

INVESTIGATION INTO THE SPATIAL DISTRIBUTION OF  
AGN COMPANION GALAXIES  
IN GRAVITATIONALLY ISOLATED ENVIRONMENTS

Janakan Sivasubramanium

A Thesis Submitted to The Faculty Of Graduate Studies  
in Partial Fulfillment of  
the Requirements for the Degree Of

Master of Science

Graduate Program in Physics & Astronomy  
York University  
Toronto, Ontario

September 2018

© Janakan Sivasubramanium, 2018

# Abstract

Active galaxies are an important subclass of galaxies, distinguished by an energetic core radiating an extraordinary amount of energy. These hyperactive cores, referred to as Active Galactic Nuclei (AGN), are driven by enhanced accretion onto a central supermassive black hole about a million to a billion times the mass of our Sun. Accretion onto a supermassive black hole may be a convincing mechanism to explain the extreme properties stemming from an active galaxy, but this proposal inevitably opens up another problem: what source provides the gaseous fuel for black hole accretion?

In this research project, we examine the possibility that these active galaxies have engaged in some form of galactic “cannibalism” of their neighbouring galaxies to acquire a fuel supply to power their energetic cores. By using data from the Sloan Digital Sky Survey (SDSS), we conduct an environmental survey around active and non-active galaxies and map out the spatial distribution of their neighbouring galaxies. Our results show that, in gravitationally isolated environments, the local environment ( $< 0.5$  Mpc) around active galaxies are seen to have an under-density or scarcity of neighbouring galaxies relative to the non-active control sample – a possible indication of a history of mergers and consumptions.

# Acknowledgments

The past two years have been an incredible learning experience. More than the technical knowledge, I believe it is my growth as a researcher and scientific thinker that have been the most valuable outcome of this experience. With this said, there have been many people along the way I would like to thank and show my gratitude. Foremost, I would like to thank my Dad, Mom and Sister for their continual support, not only through this experience but from the beginning. While most immigrant parents encourage and insist their children to pursue conventional career paths like medicine or engineering, you gave me the freedom to choose my own path – the road not taken – and create a name for myself. This was the first spark that ignited my creative spirit and hunger to learn.

I would like to show my appreciation towards many people at YorkU. I would like to thank Marlene Caplan and Janaki DeCamillis for their administrative support over the past two years. A special thanks goes out to my supervisor, Prof. Michael De Robertis, for giving me a chance to work and learn from him. I appreciate your time and work. Thank you to Prof. Adam Muzzin for taking the time out of his busy schedule to participate on my supervisory committee, and an important thanks to Prof. John Moores for taking part on my defence committee. A special acknowledgment also goes out to Prof. Tom Kirchner and Prof. Matthew Johnson for being great teachers in my courses and supporting my graduate school applications.

Lastly and most importantly, I would like to thank George James Conidis, who has been my personal coach, mentor and friend. Similar to how a compass in a magnetic field snaps to North, great leaders have the same effect on those around them. They not only teach and improve the lives of others; they have the ability to take what you know, and then restructure and align it to a greater purpose. They bring the best out of people by giving them a clearer perspective. George, you are definitely one of those great leaders.

I admire your powerful and precise scientific thinking. You taught me that the means by which we get to an answer are far more important than the answer itself. An obsession over the process and a love to break down a problem to its raw essence and analyze the fundamental gears making the whole system tick is where the minds of great physicists lie. I appreciate your pragmatic and no-BS approach to dealing with the challenges of being a researcher and, in a larger sense, the challenges of life. Thank you for not letting me quit, especially when situations seemed utterly hopeless. Thank you for teaching me to value myself and, more importantly, to protect myself from those who attempted to devalue me. Above all, thank you for believing in me.

Janakan Sivasubramanium

August 2018

# Contents

<b>Abstract</b>	<b>ii</b>
<b>Acknowledgments</b>	<b>iii</b>
<b>Table of Contents</b>	<b>v</b>
<b>List of Tables</b>	<b>ix</b>
<b>List of Figures</b>	<b>x</b>
<b>1 Introduction</b>	<b>1</b>
1.1 Why are Active Galaxies special? . . . . .	1
1.1.1 Interesting Examples of AGNs . . . . .	2
1.2 Central Problem: Supplying Fuel to the Core . . . . .	6
1.3 Pathways to Activating a Core . . . . .	7
1.4 Observational Approach:	
Investigating Routes to Activation . . . . .	12
1.4.1 First Approach: <i>Imaging the Active Galaxy</i> . . . . .	12
1.4.2 Second Approach: <i>Environmental Study of Neighbours</i> . . . . .	14
1.5 Our Approach . . . . .	17
1.5.1 Our General Model and Methods . . . . .	17

1.5.2	Important Isolation Constraint . . . . .	19
1.6	Objectives of Thesis . . . . .	20
<b>2</b>	<b>Our Model:</b>	
	<i>Defining Three Levels of Structure</i>	<b>22</b>
2.1	Structure of Our Model . . . . .	22
2.2	First Level: Individual Galaxies . . . . .	22
2.2.1	Calculating the Distance to Galaxies . . . . .	23
2.2.2	Absolute Magnitude . . . . .	26
2.3	Second Level: Host-Partner Systems . . . . .	27
2.3.1	Defining the Host . . . . .	27
2.3.2	Defining the Spatial Domain . . . . .	28
2.3.3	Defining the Partner . . . . .	29
2.3.4	Separation Distance Between Host and Partner . . . . .	31
2.3.5	Uncertainties in the Separation Distance . . . . .	31
2.4	Third Level: An Equivalent Ensemble . . . . .	33
<b>3</b>	<b>Our Methods:</b>	
	<i>Computing the Number Density Function</i>	<b>35</b>
3.1	Two Challenges with Galaxy Data . . . . .	35
3.2	Binning into Volume-Shells . . . . .	37
3.3	Quantifying Positional Uncertainty of Partners . . . . .	38
3.3.1	The Gaussian Representation of a Companion Galaxy . . . . .	38
3.3.2	Sample Calculation . . . . .	40
3.4	Computing the Number Density Function . . . . .	41
<b>4</b>	<b>Data Analysis</b>	<b>44</b>
4.1	Data Processing: Correcting for Systematic Errors . . . . .	44

4.1.1	CMB Rest-Frame Correction . . . . .	45
4.1.2	$K$ -Corrections . . . . .	46
4.1.3	Extinction through Interstellar Medium . . . . .	47
4.2	Building a Sample of Host Galaxies . . . . .	47
4.2.1	Absolute Magnitude: Constraining the Host Mass . . . . .	47
4.2.2	Redshift Limit: Spectroscopic Completeness of SDSS . . . . .	49
4.2.3	Core Identity: Assigning Spectral Sub-Classifications . . . . .	50
<b>5</b>	<b>Results</b>	<b>54</b>
5.1	Case Study (#1):	
	<i>Gravitationally Non-Competitive (GNC) Environment</i> . . . . .	56
	→ Scientific Figure: GNC Minor Ensemble . . . . .	60
	→ Scientific Figure: GNC Intermediate Ensemble . . . . .	60
	→ Scientific Figure: GNC Comparable Ensemble . . . . .	60
5.1.1	Examining the 95% Confidence Interval . . . . .	61
5.1.2	Fiber Collision in SDSS . . . . .	63
5.1.3	Colour Distribution . . . . .	64
	→ Scientific Figure: 0.0–1.0 Mpc Companion Colour Distribution . . . . .	66
	→ Scientific Figure: 1.0–2.0 Mpc Companion Colour Distribution . . . . .	66
	→ Scientific Figure: 2.0–3.0 Mpc Companion Colour Distribution . . . . .	66
5.2	Case Study (#2):	
	<i>Gravitationally Competitive (GC) Environment</i> . . . . .	69
	→ Scientific Figure: GC Mixed Ensemble – All Companions . . . . .	74
	→ Scientific Figure: GC Mixed Ensemble – Minors . . . . .	74
	→ Scientific Figure: GC Mixed Ensemble – Intermediates . . . . .	74
	→ Scientific Figure: GC Mixed Ensemble – Comparables . . . . .	74
5.2.1	Examining the 95% Confidence Interval . . . . .	74

<b>6</b>	<b>Discussion</b>	<b>76</b>
6.1	Observational Interpretation of the Results . . . . .	77
6.1.1	Case Study (#1): Gravitationally Non-Competitive Environment	77
6.1.2	Case Study (#2): Gravitationally Competitive Environment .	79
6.1.3	Comparison to Ellison et al. (2011) Study . . . . .	80
6.2	Theoretical Interpretation of the Results . . . . .	81
6.2.1	Importance of the GNC Case Study to Statistical Mechanics .	82
6.2.2	Spherically Symmetric + Isotropic Model . . . . .	83
6.2.3	Spherically Symmetric + Isotropic + <i>Isothermal</i> Model . . . .	84
6.2.4	Important Implications of AGN Number Density's Local Maximum . . . . .	86
6.3	Assumptions and Limitations of the Model and Methods . . . . .	89
6.3.1	Redshift Range and Relation to Cosmic Timescale . . . . .	89
6.3.2	Selection Bias to AGN Type . . . . .	89
<b>7</b>	<b>Conclusion</b>	<b>90</b>
	<b>Bibliography</b>	<b>93</b>



# List of Tables

1.1	Summary of AGN Classes. . . . .	5
3.1	Partner parameters for Sample Calculation from Section 3.3.2 . . . . .	40
5.1	Quantifying the scarcity of companions within the GNC environment . . .	60
5.2	GNC Environment Confidence Values . . . . .	62
5.3	Colour Distributions: P-Values from the Kolmogorov-Smirnov Test . . . .	64
5.4	Number of companions in GC Environment . . . . .	74
5.5	GC Environment Confidence Values . . . . .	75

# List of Figures

1.1	Different Type of Active Galaxies: (i) Seyfert Galaxy (NGC 5793); (ii) Quasar (3C 273); (iii) Radio Galaxy in Visible Spectrum (3C 348); (iv) Radio Galaxy in Visible/Radio/X-Ray Spectrum (3C 348); . . . . .	3
1.2	Possible Pathways to Core Activation: Different Types of Gravitational Interaction with Neighbouring Galaxies; . . . . .	9
1.3	LMC and SMC from Paranal Observatory in northern Chile; Figure adopted from Hashimoto, Funato & Makino (2003) describing radial evolution of LMC over -10 to +10 billion years; . . . . .	14
1.4	Figure adopted from Ellison et al. (2011) showing AGN fractions in galaxy pairs; . . . . .	15
1.5	Baldwin, Phillips & Terlevich (BPT) Diagram adopted from Ellison et al. (2011); . . . . .	16
1.6	Illustration of counting volume around central host galaxy; . . . . .	17
1.7	General sketch illustrating how the number density of companions may behave over a certain radial range; . . . . .	18
1.8	Illustration of Gravitationally Competitive/Non-Competitive Environment	19
2.1	Three Levels of Structure in Our Model . . . . .	23
2.2	Illustration of Non-Interacting Condition . . . . .	28

2.3	Cross-sectional illustration of the geometry associated with locating a host-partner system; . . . . .	31
3.1	Illustration of how a 3D host-partner system with five partners is projected onto 1D radial scale by assuming a spherically symmetric system; . . . . .	36
3.2	Binning into Volume-Shells . . . . .	37
3.3	Sample Calculation with Gaussian Probability . . . . .	41
4.1	CMB with and without Dipole Anisotropy . . . . .	45
4.2	Example of Galactic Spectral Energy Distribution (SED) . . . . .	46
4.3	<i>i</i> -Band Luminosity Function of Galaxies with $z \leq 0.1$ . . . . .	48
5.1	<i>Scientific Figure</i> : GNC Minor Ensemble . . . . .	57
5.2	<i>Scientific Figure</i> : GNC Intermediate Ensemble . . . . .	58
5.3	<i>Scientific Figure</i> : GNC Comparable Ensemble . . . . .	59
5.4	<i>Scientific Figure</i> : 0.0 – 1.0 Mpc Companion Colour Distribution . . . . .	66
5.5	<i>Scientific Figure</i> : 1.0 – 2.0 Mpc Companion Colour Distribution . . . . .	67
5.6	<i>Scientific Figure</i> : 2.0 – 3.0 Mpc Companion Colour Distribution . . . . .	68
5.7	<i>Scientific Figure</i> : GC Mix Ensemble – All Companions . . . . .	70
5.8	<i>Scientific Figure</i> : GC Mix Ensemble – Minors . . . . .	71
5.9	<i>Scientific Figure</i> : GC Mix Ensemble – Intermediates . . . . .	72
5.10	<i>Scientific Figure</i> : GC Mix Ensemble – Comparables . . . . .	73
6.1	Sketches of the number density solution given in Equation (6.8) for the spherically symmetric, isotropic and isothermal model. . . . .	85

# Chapter 1

## Introduction

### 1.1 Why are Active Galaxies special?

Starting in the early 20<sup>th</sup> century, our Milky Way was discovered to actually be one of many billions of galaxies populating the cosmos. As astronomers began collecting detailed catalogues of this galaxy zoo beyond our own and investigating their properties, one particular sub-class of galaxies stood out as a special outlier, known as Active Galaxies. At first glance, these objects appeared optically normal but, after closer inspection, astronomers were able to measure extreme luminosities stemming from the nucleus, referred to as *Active Galactic Nuclei (AGN)* (Netzer, 2013). These AGNs can produce an intense amount of radiation greater than the entire output released by a typical galaxy (Sabater et al., 2015). It is not necessarily this degree of energy production that is astonishing; it is the fact that a tiny volume spanning a few light-years has the ability to generate more luminosity and, at times, can outshine the entire disk of a typical galaxy, which generally spans about hundred thousand light-years (Netzer, 2013). Even more intriguing, astrophysicists learned that an AGN's energy production cannot be simply attributed to the light from stars and dust alone, known as thermal radiation – there must be some other mechanism powering these nuclei.

What is the cause of this extreme activity? Astrophysicists have strong evidence to believe that there exists a supermassive black hole anywhere from a million to a billion  $M_{\odot}$  at the centre of these active galaxies, where  $M_{\odot} (= 2 \times 10^{30} \text{ kg})$  is a solar mass unit equivalent to the mass of our Sun (Richstone et al., 1998). These cosmic

entities are like hungry galactic monsters devouring whatever gas is available from the swirling disk of gas – the accretion disk – surrounding the black hole. As this matter falls into the black hole, it heats to high temperatures via some kind of frictional force and releases an enormous amount of energy in the form of non-thermal radiation.

Interestingly, there is also evidence suggesting that all large galaxies possess central supermassive black holes and experience a certain extent of material infall; however, active galaxies have elevated this accretion process far beyond the typical intensity of normal galaxies (Netzer, 2015). To put this accretion rate into perspective, it is estimated that a  $10^8 M_{\odot}$  black hole may consume about  $1 M_{\odot}$  of gas per year to power its engine. The process is very efficient for an astrophysical phenomenon, where detailed calculations estimate 10% to 20% of the total mass-energy of the infalling matter has the ability to be converted to radiation before crossing the black hole’s horizon (Richstone et al., 1998). It is this enhanced accretion that gives rise to the observed non-stellar and intense radiation from the nucleus.

### 1.1.1 Interesting Examples of AGNs

Over the years, astrophysicists have discovered a great variety of AGNs with different spectral features, radiative outputs and large-scale structures (Fabian, 2012). One of the first investigations of active galaxies was done by Carl K. Seyfert in 1943. His findings suggested that a small population of galaxies had highly luminous galactic nuclei and possessed atypical spectral features unseen in most galaxies. These objects are now collectively known as Seyfert galaxies; Figure (1.1a) depicts a well-studied Seyfert known as NGC 5793. They have been widely studied in astrophysics because they are the most common active galaxy found in high number densities. Visually, they often appear very similar to common spiral galaxies, like our Milky Way; however, when we analyze the light from their nuclei, there are noticeable differences in the spectral features. In fact, Seyferts turned out to actually be one family member of a rich variety of active galaxies. These further discoveries transitioned AGNs from an observational curiosity into an important sub-classification of galaxies and allowed us to expand our knowledge of galaxy formation and supermassive black hole evolution. We now explore some interesting examples of active galaxies.

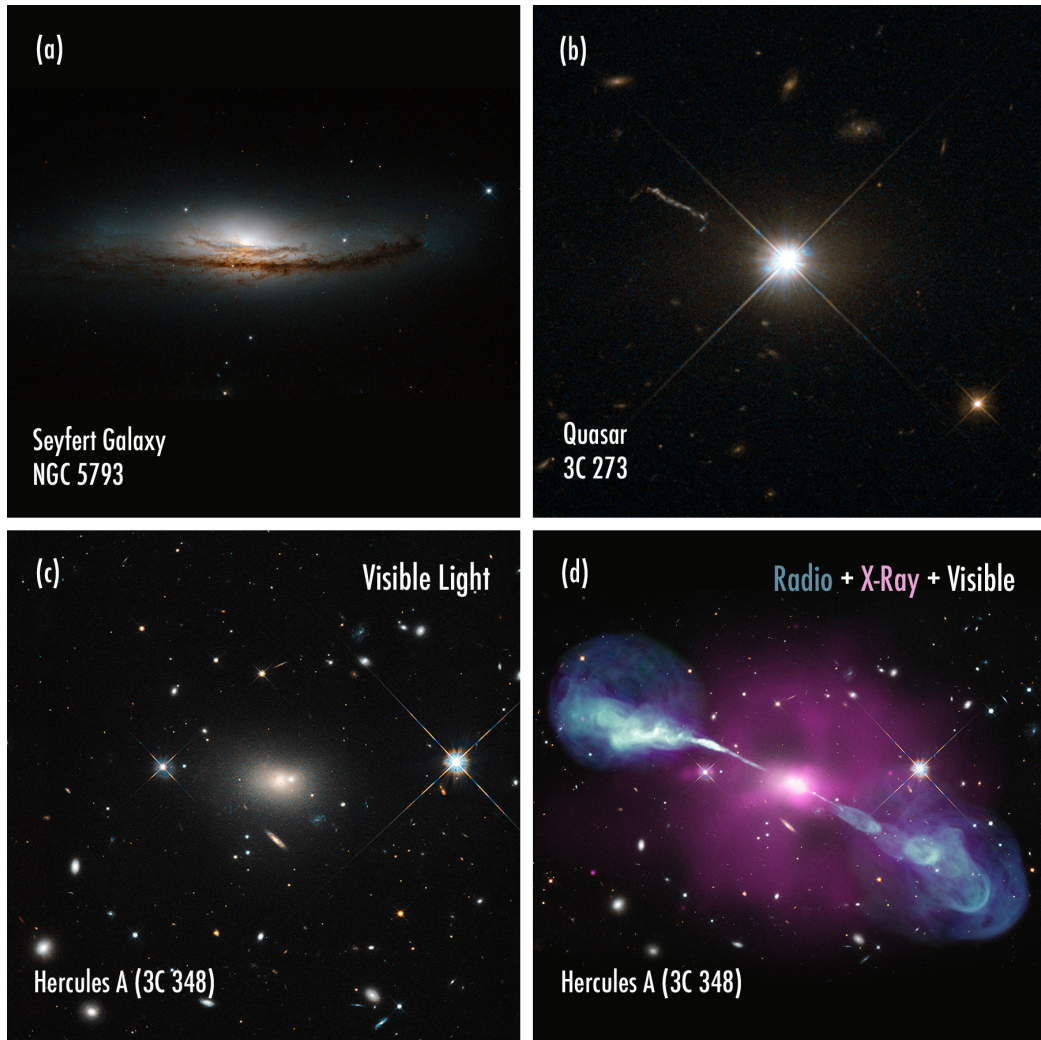


Figure 1.1: (a) Seyfert galaxy (NGC 5793). Seyferts are the most common active galaxies and particularly relevant to this thesis. (Source: NASA, ESA, & E. Perlman); (b) Quasar (3C 273). Quasars are one of the most luminous active galaxies. (Source: NASA/HST); (c and d) Two images of the same radio active galaxy, Hercules A (3C 348), in the visible spectrum (c) and a superposition of the visible, x-ray and radio spectrum (d). There are two bipolar beams extending about 1.5 million light-years in length, known as astrophysical jets. These jets represent the outflow of highly energized and ionized matter moving at relativistic speeds. They are often powered by strong magnetic fields and accretion onto a central supermassive black hole. (Source (c): NASA/STScI/HST; Source (d): NASA/STScI/CXO/SAO/NRAO/VLA/HST)

An AGN that has caught much attention over the years, especially in popular scientific literature, are Quasi-Stellar Radio Sources (Quasars). These active galaxies particularly stand out because they are one of the most luminous objects among galaxies and can be seen at far cosmological distances. The total luminosity from a typical Quasar can vary anywhere from  $10^{38}$  Watts to more than  $10^{41}$  Watts, which is almost 100,000 times more energetic than a typical galaxy like our Milky Way (Netzer, 2015). Figure (1.1b) is an image of one of the first Quasars, 3C 273, ever discovered. The observation of quasars has also led to investigations exploring the frequency of active galaxies over different cosmic timescales. In general, we see a progressively increasing presence of more luminous active galaxies in the past, where Quasars were notably much more predominant billions of years ago than now (Netzer, 2013).

Figure (1.1c) and (1.1d) depicts another active galaxy named Hercules A (3C 348). In the left image, we see Hercules A only in visible light with no particularly noticeable features; however, when we include the signal from the  $x$ -ray and radio wavelength in the right image, we suddenly see a new wealth of information. Hercules A is a special type of AGN referred to as a radio galaxy. Even though the central galaxy appears to be a regular elliptical galaxy, there are stunning bipolar extensions originating from the center. This large-scale structure is the result of the relativistic ejection of charged electromagnetic particles arising from the violent environment created by the accretion onto the supermassive black hole. Astrophysicists estimate the extension of these jets to be about 1.5 million light-years in length, which is almost 10 times the diameter of the entire Milky Way (Osterbrock & Ferland, 2006). We include a brief summary of different AGN sub-classes in Table (1.1).

Table 1.1: Summary of AGN Classes.

<b>Class</b>	<b>Sub-Class</b>	<b>Description</b>
<i>Seyfert</i>	Type 1	Weak radio emission; X-ray emission; Spiral galaxies; Variable brightness; Broad and narrow emission lines
	Type 2	Weak radio and x-ray emission; Spiral galaxies; Not variable brightness; Narrow emission lines only
<i>Quasars</i>	Radio-Loud (QSR)	Strong radio emission; Variable; Some polarization; Broad and Narrow emission lines
	Radio-Quiet (QSO)	Weak radio emission; Variable; Weak polarization; Broad and narrow emission lines
<i>Radio Galaxies</i>	BLRG	Strong radio emission; Elliptical galaxies; Variable; Weak polarization; Broad and narrow emission lines
	NLRG	Strong radio emission; Elliptical galaxies; Not variable; No polarization; Narrow emission lines only
<i>LINERs</i>		Spiral galaxies; Low-ionization emission lines



## 1.2 Central Problem: Supplying Fuel to the Core

Accretion onto a supermassive black hole may be a convincing mechanism to explain the extreme properties stemming from an AGN, but this proposal inevitably opens up another problem (Lynden-Bell, 1969). If all major galaxies have central supermassive black holes and experience a certain extent of material infall, then why are some galaxies active and others not? What pathway has permitted active galaxies to engage in enhanced accretion to power this extreme core activity? In essence, these galaxies have somehow worked out a route to transport a supply of gaseous fuel directly to the galactic core.

Across the board, active galaxies generally require anywhere from 0.1 to  $10 M_{\odot}$  worth of matter per year to feed their engines (Osterbrock & Ferland, 2006). If so, where does this supply of gas come from? At first thought, we may immediately turn to the gas in the surrounding galactic disk, but studies have revealed this gas to be relatively stable; after all, the vast majority of spiral galaxies, which are also the dominant morphology of Seyferts, are not AGN (Fabian, 2012). If there is no such fuel supply to power the engine, then it is perfectly possible for a galactic core to have a supermassive black hole but have no activity, collectively referred to as non-AGNs. Our Milky Way is an example of a non-AGN with a  $4.5 \times 10^6 M_{\odot}$  supermassive black hole with no signs of significant core activity. The existence of a supermassive black hole is a necessary condition to activate the center of a galaxy; however, it is not a sufficient condition to claim that a galaxy's core will be active (Netzer, 2013). With all of this said, active galaxies are distinguished structures that have in some way worked out this transport mechanism to deliver this activating fuel to the core.

This leads us to one of the central questions driving current research in the field of Active Galaxies: *What pathway allows AGNs to efficiently supply their cores with gaseous fuel and engage in enhanced accretion onto the central supermassive black hole compared to non-AGNs? Where does this gas originate from?*

### 1.3 Pathways to Activating a Core

There exists a great deal of literature exploring how active galaxies may have received their fuel supply and discussions on various pathways to activation. Overall, researchers have approached the question via two routes: (1) internal mechanisms and (2) external mechanisms. As for internal means, secular evolution involves scenarios whereby existing gaseous material in the disk grows unstable from a galaxy's *own* self-perturbations and this instability ultimately plunges matter into the core. For instance, the possibility of stellar bars as a pathway has been considered as a viable option. These bar structures are common morphological features found in many spiral galaxies and research suggests they may give way to funneling gaseous material into the core. Cisternas et al. (2015) investigated this pathway and found that the role of bars may not be a convincing mechanism to deliver a sufficient amount of fuel to the central 100 pc and power black hole accretion. Another possible internal source would be nuclear star clusters. Seth et al. (2008) studied galaxies that hosted both nuclear star clusters and AGNs to examine any correlations between the two features. They found that the fraction of galaxies with nuclear star-cluster were equally likely to have AGN and non-AGN characteristics; there were no strong correlations.

With this said, the focus of this thesis is particularly directed at the possibility of an external source being the main culprit responsible for triggering gas inflow and, ultimately, initiating core activity. What are these external sources? The modern definition of a galaxy is regarded as a gravitationally bound collection of stars and gas situated in an encompassing dark matter halo (Mo, Bosch, & White, 2010). However, galaxies themselves may belong to larger gravitational structures forming a hierarchical framework of the universe, such as galaxy pairs, groups, and clusters. These neighbour galaxies are constantly interacting with each other via long-range gravitational forces.

Over the years, researchers have investigated whether an active galaxy's neighbours may have possibly played an important role in initiating core activity. There are two main pathways allowing neighbour galaxies to stimulate gas inflow: (i) a direct contribution of fuel, whereby the neighbour merges with the host and directly supplies its reserve of gas to the core and/or (ii) the physical closeness of a neighbour induces instabilities in the host's existing gas supply, which gives way to radial movement of gas to the core (Netzer, 2013). While we can group all of these possibilities as

gravitational interactions, different interactions have acquired special attention over the years.

### **Galactic Collision**

Galactic collisions are an example of one of the most direct ways a neighbour galaxy can supply fuel to the core. If the typical diameter of a major galaxy is anywhere between 20 to 40 kiloparsec (kpc), then galaxy pairs within 1000 kpc or 1 megaparsec (Mpc) are often seen to be more strongly interacting and, depending on the orbital configurations, approaching trajectories can result in direct inbound collisions under their mutual gravitational attraction (Binney & Tremaine, 2008). Figure (1.2a) depicts an example of a galactic collision – the spiral galaxy NGC 2207 is undergoing a direct collision with a smaller neighbour galaxy IC 2163. It is interesting to note that in a galactic collision the individual stars themselves do not collide, but rather the gas and dust from both members can experience significant compressions and shocks.

In terms of galactic collisions as a pathway to AGN activation, these kind of gravitational interactions can be both beneficial and detrimental to promoting core accretion. It is a challenge to determine what particular kinds of collision can lead to AGN activity because modeling galactic collisions is extremely difficult via analytical methods, and often requires detailed numerical simulations or high-resolution imaging from telescope data. In general, there are four important properties that influence the final structure of a merger: (i) mass ratio between the colliding pair (if a progenitor’s mass ratio is less than 1/3, then it is referred to as a minor merger); (ii) morphologies of the progenitors (disk or elliptical); (iii) gas mass fraction of the progenitors (mergers with gas-rich encounters referred to as wet mergers); (iv) orbital properties (Mo, Bosch, & White, 2010). In terms of AGNs, we would expect minor and wet mergers with orbital configurations that do not entirely disrupt existing disk structure to be the most favorable collisions leading to core activity (Combes et al., 2009).

### **Galactic Cannibalism**

Another important scenario is galactic cannibalism, whereby the orbit of a smaller neighbour gradually decays into the host via the process of dynamical friction. The influence of dynamical friction can be thought of as a “gravitational drag” experienced by a smaller body as it moves in the presence of a larger gravitational body; as a

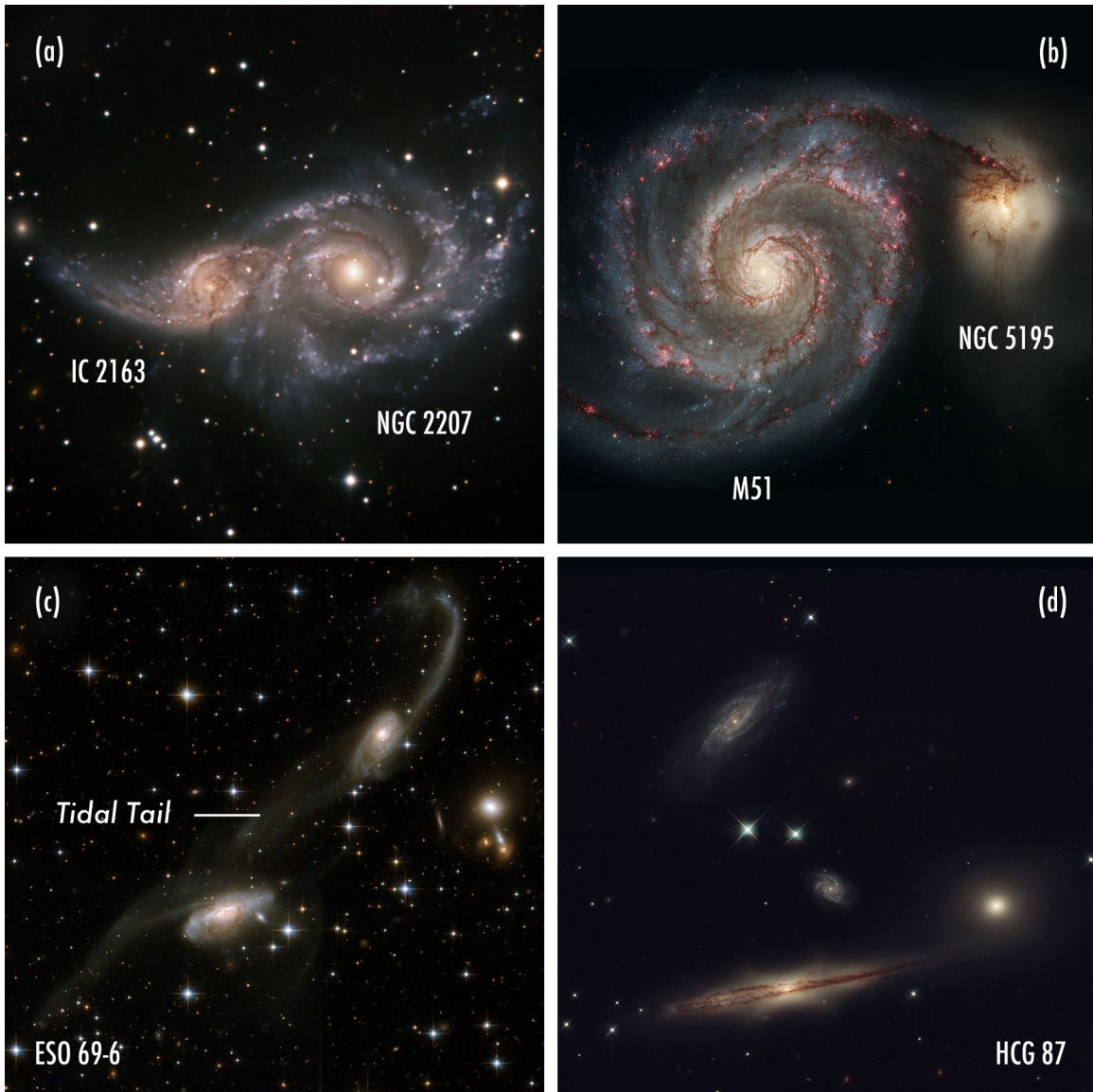


Figure 1.2: (a) Galactic collision between NGC 2207 and small neighbour IC 2163 (*Source: ESO*); (b) Galactic cannibalism of active (Seyfert) galaxy M51 of smaller dwarf neighbour (NGC 5195) (*Source: ESA, NASA*); (c) Small compact galaxy group, HCG 87. Close proximity of neighbour galaxies contained within projected diameter of  $> 0.1$  Mpc situates group members in an asymmetric gravitational potential, which may possibly lead to gas inflows. Known as galactic harassment (*Source: Sally Hunsberger (Lowell Obs.) Jane Charlton (Penn State) et al.*); (d) The system ESO 69-6 of two interacting galaxies with elongated tidal tails stretching out between them like a bridge. (*Source: NASA, ESA, Hubble Heritage*)

consequence, there is a loss in angular momentum and the orbital trajectory begins to decay (Ogiya & Burkert, 2016). This decaying process would allow a larger host to consume smaller partners over reasonable cosmological timescales. Even though the initial concept proposed by Chandrasekhar (1943) involved a large body transversing through a cloud of smaller bodies, this phenomenon is still relevant for a large host galaxy and its interaction with smaller partners. The Chandrasekhar formula says that the velocity of an orbiting smaller companion  $\vec{v}_c$  in the presence of a large host experiences the following deceleration (Ogiya & Burkert, 2016):

$$\frac{d\vec{v}_c}{dt} = -4\pi G^2 M_c \ln(\Lambda) \rho_{host} \frac{\vec{v}_c}{v_c^3}, \quad (1.1)$$

where  $M_c$  is mass of the companion,  $\rho_{host}$  is the mass density distribution of the host,  $\ln(\Lambda)$  is the Coulomb logarithm, and  $v_c$  is the speed. From this formula, we immediately observe that if the companion has any tangential velocity component, then it will necessarily have a negative and tangential acceleration component, which leads to an angular momentum loss and a gradual spiraling towards the system's center-of-mass. This is why dynamical friction is often referred to as a “gravitational drag”.

Figure (1.2b) shows the Seyfert galaxy M51 undergoing a strong interaction with a neighbouring dwarf galaxy (NGC 5195). At this stage, the neighbours have begun merging and a common gaseous envelope has formed from exchanged material. These kind of satellite galaxies (less than 10% the mass of the host) are ideal candidates to be cannibalized because of their mass difference relative to the host and their general abundance. An interesting calculation by Binney and Tremaine (2008) roughly estimate the number of satellites consumed by a large host via dynamical friction over a Hubble time of about 13 billion years is equivalent to  $\Delta L \approx 0.13L_{Host}$ , where is  $L_{Host}$  is the current luminosity of the host. In other words, a typical giant galaxy has eaten one or two satellites equivalent  $\approx 10\%$  of its own luminosity. Another interesting idea worth mentioning is that gravitationally bound companions may play different roles for a host in the consumption process, as opposed to unbound companions. For instance, a study by Filippenko et al. (1998) showed that nearly half of all spiral galaxies have some level of non-thermal activity in their centres; however, there is no compelling evidence that half of all galaxies are merging or have recently merged. This may be evidence that a nearby bound smaller satellite may have been consumed to power the core.

## Galactic Harassment and Tidal Stripping

Neighbours do not necessarily have to directly merge with the host via a collision or cannibalism process to activate the core. Ultimately, the stimulation of gas inflow is what leads to the onset of enhanced accretion. It turns out that the physical closeness of a neighbour galaxy can also lead to this stimulation (Ellison et al., 2011). For instance, the close proximity of a comparable-sized neighbour can situate a host galaxy in an asymmetric gravitational potential. This imbalance may give rise to stresses and strains to transport gas into the core (Haan et al., 2009). As an example, Figure (1.2d) illustrates a small compact group of galaxies known as HCG 87 that contain a collection of galaxies within close proximity. If the typical distance between major galaxies is  $\approx 1.0$  Mpc, then astronomical measurements indicate that this group has a projected diameter around 0.1 Mpc. Within this collection itself, there are two active galaxies close to other comparable-sized galaxies, suggesting that gravitational interaction with close neighbours may be possibly assisting core activity.

The nearness of a neighbour can also exert tidal forces such that gaseous material is striped from the outskirts. This type of gravitational interaction may give rise to thin, elongated stretches of stars and gaseous material, known as tidal streams and tails, allowing for a direct exchange of matter without direct merger (Putman et al., 2003). Figure (1.2c) shows an example of such a system of two interacting galaxies (ESO 69-6) with long elongated tidal tails stretching out.

## 1.4 Observational Approach: Investigating Routes to Activation

We have introduced Active Galaxies as an important sub-class of galaxies, distinguished by an energetic core, or AGN, radiating an extraordinary amount of energy. This radiation is not the result of typical stellar or thermal activity as found in most galaxies, but, rather, astrophysicists have strong evidence to believe that this hyperactive core is driven by enhanced accretion onto a central supermassive black hole. However, the presence of a supermassive black hole is not unique just to AGNs; most large galaxies, like our Milky Way, also harbour these black holes and, yet, do not have extreme core activity – collectively referred to as non-AGNs (Netzer, 2013). In essence, the primary difference between AGNs and non-AGNs is that active galaxies have found some way to transport fuel to their nucleus. This brings us to an important open question: what pathway allows these active galaxies to supply gaseous fuel to power their active cores?

In terms of plausible mechanisms, there seem to be many routes to activating a core. The focus of this thesis is directed at understanding how neighbour galaxies via gravitational interaction with a host may stimulate gas inflow. By gravitational interactions, we are referring to situations whereby a neighbour galaxy makes a direct contribution of gas to the host and/or the physical closeness of a neighbour induces gravitational disturbances in the existing gas of the host. Any of these situations can potentially lead to the onset of enhanced accretion and, thus, activate the core.

In this section, we address how researchers have investigated and tested these possibilities to examine their validity. We present two important approaches, which include capturing high-resolution images of active galaxies with telescopes and studying their surroundings to search for particular environmental traces indicative of gravitational interactions.

### 1.4.1 First Approach: *Imaging the Active Galaxy*

The first approach involves taking high-resolution imaging of the active galaxy and searching for morphological evidence of past mergers and gas inflow. For instance, a study by Combes et al. (2009) inspected the disk morphology of the active (LINER)

galaxy NGC 1961. Compared to other disk galaxies, this galaxy stands out because of a perturbed and deformed galactic structure with a very large radial extent, suggesting that NGC 1961 may have undergone a direct head-on collision. This may have ultimately driven cold gas into the core of the galaxy and initiated AGN activity.

Major mergers can often lead to significant distortions and damages to the integrity of a host's existing disk, which may also conversely inhibit efficient gas inflow and, thus, prevent core activity. However, minor mergers with smaller-mass neighbours may be a more effective process. For instance, a study by Tanaka, Yahi & Taniguchi (2017) search for morphological evidence of past minor mergers in the Seyfert galaxy, NGC 1068. They used deep optical imaging from the Subaru Telescope and reported at least three Ultra Diffuse Objects (UDOs) at a radial distance of 45 kpc away from the active core of NGC 1068. This evidence of distorted disk morphology suggests that NGC 1068 may have been involved in a past merger that did not entirely disrupt the integrity of the disk but, at the same time, may have provided subtle changes in the gas inflows and potentially triggered nuclear activity.

The effects of dynamical friction, which allows for a slower and less-dramatic cannibalism of smaller neighbours, is more challenging to study via these imaging techniques. One astrophysical system that has received attention in the light of dynamical friction is the orbital decay of the Milky Way's two notable satellite galaxies: the Large Magellanic Cloud (LMC) and the Small Magellanic Cloud (SMC), as seen in the left of Figure (1.3). A study by Hashimoto, Funato & Makino (2003) investigate the orbital evolution of satellite galaxies, in general, using N-body numerical simulations. The right-side plot in Figure (1.3) attempts to predict the decay of the LMC by modeling the satellite's radius (in kpc) from the Milky Way over 10 billion years into the future and from the past (the simulation assumes the LMC's mass to be  $2 \times 10^{10} M_{\odot}$ , and located at 50 kpc with speed of  $\approx 340$  km/s). Since the Milky Way has a disk radius around 15 kpc, the study estimates the LMC may encounter our galaxy anywhere within the next 5 to 10 billion years. The  $\Lambda$  parameter is known as the Coulomb logarithm, which is dependent on the distribution and kinematics of the dark matter halo.

Beside directly merging with the Milky Way, tidal forces induced on the LMC and SMC by our Galaxy has sheared off gaseous material, leading to tidal tails and



streams. Putman et al. (2003) conducted spectroscopic studies to reveal the satellites are actually connected by a low metallicity bridge of gas, or Magellanic Bridge, and share a common gaseous envelope. This is observational evidence that the LMC and SMC have been merging with the Milky Way via dynamical friction over an estimated timescale of 2 to 6 Gyr. Even though our Milky Way’s central  $4.5 \times 10^6 M_{\odot}$  supermassive black hole is not fully active, some researchers speculate that the supply of gas from the LMC and SMC may stimulate core accretion.

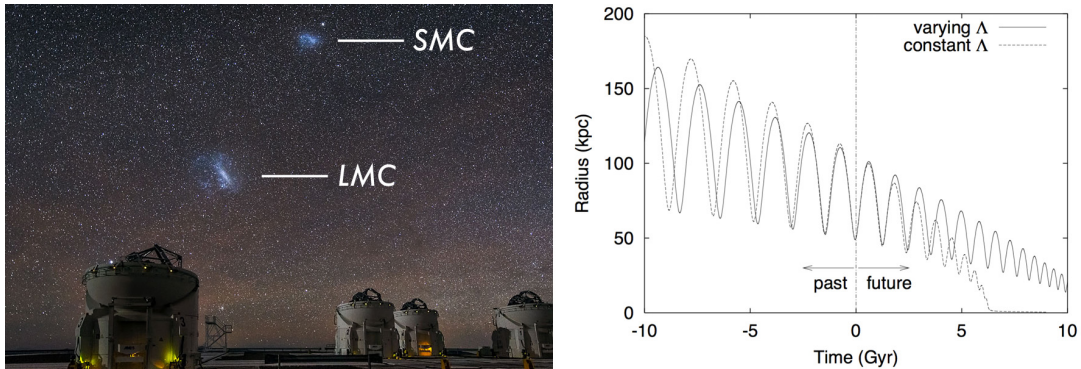


Figure 1.3: (Left) Image of the Paranal Observatory in northern Chile and the nighttime sky containing a view of the Milky Way’s two notable satellite galaxies: the Large Magellanic Cloud (LMC) and the Small Magellanic Cloud (SMC) (Source: ESO/J. Colosimo); (Right) Radial evolution of the LMC over  $-10$  to  $+10$  billion year (Gyr) time period from today. Figure adopted from Hashimoto, Funato & Makino (2003).

### 1.4.2 Second Approach: *Environmental Study of Neighbours*

The second approach to studying the influence of neighbouring galaxies involves surveying the surrounding environment of a host. The reasoning is that if a host had indeed engaged with its neighbours to stimulate gas inflow and activate its core, then there should be traces seen in the environment indicative of a past violent and interactive history, which led to a direct merger. Along the same lines, if the closeness of a neighbouring galaxy is stimulating gas inflow and invigorating core activity, then current observations of the surroundings should be indicative of such an environment of close-range companions to the host.

One of the challenges of conducting an environmental study is defining the particular spatial domain to be surveyed. Galaxies may be embedded in a hierarchical framework of different structures; however, there are no concrete and clear-cut defini-

tions distinguishing these different structures. If the mean number density of galaxies is  $\approx 0.01 \text{ Mpc}^{-3}$ , then any region of galaxy clustering denser than this mean number density is often regarded as a galactic structure of interest (Osterbrock & Ferland, 2006). To start, two galaxies within 1.0 Mpc of each other are often seen in bound configurations where they are gravitationally interacting – they are known as galaxy pairs. Beyond pairs, a significant number of galaxies in our present-day Universe are also arranged into groups and clusters. While there is no sharp division between a group and cluster, any volume where the number of galaxies is a few tens to a few hundred times the mean number density is regarded as a group or cluster. A radius of 1 to 3 Mpc is often regarded as a group radius with 10 to 30 galaxies, while a radius less than 10 Mpc with fewer than 100 galaxies is often considered as a cluster (Mo, Bosh, & White, 2010).

Researchers have investigated the distribution and properties of AGNs in these different levels of structure. For instance, a study by Ellison et al. (2011) explore the idea of galaxy pair interaction as a possible trigger of AGN activity by examining a very local environment within a projected radius of 0.08 Mpc. By surveying galaxies with close companions from the Sloan Digital Sky Survey (SDSS), they found a significant increase in the AGN fraction in close pairs with projected separation  $> 0.04 \text{ Mpc}$  by an average factor of 2.5 relative to the control sample, with an increase in the AGN fraction strongest in equal mass galaxy pairs and weakest in unequal mass pairs.

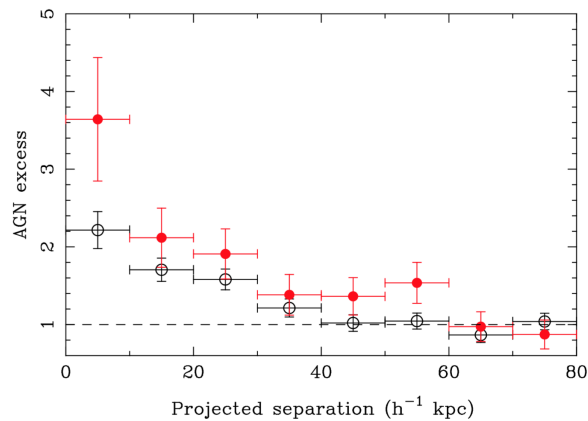


Figure 1.4: Figure (3) from Ellison et al. (2011). It shows AGN excess, which is a measure of the fraction of AGN in the pairs relative to the fraction of AGN in the control sample, is plotted as a function of projected separation. Black open symbols show galaxies at  $z < 0.1$  and red filled points show galaxies at  $z \geq 0.1$ .

Satyapal et al. (2014) conducted a mid-infrared to study of AGNs in merger circumstances and galaxy pairs to understand how AGNs may be triggered by gravitational interactions. The researchers initially collected a sample of galaxy pairs and post-mergers from the Sloan Digital Sky Survey and then matched the objects to the Wide Field Infrared Sky Explorer (WISE) database. Relative to a mass-, redshift-, and environment-matched control sample, the fraction of AGNs in pairs were found more commonly within closer projected separations of  $< 100$  kpc.

A study by Khabiboulline et al. (2018) aimed to measure another indicator of AGN activity beyond spatial distributions. They examined how the ionization conditions in AGN activity varied across different environments from galaxy pairs to clusters for  $z < 0.2$ . They measured the strength of AGN activity by considering an active galaxy's position on the BPT diagram (see Figure (1.5)). Their results indicate that a galaxy's interaction enhances AGN ionization activity toward the top right of the BPT diagram, especially in galaxy-pair interactions within a projected radius of 100 kpc and AGNs found in larger cluster environments where starforming activity is more common.

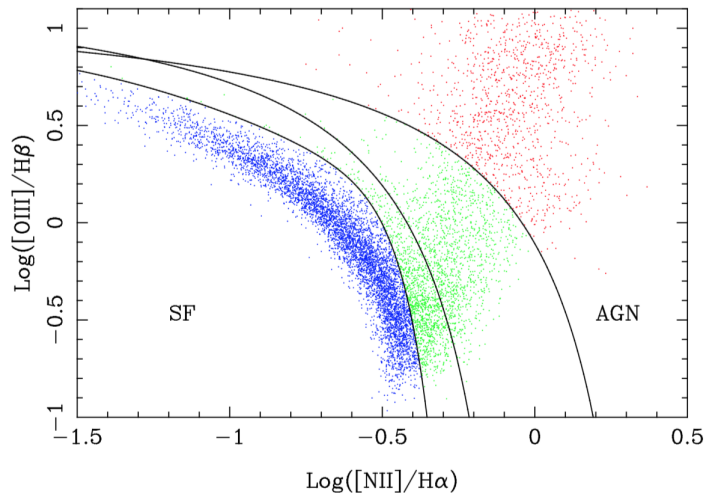


Figure 1.5: The Baldwin, Phillips & Terlevich (BPT) diagram plots the relative fluxes from  $[\text{OIII}]/\text{H}\beta$  and  $[\text{NII}]/\text{H}\alpha$  for a galaxy. It is often used as a diagnostic test to determine and classify galaxies as AGNs (denoted in red) or Star-Forming (SF) (denoted in blue) based on their relative positioning on the diagram. Figure taken from Ellison et al. (2011).

Beyond the immediate surrounding of galaxy pairs, researchers have also investigated the distribution of AGNs in clusters and groups of galaxies in order to study their evolution and how they are correlated with their environment on a scale beyond

1.0 Mpc. An important question involves asking: is the evolution of AGNs in clusters different from AGN evolution in non-cluster environments (referred to as field AGNs)? Martini, Mulchaey & Kelson (2007) studied the distribution of 35 AGNs in eight galaxy clusters with  $0.06 \leq z \leq 0.31$ . These researchers found that the most luminous AGNs ( $L_{X\text{-ray}} > 10^{42}$  ergs s<sup>-1</sup>) are more centrally concentrated compared to other non-AGN cluster members with similar luminosities.

## 1.5 Our Approach

### 1.5.1 Our General Model and Methods

The challenge of understanding the pathway active galaxies have taken to activate their cores is an open problem that may be explored from many different angles. In this thesis, our approach to understanding how these galaxies may have become active involves conducting an environmental survey of their surroundings. We use data from the Sloan Digital Sky Survey (SDSS) – a monumental astronomical surveying project that imaged 35% of the sky in a variety of filters and collected a database of over 500 million objects.

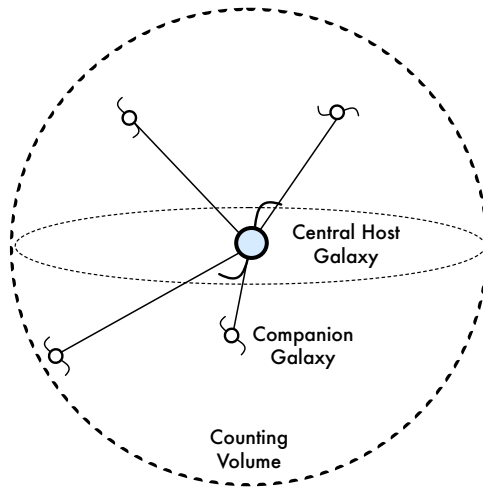


Figure 1.6: Around a (non-AGN or AGN) host galaxy, we consider spherically symmetric volume and search for neighbour galaxies, referred to as companions (or partners) of the central host, within this volume. A host and its partners are collectively known as a host-partner system. Once we have an ensemble of these host-partner systems, we investigate how the companion number density  $n(r)$  (i.e. number of galaxies per unit volume) varies over distance  $r$  from the host.

From this extensive database, we first establish a target sample of AGN galaxies and a control sample of non-AGN galaxies normalized under certain macroscopic parameters such as distance range (measured in astrophysics by redshift  $z$ ), galaxy shape, and mass. The matched galaxies in this collection will be referred to as host galaxies. Around each host galaxy, we consider a spherical volume and identify the

neighbouring galaxies within this volume, which we refer to as companions (or partners) of the central host. Once we have identified and established these host-partner systems, we investigate how the number density of companions (i.e. the number of galaxies per unit volume) varies as a function from the central host.

Ultimately, we want to investigate whether the physical presence of these companion galaxies may be responsible for core activity in a host. Our hypothesis is that, if companion galaxies via some form of gravitational interaction are indeed responsible for triggering an AGN, then we would expect some observable difference in the number density of AGN companions compared to the number density of non-AGN companions. Our project aims to investigate whether there possibly exists such a difference. Even though we acknowledge there are many different forms of gravitational interactions (as described in the previous section), our project is not necessarily interested in these specific details. To answer the questions, (i) how intensely are companion galaxies interacting with their host and (ii) which particular form of gravitational interaction is being invoked, we can essentially distill these two questions to investigating the following question: How does the number density of companions vary around a host?

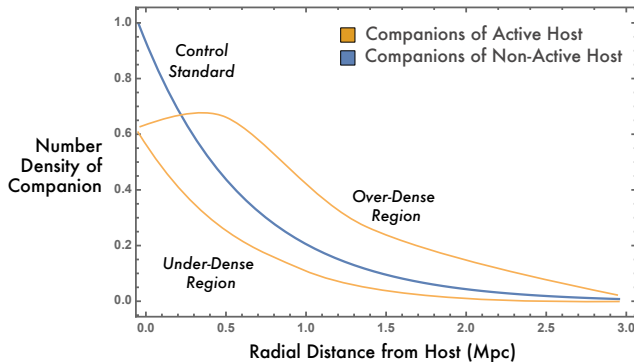


Figure 1.7: A sketch generally illustrating how the number density of companions may behave over a certain radial range. By observing how the number density of AGN companions varies relative to the non-AGN control sample, we can understand whether these active host are placed in a *under-*, *over-*, or *equally-dense* environment. This comparison allows us to directly study the relative environment of active and non-active host and make inferences about the cause of core activity from environmental differences.

The number density of companions has important interpretational value and may be used to understand the statistical behaviour of companions around a host. In our project, the non-AGN number density will give us a control standard that represents

the typical clustering of companions such that a host is not seen to be active. Now, by observing how the AGN number density varies relative to the control, we can measure if AGN hosts are, on average, situated in *under-*, *over-*, or *equally-dense* environments compared to their non-AGN counterparts. This difference between the AGN and non-AGN number density has important interpretational value in this project allowing us to reason whether gravitational interaction with companions may possibly lead to core activity.

### 1.5.2 Important Isolation Constraint

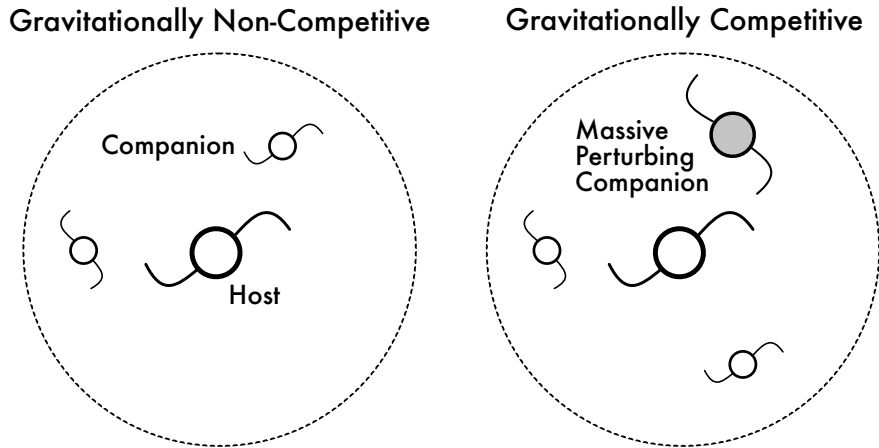


Figure 1.8: The central galaxy may be the *mathematical* host of the surrounding volume, but, whether or not it is the *physical* host of the volume depends on the central host’s gravitational dominance. In the Gravitationally Non-Competitive (GNC) environment (left), there are no comparable-sized companions in the volume; therefore, the clustering of lower-mass companions is predominantly determined by the gravitational presence of the central host. However, if there is a comparable-sized partner (right), then the central host has to compete with this massive partner for other companions.

One of the key ideas distinguishing our project is the consideration and exploration into an important isolation constraint referred to as *Gravitational Competitiveness* (GC). As mentioned above, our methodology and model involves establishing a sample of non-AGN and AGN hosts and then searching around them for companions within a certain volume. By placing an object at the center of a volume, it only defines the central galaxy to be the *mathematical* host. However, what does it mean for a galaxy to be a *physical* host in its surrounding? A physical host must be the gravitationally dominant presence in this volume. However, if there is a companion of

comparable-mass in this volume, then the central host is not the dominant source of gravity. The central host has to *compete* with the other comparable-sized partner(s) for the clustering of lower-mass companions. This physical circumstance is what we refer to as Gravitational Competitiveness.

With all of this said, we adopt a model that is conscious of the gravitational environment of the host. We want to investigate whether the gravitational dominance of a central host plays an important role in determining the spatial distribution of companions. This is a subtle condition that may not have been fully appreciated by previous researchers.

## 1.6 Objectives of Thesis

To summarize, our project aims to investigate the following relationships:

- Even after AGN and non-AGN host galaxies have been matched within certain macroscopic parameters, does the spatial distribution of companions depend on core activity of the host?
- How does the mass of a companion influence how it clusters around a host? Is there radial bias for different mass partners?
- How does a host's gravitational dominance (i.e. the Gravitational Competitiveness constraint) influence the spatial distribution of companions?

From this point on, the thesis will adhere to the following outline. In *Chapter (2): Our Model*, we clearly define the model we use to develop the statistics associated with the number density. We introduce the meaning of an Equivalent Ensemble and the important parameters that identify an ensemble. We engage in an important discussion about calculating distances to and between galaxies. The detailed uncertainty considerations in distance calculations play an important part throughout the project. In *Chapter (3): Our Methods*, we address the challenge of locating of galaxies with positional uncertainties. We present important probabilistic tools like representing the position of galaxies as Gaussian functions and ensemble averages to determine the average number in different radial volume-shells.

In *Chapter (4): Data Analysis*, we delve into the data processing methods applied to the galaxy data from the Sloan Digital Sky Survey (SDSS). We address the important idea of selecting a host, completeness limits and potential systematic biases. In *Chapter (5): Results*, we put together all the developed ideas to study two important case studies: (i) the Gravitationally Non-Competitive (GNC) Environment and (ii) Gravitationally Competitive (GC) Environment. In each case study, we examine different host-partner configurations to investigate the spatial distribution of companions around their host galaxies and examine how core activity, partner mass, and the gravitational-competitive condition influences this spatial clustering. The possible interpretations and implications behind these results are explored in *Chapter (6): Discussion*. For instance, we discuss how the observation of an under-dense environment within the inner 0.5 Mpc of AGN host may be indicative of a past history of mergers. Finally, in *Chapter (7): Conclusion*, we summarize our main findings, interpretations and briefly discuss future works.



# Chapter 2

## Our Model:

### *Defining Three Levels of Structure*

#### 2.1 Structure of Our Model

The ultimate goal is to be able to compute the number density of companions around an ensemble of AGN and non-AGN host galaxies. Another way of thinking about the number density function is that it is statistical description of where we, on average, expect to find companions around a host. To form this description, a single host-partner system cannot give us a distribution; we need to consider an ensemble of equally “configured” host-partner systems and examine this ensemble’s statistics.

In this chapter, we discuss the schemes we use to organize raw galaxy data into a structured model. This is briefly illustrated in Figure (2.1). Here are the three levels of structure in increasing order of complexity: (1) Individual Galaxies, (2) Host-Partner System, and (3) Equivalent Ensemble. We discuss the important parameters associated with each level and how these levels are organized. It is important to note we assume a spherically symmetric distribution and only attempt to understand the radial clustering of companions around host.

#### 2.2 First Level: Individual Galaxies

Galaxies are the most basic units in this project. They are treated like point particles located in 3D space. To uniquely locate a galaxy, we need its angular position on the

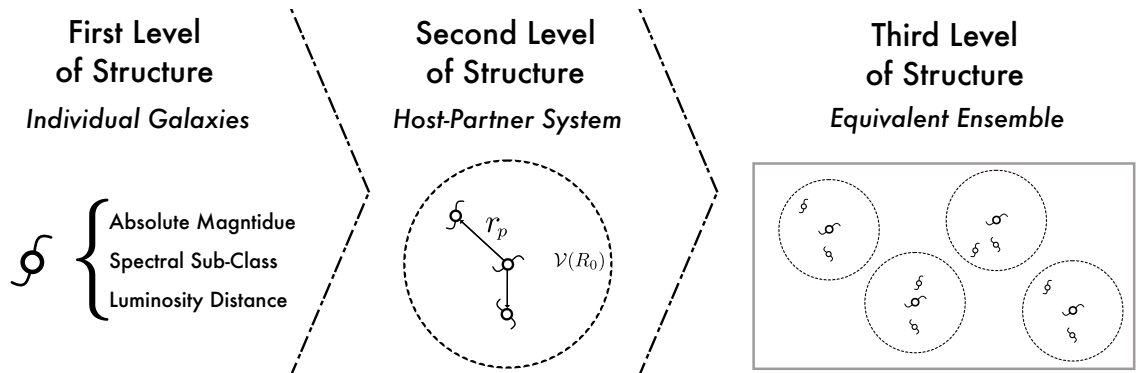


Figure 2.1: Three Levels of Structure in Our Model: (i) First level consist of individual point-like galaxies, characterized by different parameters; (ii) Second level is a single host galaxy at the center of a counting volume  $\mathcal{V}(R_0 = 3.0 \text{ Mpc})$  along with companion galaxies separated at  $r_p$ . A host and its companions are collectively referred to as a host-partner system; (iii) Third level consist of a collection of “similar” host-partner systems, referred to as an Equivalent Ensemble.

celestial sphere (specified by two coordinates, the declination  $\delta$  and the right ascension  $\alpha$ ) and a separation distance from Earth to the galaxy  $d$ .  $\delta$  and  $\alpha$  are raw parameters from SDSS but we cannot directly measure the separation distance to the galaxy  $d$  – it must be inferred from other measurements. In this section, we describe how we use raw positional parameters to compute the separation distance, its uncertainties, and how the intrinsic brightness of a galaxy is determined.

### 2.2.1 Calculating the Distance to Galaxies

For centuries, telescopes have provided stunning images of the cosmos with highly precise measurements of angular separations; however, these two-dimensional representations cannot immediately provide us with information on the depth of celestial objects. In fact, determining the distance to galaxies is one of the most challenging tasks in astrophysics. There are many different types of cosmic distance estimators, but Hubble’s law is often the most flexible and accurate estimation of distance, and it is how we estimate distances in this project.

In 1929, the astronomer, Edwin Hubble, noticed that the characteristic lines in the spectra of almost all galaxies outside our local environment seemed to be shifted in some regular manner to a longer wavelength than what was expected. This wavelength stretch is known as a redshift and it may be quantified by measuring the change in

the wavelength,

$$z = \frac{\Delta\lambda}{\lambda_0} = \frac{\lambda - \lambda_0}{\lambda_0}, \quad (2.1)$$

where  $\lambda$  is the observed wavelength and  $\lambda_0$  is (emitted) rest-length wavelength from the galaxy. Over the century, studies into relativity theory revealed that this redshift is analogous to a cosmological Doppler shift, but, rather than a result of a relative motion between Earth and the observed galaxies, the spacetime between us is expanding and, thus, the light waves are stretched in the process of reaching us. For simplicity, we avoid attributing spacetime with a speed and, rather, assign a recessional velocity  $v_{rec}$  to the observed galaxy and model the redshift as an analogous cosmological Doppler shift. It can be shown that, for  $z \ll 1$ , we may relate the redshift to the recessional velocity of a galaxy via the relationship

$$z = v_{rec}/c,$$

where  $c$  is the speed of light. Hubble (1929) was the first to propose a relationship between the distance to a galaxy  $D$  and its recessional velocity,

$$D = \frac{v_{rec}}{H_0} \quad \text{or, equivalently,} \quad D = \frac{c z_{rec}}{H_0}, \quad (2.2)$$

where  $z_{rec}$  is the redshift resulting from the recessional velocity and  $H_0 = 67.74 \pm 0.46$  km/s/Mpc (PLANCK, 2015) is a proportionality constant known as the Hubble constant, which relates the recessional rate of galaxies over separation distances.

The above description has an important assumption that requires careful consideration. We have assumed that, relative to some local rest frame, the galaxies have no motion; however, this is not true. Galaxies are three dimensional objects with three dimensional velocity components evolving in a gravitational potential. This intrinsic motion of the galaxy leads to deviations from the Hubble flow, and we must be careful and understand which particular component of a galaxy's motion is contributing to the redshift. A galaxy's three-dimensional velocity  $\mathbf{v}_{gal}$  may be decomposed into two components: a speed along the radial or line-of-sight from Earth  $v_r$  and a tangential speed along the plane-of-the-sky  $v_t$ , where the magnitude of  $\mathbf{v}_{gal}$  is

$$v_{gal}^2 = (v_r)^2 + (v_t)^2. \quad (2.3)$$

When it comes to distance estimations via spectroscopic redshifts, it is only the line-of-sight translation  $v_r$  that contributes to the redshift. However, there are two further components contributing to the line-of-sight velocity. This includes the recessional velocity arising from the expansion of the universe  $v_{rec}$  and the galaxy's intrinsic motion in its local environment, referred to as its peculiar motion  $v_{pec}$ . Therefore, we may further decompose the line-of-sight (radial)  $v_r$  component into,

$$v_r = v_{rec} + v_{pec}^{(r)}, \quad (2.4)$$

where  $v_{pec}^{(r)}$  is the peculiar velocity component along the radial or line-of-sight direction. It is here where we have to be careful. The redshifts measured from SDSS are a consequence from the full velocity component  $v_r$ , i.e.  $z_{SDSS} = v_r/c$ ; however, the redshift inputted into Hubble's law is the shift resulting from the recessional velocity:  $z_{rec} = v_{rec}/c$ .

We take care and combine the components in the following manner. We know that,

$$v_r = v_{rec} + v_{pec}^{(r)} \Rightarrow v_{pec}^{(r)} = v_r - v_{pec}^{(r)} \quad (2.5)$$

$$\Rightarrow z_{rec} = z_{SDSS} - v_{pec}^{(r)}/c. \quad (2.6)$$

The term  $v_{pec}^{(r)}/c$  is a correctional term that accounts for the shift resulting from the peculiar motion of a galaxy. With this information, we may update Hubble's law to be,

$$D = \frac{cz_{rec}}{H_0} \rightarrow \frac{c}{H_0} \left( z_{SDSS} - \frac{v_{pec}^{(r)}}{c} \right). \quad (2.7)$$

Based on typical values cited in the literature, we estimate  $v_{pec}^{(r)} = (150 \pm 100)$  km/s (Mo, Bosch & White, 2010). We may compute the uncertainty in the distance  $D$  from,

$$\Delta D^2 = \left( \frac{\partial D}{\partial z_{SDSS}} \Delta z_{SDSS} \right)^2 + \left( \frac{\partial D}{\partial v_{pec}^{(r)}} \Delta v_{pec}^{(r)} \right)^2 \quad (2.8)$$

$$\Delta D = \frac{c}{H_0} \sqrt{(\Delta z_{SDSS})^2 + (\Delta v_{pec}^{(r)}/c)^2}. \quad (2.9)$$

This error consideration plays an important role in the calculation of the separation distance in Section 2.3 and, ultimately, in how the number density is computed in Section 3.3.

Along with this information about distance measures and relationships to redshift  $z$ , we also mention one other important concept related to the project. The distance measure  $D$  is actually the distance to galaxies calibrated to our current time from the Big Bang. This calibrated distance is referred to as the co-moving distance  $D$ . If we were to consider the expansion of spacetime, this new distance, referred to as the proper distance  $d$ , must be multiplied by a factor of  $(1 + z)$ ,

$$d = (1 + z)D. \quad (2.10)$$

From now on, when we discuss the “distance to a galaxy”, we are actually referring to the proper distance  $d$  that is equal to the co-moving distance  $D$  multiplied by the factor of  $(1 + z)$ .

## 2.2.2 Absolute Magnitude

Another computed variable associated with a galaxy is its absolute magnitude  $M$ . The absolute magnitude of an object is defined to be the object’s apparent magnitude, or brightness in the sky, if it were located at distance of 10 pc. It may be computed by the relation,

$$M = m - 2.5 \log \left( \frac{F}{F_{10}} \right), \quad (2.11)$$

where  $m$  is the measured apparent magnitude,  $F$  is the measured flux from the galaxy and  $F_{10}$  would be the apparent flux if it were placed at 10 pc. It is important to note that we take into consideration cosmological effects, like the expansion of spacetime. The above flux is equivalent to

$$F = \frac{L_{\text{Host}}}{4\pi d_L^2}, \quad (2.12)$$

where  $L_{\text{Host}}$  is the intrinsic luminosity of the host galaxy and  $d_L$  is the *luminosity* distance to the host. The luminosity distance  $d_L$  is related to the distance  $d$  via the formula:  $d_L = (1 + z)D$ . Combining these results together, we get

$$M = m - 5 \log \left( \frac{1+z}{10 \text{ pc}} \times D \right), \quad (2.13)$$

where  $z$  is the measured redshift of the galaxy. It is important to note that, since the apparent magnitude itself is dependent on which particular wavelength, or passband, you observe the galaxy, the absolute magnitude is also dependent on the observed passband.

## 2.3 Second Level: Host-Partner Systems

We have established the idea of galaxies being fundamental point-like units spread out in space with associated parameters like distance  $d$  and absolute magnitude  $M$ . However, our project is not necessarily how these galaxies are situated relative to us on Earth, but rather we want to investigate their surrounding environment. In this section, we build the second level of our model: the *Host-Partner System*. As described in the introduction, this involves defining a galaxy as a host and searching for neighbouring galaxies, referred to as companions, within a certain volume. We now discuss the process of selecting host galaxies, defining the spatial volume around these host galaxies, and how we find associated partners.

### 2.3.1 Defining the Host

We define the parameters used to determine whether a galaxy is considered a host, and, in Chapter (4), we discuss the the full numerical details. From SDSS, any galaxy that satisfies the following three conditions is considered a host:

1. Redshift Limit:  $0.01 \leq z \leq z_{Upper}$ . Since galaxies become fainter with larger distance (or redshift) separations and SDSS has a minimum brightness cutoff, then there is a maximum distance (or redshift) we can observe a galaxy before it becomes too faint and is not registered in SDSS's spectroscopic catalog;
2. Absolute magnitude range:  $M \pm \sigma$ , where  $\sigma$  represents a bin size around the average value  $M$ . The luminosity of a galaxy is proportional to its mass and, since this project is centered around the idea of clustering in a host's gravitational field, we want to localize the mass or, equivalently, the absolute magnitude of our host;

3. Spiral Confidence Value:  $s > 0.6$ . Majority of active galaxies are Seyferts, whose dominant morphology is spiral. Therefore, we aim to select spiral host galaxies;
4. Core Identity:  $C = \text{AGN}$  or  $C = \text{non-AGN}$ . A host can either be a AGN or non-AGN according the spectral sub-classifications determined by SDSS.

### 2.3.2 Defining the Spatial Domain

Once we have a collection of host galaxies, we define a spherically symmetric volume around each galaxy. We refer to this volume as the *Counting Volume*  $\mathcal{V}(R_0)$ , where  $R_0$  is the radius of this domain. Throughout this project, we use the value  $R_0 = 3.0$  Mpc. To put 3.0 Mpc in perspective, the typical diameter of disk galaxies is around 0.02 to 0.04 Mpc and the distance between major galaxies is about  $\approx 1$  Mpc (for instance, the distance between our Milky-Way and our nearest major neighbour, Andromeda or M31, is about 0.8 Mpc). Our spatial distribution will be surveyed from this volume.

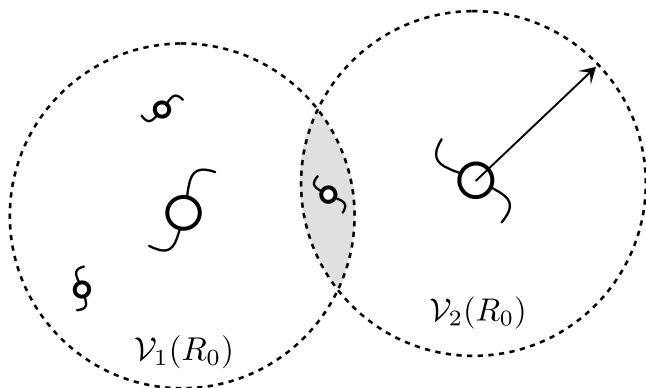


Figure 2.2: Cross-sectional diagram of two host within a counting volume  $\mathcal{V}_1$  (containing 3 associated partners) and  $\mathcal{V}_2$  (containing 1 associated partner). Non-Interacting condition is violated, as indicated by middle shaded region; therefore, only one of these host is allowed into the sample.

An important constraint associated with the counting volume is the *Non-Interacting Condition*. Even though a single host may be associated with one or more partners, we need, however, to ensure that a single partner is only associated with one unique host. In our search algorithm, this translates to the condition that the counting volumes associated with each individual host cannot overlap (See Figure (2.2)). Physically, this condition may be regarded as a constraint to control the tolerated extent of host-to-host gravitational interaction. Also, statistically, we may run into the problem of over-counting host-partner relationships and biasing our distribution if we do not implement this condition. If there were any overlapping pairs of host galaxies (which

was about fewer than 8% of our population), one of the host was arbitrarily chosen to be in the final host sample and the other one was disregarded. There was no particular prefer over one host.

### 2.3.3 Defining the Partner

Once we have a collection of host galaxies, any neighbour galaxies within a 3.0 Mpc volume is defined to be a companion (or partner) associated with the central host. We now discuss two important parameters associated with these companions.

#### Mass Ratio $\mu$ Between Host and Partner

Since the strength of a gravitational field is proportional to the mass of the interacting objects, the mass ratio between the host and partner plays an important role. However, we can not directly measure the mass of a galaxy  $S$  through the data provided by SDSS; we can only measure a galaxy’s brightness, or apparent magnitude  $m$ , in the sky. In this section, we derive a relationship between a galaxy’s apparent magnitude and its mass.

Suppose a host and partner galaxy have a mass of  $S_{host}$  and  $S_{Partner}$ , respectively, then the mass ratio  $\mu$  between these two objects may be defined as,

$$\mu \equiv \frac{S_{Partner}}{S_{Host}}. \quad (2.14)$$

This mass definition is not immediately useful because we can not directly “observe” the mass of a galaxy through SDSS; it must be inferred from the luminosity  $L$  of the object. If we assume that there exists a consistent mass-to-light ratio  $\gamma$  for both the partner and host such that  $S = \gamma L$ , then we can express the mass ratio between a partner and its host in terms of the luminosity:

$$\mu = \frac{S_{Partner}}{S_{Host}} = \frac{L_{Partner}}{L_{Host}}, \quad (2.15)$$

where it is important to note that we assume the mass-to-light ratio  $\gamma$  between the host and partner is the same. We may relate this expression to magnitudes by taking



the difference of the absolute magnitudes between the partner and the host,

$$M_{Partner} - M_{Host} = -2.5 \log \left( \frac{F_{Partner}}{F_{Host}} \right) \quad (2.16)$$

$$= -2.5 \log \left( \frac{L_{Partner}}{L_{Host}} \right) = -2.5 \log(\mu), \quad (2.17)$$

$$\Rightarrow \mu = 10^{-(M_{Partner} - M_{Host})/2.5} = 10^{-\Delta M/2.5}. \quad (2.18)$$

We have assumed the flux ratio to be equivalent to the luminosity ratio because the distance of separation between us and the galaxies are much larger than the individual separation between the host and partner.

This formula gives us a direct means to estimate how the mass ratio  $\mu$  between the partner and host is related to their absolute magnitude difference. For this project, we aim to confidently find partners with a mass ratio of  $\mu \geq 0.05$  or 5% the mass of the host. Here are some sample mass ratios:

$$\mu = \begin{cases} 1.0 & \text{if } \Delta M = 0 \\ 0.6 & \text{if } \Delta M = 0.555 \\ 0.3 & \text{if } \Delta M = 1.307 \\ 0.1 & \text{if } \Delta M = 2.500 \\ 0.01 & \text{if } \Delta M = 5.000 \end{cases}$$

One interesting idea worth mentioning is a possible systematic error that may arise from using a galaxy's luminosity as a proxy for mass, especially in the case of dealing with active galaxies. Since active galaxies have particularly bright galactic cores, if we are not careful, the inclusion of this luminous core in our total estimate of a galaxy's luminosity may misrepresent the galaxy's mass as higher than the actual value. In our particular project, our selection process of active galaxies has a preference for Seyferts. These active galaxies have much less luminous cores (on average, about 5% to 15% the total stellar light (Netzer, 2013)) compared to very luminous AGNs like Quasars; therefore, this effect is not expected to introduce a serious bias.

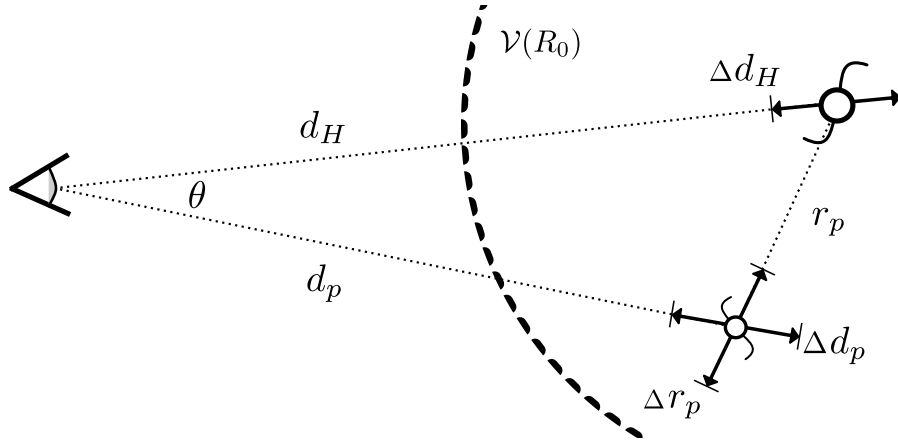


Figure 2.3: Schematic diagram illustrating the geometry associated with locating a host-partner system. The host and partner are recorded to be located at distance of  $d_H \pm \Delta d_H$  and  $d_p \pm \Delta d_p$ , respectively (See Section 2.2 for distance calculation from redshift). Once  $d_H$ ,  $d_p$ , and the subtended angle between the host and partner  $\theta$  are known, the separation distance  $r_p$  is computed from Equation (2.19). Its error relation  $\Delta r_p$  is given in Equation (2.23). If  $r_p$  is less than the Counting Volume  $\mathcal{V}$  radius of  $R_0 = 3.0$  Mpc, then galaxy is labeled a companion of the host.

### 2.3.4 Separation Distance Between Host and Partner

We have discussed a great deal about computing distance to galaxies; however, to understand the statistics of host-partner systems, we need to be able to determine the distance between a host and its partners. To determine the separation distance  $r_p$ , we can use the geometry depicted in Figure (2.3). Using the cosine law,  $r_p$  can be determined:

$$r_p = \sqrt{(d_H)^2 + (d_p)^2 - 2d_H d_p \cos(\theta)}, \quad (2.19)$$

where  $d_H$  and  $d_p$  are the distances computed via spectroscopic redshifts outlined in Section 2.2 and  $\theta$  (as shown in Figure (2.3)) is the subtended angle between the host and partner. In fact, the definition of a partner galaxy may be more precisely defined to be: if a neighbour galaxy has  $r_p \leq 3.0$  Mpc, then it is a companion of the central host.

### 2.3.5 Uncertainties in the Separation Distance

The uncertainty associated with  $r_p$  is a much more involved calculation that is dependent on the unique uncertainty associated with the distance to the host-partner system

and the subtended angle between them. To start, we begin with the general uncertainty relation for a function  $f(x_1, x_2, \dots, x_n)$  of  $n$ -variables each with independent random errors  $\Delta x_n$ :

$$(\Delta f)^2 = \left( \frac{\partial f}{\partial x_1} \Delta x_1 \right)^2 + \dots + \left( \frac{\partial f}{\partial x_n} \Delta x_n \right)^2. \quad (2.20)$$

As for our case, we are dealing with a function of three variables  $r_p(d_H, d_p, \theta)$ . However, the greatest uncertainty is found in  $d_H$  and  $d_p$ , and the error in  $\theta$  may be negligible. To explain, suppose we have a host located at distance 150 Mpc (a typical scale for our project) and a partner 0.5 Mpc from the host (for simplicity, assume along the plane of the sky). Rewritten in terms of our current variables, this would correspond to a separation distance of  $r_p = 0.5$  Mpc and a subtended angle of  $\theta = \arctan(0.5/150) \approx 0.0033$  radians. SDSS has an angular resolution with a typical uncertainty of  $\Delta\theta = 1$  arcsecond  $\approx 4.8 \times 10^{-6}$  radian, and the typical uncertainty in separation distance may be  $\Delta r_p = 0.05$  Mpc. From this, if we were to consider, as required above, the square of the fractional uncertainty,

$$\left( \frac{\Delta\theta}{\theta} \right)^2 = \left( \frac{4.8 \times 10^{-6}}{0.0033} \right)^2 \quad (2.21)$$

$$= 2.115 \times 10^{-6} \ll \left( \frac{\Delta r_p}{r_p} \right)^2 = \left( \frac{0.05}{0.5} \right)^2 = 0.01, \quad (2.22)$$

then we clearly see that uncertainty in the resolving the radial position of galaxies is much greater than the uncertainty in determining their angular separation. With this information, we may compute the specific form to be,

$$\begin{aligned} (\Delta r_p)^2 &= \left( \frac{\partial r_p}{\partial d_H} \Delta d_H \right)^2 + \left( \frac{\partial r_p}{\partial d_p} \Delta d_p \right)^2 \quad (2.23) \\ &= \frac{d_h^2 \Delta d_h^2 + \cos^2(\theta) (d_p^2 \Delta d_h^2 + d_h^2 \Delta d_p^2) - 2d_h d_p \cos(\theta) (\Delta d_h^2 + \Delta d_p^2) + d_p^2 \Delta d_p^2}{d_h^2 + d_p^2 - 2d_h d_p \cos(\theta)} \end{aligned}$$

The typical range of  $\Delta r_p$  can vary depending on a partner's relative positioning to the host.  $\Delta r_p$  plays an important role in the upcoming sections because we need to know confidence value when we are placing galaxies in numerical bins to calculate the number density.

## 2.4 Third Level: An Equivalent Ensemble

Our third and final level of structure involves collecting host-partner systems that are “similar” in configuration. This collection of equally-configured host-partners systems is referred to as an Equivalent Ensemble. In this work, we define two or more host-partner systems to be “similar” if the mass ratio  $\mu$  of all the partners are localized within a certain range. By restricting the values of  $\mu$ , this allows us to consider an important constraint for this project known as Gravitational Competitiveness (GC). By our definition, if the environment is Gravitationally *Non-Competitive*, then all partners in the counting volume have  $\mu \leq 0.6$ .

## *Summary of Chapter (2)*

In this chapter,

- We outlined three levels of structure to our model: (1) Individual Galaxies; (2) Host-Partner Systems; (3) Equivalent Ensemble;
- Individual galaxies are the most fundamental level of structure, and are treated as point-like units. They are characterized by various parameters like their morphology, their separation distance  $d$  (computed from the spectroscopic redshift  $z$  and Hubble's law), and absolute magnitude  $M$ . A certain subset of these galaxies were considered as host galaxies;
- Once we have a sample of host galaxies, we consider a spherical volume of radius 3.0 Mpc centred around each host and search for neighbouring galaxies within this volume, referred to as companion (or partner) galaxies. A host and its companions form a single unit: the host-partner system;
- Our final level of structure is a collection of “similar” host-partner systems, referred to as an Equivalent Ensemble. Two host-partner systems are considered similar if each system's companions are localized within a certain host-partner mass ratio  $\mu$  range;
- We have now established a model. In the next chapter, we discuss how we may use this model to examine the distribution of companions around active and non-active host galaxies, i.e. compute the number density of companions.

# Chapter 3

## Our Methods:

### *Computing the Number Density Function*

#### 3.1 Two Challenges with Galaxy Data

One of the core questions in this research is: *How does the surrounding environment of neighbouring galaxies compare around AGN and non-AGN hosts?* The number density function  $n$  is the important measure that gives a quantitative description of host's environment and the extent of companion clustering. This distribution determines the number of companion galaxies per volume around a central host and, since we have assumed a spherical symmetry, this number density is a function of the separation distance  $r$  from the host:  $n = n(r)$ . To mathematically describe this idea, we may define the number density function  $n(r)$  to be,

$$n(r) = \frac{dN(r)}{dV}, \quad (3.1)$$

where  $N(r)$  is the number of galaxies contained within a differential volume  $dV$ . This may be a good starting point and a mathematically elegant definition, but it is not immediately useful to us when dealing with galaxies.

Let's consider an example. Suppose we have a host-partner system with five companions within the 3.0 Mpc volume around the central host. Even though these five companions may have different polar  $\theta$  and azimuthal  $\phi$  angles relative to each

other, in our spherically symmetric model, we are only concerned with their radial separation  $r$  from the central host located at  $r = 0$ . Therefore, this 3D problem of understanding companion positions is reduced to a 1D radial scale. The idea is illustrated in the top of Figure (3.1). From this Figure, we also begin to see two distinct features of galaxy data that pose a challenge and must be carefully dealt with: (i) they are discrete and (ii) contain positional uncertainties.

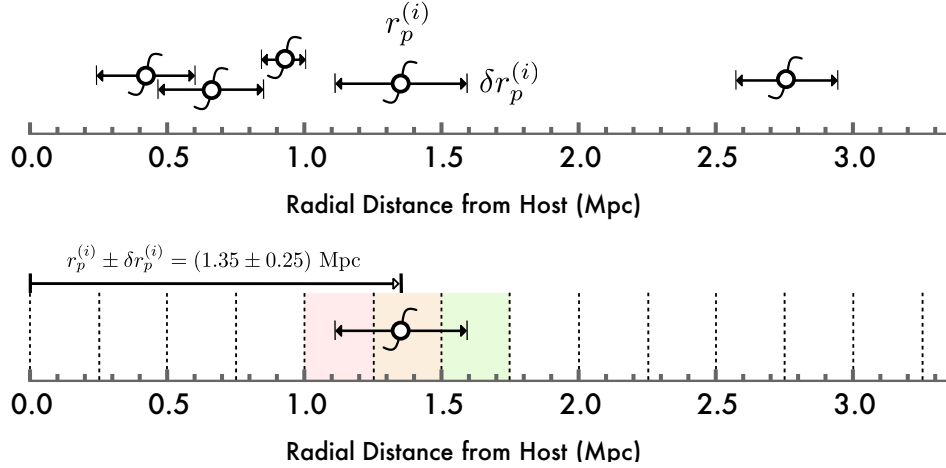


Figure 3.1: (*Top*) Illustration of how a 3D host-partner system with five partners is projected onto 1D radial scale by assuming a spherically symmetric system. Not only are the galaxy data discrete, but they have positional uncertainties associated with them. (*Bottom*) Figure shows how the positional uncertainties associated with a partner can spread across different bin separators (the dotted lines). Rather than assigning partners in a yes-or-no manner to one bin, we represent these partners as Gaussian probabilities and ask what is the probability of finding a partner in a particular bin.

To deal with discreteness, we introduce the idea of binning into Volume-Shells. That is, the total 3.0 Mpc volume around a host is partitioned into spherically symmetric volume-shells. If  $n = dN/dV$  represents how many galaxies are contained in an “infinitesimal volume”  $dV$ , this question has now been re-framed to be: how many galaxies are contained in a volume-shell bin?

The more subtle challenge is the second one: how do you “count” the number of galaxies contained in a volume-shell bin? If galaxies were just truly point-like entities in space with perfectly resolved positions, then the answer to the above question would be trivial – this is not the case. Galaxies have positional uncertainties and, therefore, they do not have unique positions. This is illustrated at the bottom of

Figure (3.1). In this Figure, we see a partner located at a distance of 1.35 Mpc but, because of its positional uncertainty of  $\pm 0.25$  Mpc, the companion's separation from the host is smeared in-between  $(1.35 - 0.25 =)$  1.15 Mpc and 1.60 Mpc. The dotted lines occurring every 0.25 Mpc mark the boundary of numerical volume-shell bins. The problem begins when we ask: What bin does the companion, whose average separation is 1.35 Mpc, belong in? Do we count the partner to belong in the red, orange, or green bin? This is the challenge of counting data with positional uncertainties.

In this chapter, we address how we go about dealing with these two challenges. Section 3.2 deals with the binning scheme associated with volume-shells. Section 3.3 discusses how we overcome the positional uncertainty challenge by representing a partner's position as a Gaussian probability function and considering the probability of finding companions in a bin. Lastly, we put all this information together in Section 3.4 and reveal how we transform the above differential expression into a discrete expression to compute the number density for a single host-partner system and, ultimately, an ensemble of many host-partner systems.

## 3.2 Binning into Volume-Shells

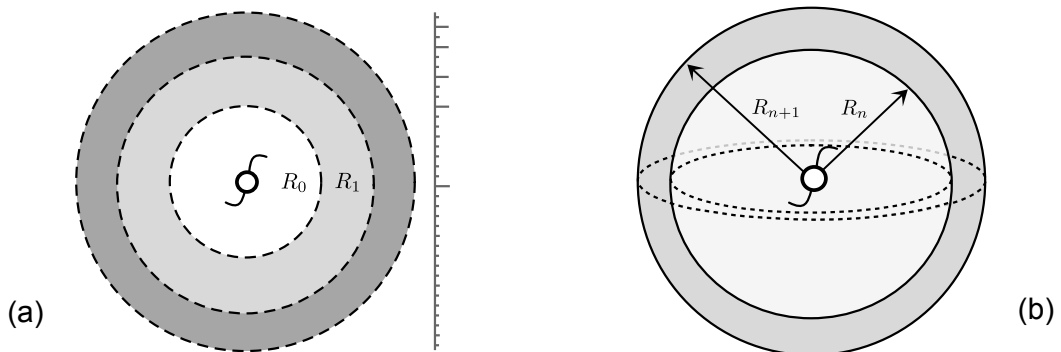


Figure 3.2: (a) Cross-sectional view of spherically symmetric volume-shells around a host. Each of these shells have a radius  $R_i$  from the host and are separated by the same distance of  $\Delta R = 0.25$  Mpc; (b) Spherical shell is a three dimensional volume around a host.

As illustrated in Figure (3.2), we take the total  $R_0 = 3.0$  Mpc volume around the host and partition this volume into equal-width segments of  $\Delta R = 0.25$  Mpc, which corresponds to 12 total volume-shell bins in this particular 3.0 Mpc volume. The



different radii are,

$$R_m = \{0.00, 0.25, 0.50, 0.75, \dots, 2.75, 3.00\} \text{ Mpc.} \quad (3.2)$$

It is important to note that we try to keep the width of shells above 0.1 Mpc.

### 3.3 Quantifying Positional Uncertainty of Partners

#### 3.3.1 The Gaussian Representation of a Companion Galaxy

When it comes to dealing with galaxy data, we began this chapter by bringing our attention to two important challenges: their discrete nature and positional uncertainties. The previous section addressed the challenge of discreteness by partitioning the counting volume of 3.0 Mpc into volume-shells and counting in these shells, as opposed the abstract idea of infinitesimal volumes  $dV$ . Now, in this section, we directly address the issue of dealing with galaxy data that have positional uncertainties. The bottom of Figure (3.1) demonstrated that if a spread in a companion's position stretched across more than one bin then it was ambiguous as to which bin the galaxy belongs in. As opposed to considering the companions as point-like entities, we resolve this issue by representing partners' positions as Gaussian probabilities and, rather than asking in a black-and-white fashion which bin the partner belongs to, we re-frame the question to be: what is the probability of finding a companion in a certain bin?

In general, the Gaussian probability density can be stated as,

$$p(x) = \frac{1}{\sqrt{2\pi(\sigma)^2}} \exp \left[ - \left( \frac{x - \langle x \rangle}{\sqrt{2}\sigma} \right)^2 \right], \quad (3.3)$$

where  $\langle x \rangle$  is the mean value of some random variable  $x$ ,  $\sigma$  is the standard deviation, and  $\int_a^b p(x)dx$  represents the probability of finding  $x$  in the interval  $[a, b]$ . Now, in terms of galaxies, if we were to measure a separation distance between a host and its partner to be  $r_p \pm \delta r_p$ , then, from this statistical perspective, this is equivalent to saying that the *mean* separation of the partner is  $\langle r \rangle \equiv r_p$  and the range in which we believe the position to lie, or its *standard deviation*, is  $\sigma_r \equiv \pm \delta r$ . This allows us to say that the probability density associated with a partner is

$$p(r) = \frac{1}{\sqrt{2\pi}(\delta r_p)^2} \exp \left[ - \left( \frac{r - r_p}{\sqrt{2}\delta r_p} \right)^2 \right], \quad (3.4)$$

where  $r_p$  is a companion's mean separation distance from the host and a standard deviation of  $\delta r$ . It is important to note that the Gaussian is technically normalized along an infinite domain but, our spatial distributions are surveyed in a 3.0 Mpc domain. Since  $\delta r \ll 3.0$  Mpc, we simply assume a sufficient normalization occurs after  $3\delta r$  and any remaining probability contribution is rounded off as numerical/counting errors. Also, if there are any Gaussians at the edge of the counting volume, we integrate beyond the limit of 3.0 Mpc to ensure we include their number density in the final bin.

To model multiple companions, we may consider the superposition of these functions. Suppose we measure a host to have  $N_p$  partners, then the probability of finding a galaxy in the range  $[R_n, R_{n+1}]$  is

$$\begin{aligned} P(R_n \leq r \leq R_{n+1}) &= \int_{R_n}^{R_{n+1}} p(r) dr & (3.5) \\ &= \frac{1}{\sqrt{2\pi}N_p} \int_{R_n}^{R_{n+1}} \sum_i \frac{1}{\delta r_i} \exp \left[ - \left( \frac{r - r_p^i}{\sqrt{2}\delta r_i} \right)^2 \right] dr, & (3.6) \end{aligned}$$

where now  $r_p^i$  and  $\delta r_p^i$  represents the separation and uncertainty of the  $i^{th}$  partner. If we want to evaluate the typical number of partners  $N(r)$  in this range, then we simply multiply by the total number of partners  $N_p$ ,

$$N(R_n \leq r \leq R_{n+1}) = \int_{R_n}^{R_{n+1}} N_p p(r) dr. \quad (3.7)$$

After presenting this continuous probability model of locating partners around a host, it is important to mention that we have assumed a spherical symmetric probability distribution. The full separation distance vector is not only characterized by its magnitude  $r_p$ ; to uniquely locate a galaxy, we need to specify a polar angle  $\theta$  and azimuth angle  $\phi$ . However, since this project is aimed at investigating the influence of gravitational interactions between host and partners, we assume that the probability of finding a galaxy at a  $r$  radius is independent of  $\theta$  and  $\phi$ .

### 3.3.2 Sample Calculation

We now consider a quick example with an actual host galaxy from SDSS to show numerical calculations using the developed tools. Our sample host is a galaxy with the following properties:

- Non-AGN Spiral galaxy;
- Redshift of  $z \pm \delta z = (0.04425 \pm 0.00001)$
- $d_H \pm \delta d_H = (193.81 \pm 0.05)$  Mpc
- Within a 3.0 Mpc volume around this host, there are  $N_p = 6$  galactic partners.

Furthermore, the distance to each partner  $d_p \pm \delta d_p$ , their separation distances  $r_p \pm \delta r_p$  and their subtended angles  $\theta$  (See Figure (2.3) for parameters) are provided in the below table. Now, each  $r_p^{(i)}$  and  $\theta_i$  can be associated with a Gaussian function and their superposition represents the total probability distribution.

	<b>Partner 1</b>	<b>Partner 2</b>	<b>Partner 3</b>	<b>Partner 4</b>	<b>Partner 5</b>	<b>Partner 6</b>
$d_p \pm \delta d_p$	193.04±0.03	194.39±0.03	194.71±0.04	192.24±0.04	195.40±0.06	193.02±0.03
$r_p \pm \delta r_p$	2.00 ± 0.02	0.86 ± 0.04	0.91 ± 0.06	1.58 ± 0.06	1.66 ± 0.07	1.44± 0.03
$\theta$	0.00952	0.00330	0.000559	0.000906	0.00250	0.00622

Table 3.1: Parameters associated with  $N_p = 6$  partners near the non-AGN host listed above. The distance to the partner is  $d_p$  (Mpc), the separation distance between the host and partner is  $r_p$  (Mpc), and the subtended angle between the host and partner is  $\theta$  (radian). See Figure (2.3) for the setup's geometry.

As an example, we ask the question: what is the probability of finding a partner within the interval 0.5 Mpc to 1.5 Mpc? We simply integrate by substituting the parameters from Table (3.3.2),

$$P(0.5 \leq r \leq 1.5) = \int_{0.5}^{1.5} p(r) dr \quad (3.8)$$

$$= \frac{1}{\sqrt{2\pi}(6)} \int_{0.5}^{1.5} \sum_{i=1}^6 \frac{1}{\delta r_i} \exp \left[ - \left( \frac{r - \langle r_i \rangle}{\sqrt{2}\delta r_i} \right)^2 \right] dr \quad (3.9)$$

$$= 0.513739. \quad (3.10)$$

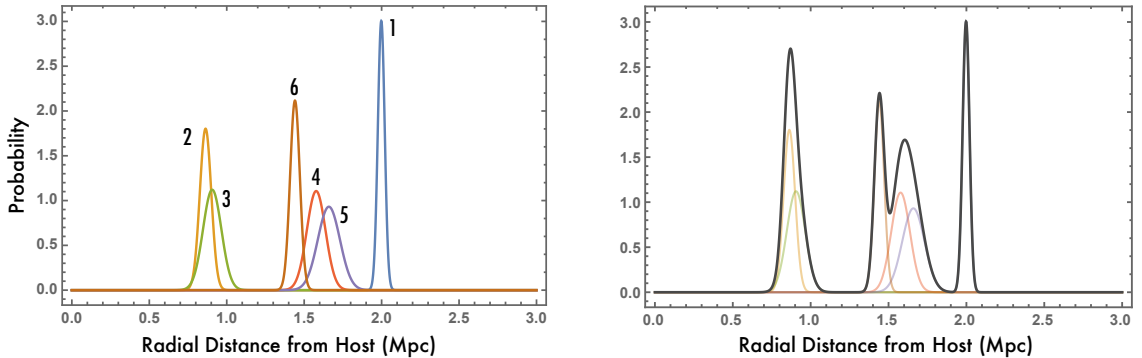


Figure 3.3: A single host-partner system with six partners. The host is a non-AGN spiral galaxy and located at a distance of  $d_H \pm \delta d_H = (193.81 \pm 0.05)$  Mpc. The six companions have been represented as six Gaussian functions (left) and their superposition represents the entire host-partner system (right). The width of the Gaussians vary because the separation uncertainties depend on different variables, as calculated in Section 2.3.

Therefore, there is  $\approx 51.3\%$  chance you will find a partner within 0.5 Mpc to 1.5 Mpc for this system. To determine, the typical number of partners within this range, we evaluate,

$$N(0.5 \leq r \leq 1.5) = \int_{0.5}^{1.5} N_p p(r) dr \quad (3.11)$$

$$= 6 \int_{0.5}^{1.5} p(r) dr \quad (3.12)$$

$$= 6 \times 0.513739 = 3.08 \text{ partners.} \quad (3.13)$$

### 3.4 Computing the Number Density Function

We began with a number density function that was continuous:

$$n(r) = \frac{dN(r)}{dV}. \quad (3.14)$$

This formula tells us that the number density of companions is the number of companion galaxies contained in an infinitesimal volume  $dV$  at a separation distance  $r$  from the host.

However, as we discussed in the previous two sections, galaxy data are discrete and contain positional uncertainties. The above definition may capture the interpretation of the number density, but it is not computationally useful to us. We resolved this

issue by introducing two ideas: (i) binning the discrete data into volume-shells; (ii) counting companions with positional uncertainties by representing them as a Gaussian probability. Now, the above definition of number density becomes,

$$n(r) = \frac{dN(r)}{dV} \rightarrow n(R_n, R_{n+1}) = \frac{N(R_n \leq R \leq R_{n+1})}{V_{shell}}, \quad (3.15)$$

where  $N(R_n \leq R \leq R_{n+1})$  is the integral expression developed in Equation (3.7) and  $V_{shell} = (4\pi/3)(R_{n+1}^3 - R_n^3)$  is the volume of a shell between the range  $[R_n, R_{n+1}]$ .

For thoroughness, we can calculate the number density for the sample system illustrated in the previous section. We asked the question how many partners were expected in-between the range of 0.5 Mpc to 1.5 Mpc. The answer was  $N(R_n, R_{n+1}) = N(0.5, 1.5) = 3.08$ . This would correspond the following number density,

$$n(0.5, 1.5) = \frac{N(0.5, 1.5)}{V_{shell}} = \frac{3.08}{\frac{4}{3}\pi(1.5^3 - 0.5^3)} = 0.226 \text{ Mpc}^{-3}. \quad (3.16)$$

It is important to note that all the calculation up to this point have been for *one* host-partner system. This is just the second-level of our model. The values of  $n(R_n, R_{n+1})$  given above do not represent a distribution. To form a proper statistically distribution, we need to find “identical” copies of similar host-partner systems, or an equivalent ensemble, and compute the  $n(R_n, R_{n+1})$  for each host-partner system. The average in each bin would represent the number density in that range.

## *Summary of Chapter (3)*

In this chapter,

- Once we established a model, we characterize and measure the distribution of companion galaxies around active and non-active host by studying the number density function;
- The number density  $n$  is a measure of the number of galaxies contained in a unit volume around a host. Since we assumed our system to be spherically symmetric, we are only concerned with variation along the radial direction  $n = n(r)$ ;
- If the galaxy data from SDSS were representative of perfectly resolved point-like entities, then it would be straightforward to compute the number density function – however, this is not the case. Galaxies have positional uncertainties that must be taken into account when counting companions around a host;
- To manage these positional uncertainties, we represented partners as Gaussian probabilities and, instead of asking how many galaxies were in different numerical bins, we re-framed the binning scheme to compute the probability of finding companions in a particular bin;
- In the next chapter, we discuss how initial data from SDSS was collected and calibrated before computing the number density function.

# Chapter 4

## Data Analysis

We have discussed a great deal about developing a methodology to study the environment of companions around host galaxies. However, before we can work out any kind of statistical conclusions, we must build a complete set of galaxies that meet our scientific objectives. We must take careful steps to ensure our selection criteria correctly isolate the intended objects and do not contain any contamination that may bias the data and, ultimately, compromise the resulting conclusions. In this chapter, we directly discuss the task of establishing a well-calibrated galaxy sample from the Sloan Digital Sky Survey (SDSS) database.

### 4.1 Data Processing: Correcting for Systematic Errors

Galaxy data from SDSS has inherent systematic errors that need to be corrected for. Here are three important calibrations and systematic corrections that need to be considered:

1. CMB Rest-Frame Correction
2. *K*-Corrections to Redshifts
3. Extinction from Interstellar Medium
  - (i) Internal extinction from the Milky Way
  - (ii) External extinction from observed galaxy's interstellar medium

In this work, the calibrated data were taken from catalogs personally developed by G. J. Conidis. A full description of the methods can be found in the works: Conidis, G. J., (2013). Analogues of the Local Sheet. *Master of Science Thesis in Physics and Astronomy*. York University, Toronto Canada. Nevertheless, for thoroughness, we briefly discuss the physical significance of these corrections in the next sections.

#### 4.1.1 CMB Rest-Frame Correction

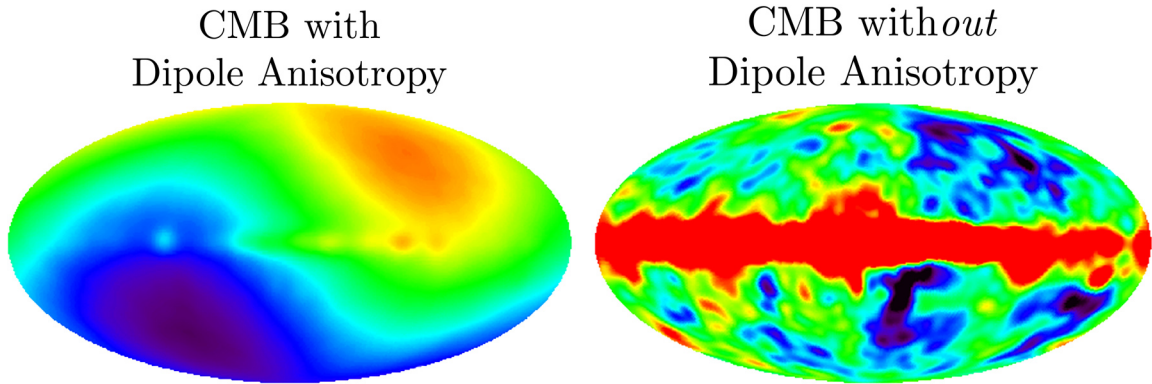


Figure 4.1: Map of the CMB captured by the Planck Telescope. Figure includes (*left*) image of the CMB with the dipole anisotropy and (*right*) without the dipole anisotropy. Figure adopted from Liguori, Matarrese & Moscardini (2003).

Initial measurements on the Cosmic Microwave Background (CMB) revealed the existence of a dipole anisotropy on the CMB’s temperature map (See Figure (4.1)). This provided compelling evidence that our solar system has a peculiar motion. If we were to consider all the contributions to this peculiar motion, like our Sun’s motion in the Milky Way, our attraction to M31, etc., we find that our Local Group has a peculiar speed of about  $600 \text{ km s}^{-1}$  moving away from the Local Void. These ideas are relevant to understanding galaxy data because any large-scale redshifts taken from Earth will inherently be affected by this peculiar motion. Tully et al. (2008) discuss the corrections for three types of motion: (i) the orbital velocity of the Sun in the Milky Way; (ii) the Milky Way’s motion about the Local Group’s centre of mass; (iii) the Local Group’s motion about the Virgo Cluster. All of these motions are characterized by a single rest-frame, referred to as the CMB rest-frame.



### 4.1.2 $K$ -Corrections

When we want to characterize the light emitted from astrophysical objects, the spectral energy distribution (SED) is an important measure that plots the emission energy over frequency (or wavelength) of light emitted. Some sample SEDs are depicted in Figure (4.2). With this said, there is an important idea to keep in mind when computing SEDs. Because of the expansion of the Universe, the observed SED is redshifted with respect to the rest-frame SED. This creates a potential problem when observing galaxies. Since we image galaxies only through a particular passband, we are actually looking at these objects in different rest-frame wavebands. Therefore, if there are two identical galaxies but at different redshifts, various observational properties like absolute magnitude and colours may appear to be different compared to their respective rest-frames values. The transformation aimed at correcting for this potential systematic error is referred to as the  $K$ -correction. The methods used to apply the  $K$ -corrections were developed by Blanton et al. (2005).

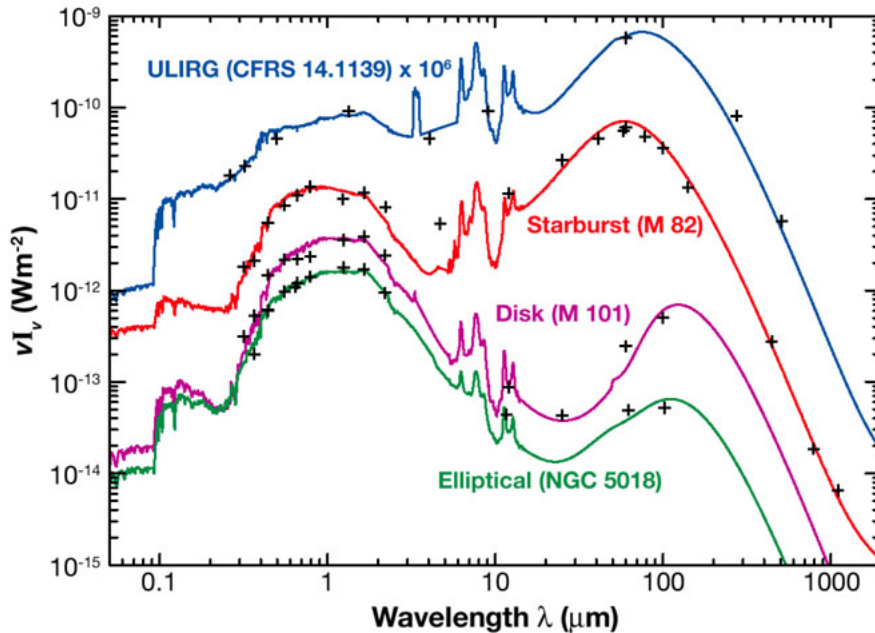


Figure 4.2: Sample spectral energy distributions (SED) of four different galaxies with different morphologies and features. The SED is a unique profile associated with an astrophysical object that portrays the energy emission from the object. Figure adopted from Galliano (2004).

### 4.1.3 Extinction through Interstellar Medium

When light passes through the interstellar medium, the incident light can be absorbed or scattered. Therefore, the light emitted from an astrophysical source after interacting with the interstellar medium (ISM) can be attenuated, confusing the actual physical processes occurring. The corrections performed to photometric measurements to account for this effect are referred to as extinction corrections. There are two type of corrections: (a) internal extinction correction, referring to the light passing through the Milky Way’s ISM, and (b) extragalactic extinction correction, light passing through an observed galaxy’s own ISM. Due to various scattering and absorption processes, observed astrophysical objects behind columns of dust often appear redder than the source. If we do not correct for these systematic errors, then we may end up misrepresenting the apparent magnitudes of galaxies. The York Extinction Solver (YES) (developed and published by McCall (2004)) was used to estimate the internal extinction in each passband by specifying the spectral energy distribution (SED) of the galaxy.

## 4.2 Building a Sample of Host Galaxies

In Section 2.3, we discussed four parameters that determined the identity of a host galaxy:

1. Absolute magnitude range:  $M \pm \sigma$
2. Redshift Limit:  $0.01 \leq z \leq z_{upper}$
3. Core Identity:  $C = \text{AGN}$  or  $C = \text{non-AGN}$
4. Spiral Confidence Value:  $s > 0.6$

We now justify these constraints and discuss their specific numerical values.

### 4.2.1 Absolute Magnitude: Constraining the Host Mass

The host galaxy sample selection is an optimization problem aimed at maximizing the number of host galaxies and localizing their mass. If this were the goal, by examining the luminosity function depicted in Figure (4.3), it would be best to place a broad absolute magnitude bin centered around the maximum of the luminosity function.

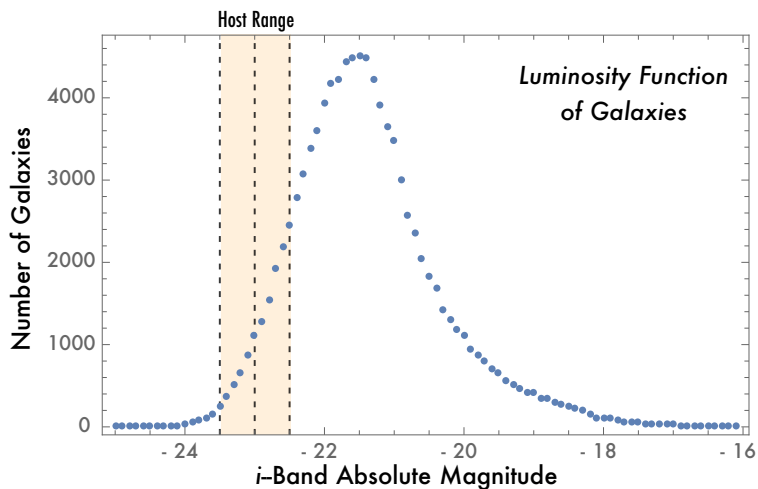


Figure 4.3:  $i$ -band luminosity function for 100,000 galaxies within  $z \leq 0.1$  of SDSS. Plot has a bin size of 0.1 and shows the greatest abundance of galaxies centered around -21.5. The shade orange region shows the absolute magnitude range of the host galaxies used in this research.

However, we need to be careful and consider other factors. If we make the width of the absolute magnitude bin too wide, then the mass of the host will not be constrained within a limit. Since this project aims at understanding how partners gravitationally cluster around a host, we need to be able to localize the mass of the host within a certain range. At the same time, another important effect takes place; it is the spectroscopic completeness limit. If a galaxy is fainter than a certain threshold ( $m_r \geq 17.77$ ) then SDSS will not provide spectroscopic information of that particular object, which is needed for the redshift and distance estimates. Therefore, the faintest partner of the faintest host is placed at the completeness limit and ultimately determines the redshift limit. A deeper redshift increases the volume of selection and allows for a larger selection of host galaxies.

All of these ideas indicate that selecting the absolute magnitude range of the host is an optimization problem that aims at maximizing the number of host galaxies and constraining their mass. After considering these details, we were able to determine that the  $i$ -band absolute magnitude range that generally best fit this description would be  $M_{host} = -23 \pm 0.5$  or  $-23.5 \leq M_{host} \leq -22.5$ . This range is indicated by the orange shaded region in Figure (4.3). We particularly chose the  $i$ -band because it is not expected to be as sensitive to star formation and interstellar extinction that would lead us to overestimate the luminosity of a galaxy's stellar component and, thus, the

luminous mass.

### 4.2.2 Redshift Limit: Spectroscopic Completeness of SDSS

The redshift limit plays an important role in constraining the selection of host galaxies. The upper bound on  $z \leq z_{upper}$  is a consequence of the spectroscopic completeness cutoff. To explain, all of our distance estimates in this project stem from the spectroscopic redshift and its relation to distance given by Hubble's law. However, SDSS does not provide spectroscopic information for all galactic objects. If a galaxy is fainter than 17.77 magnitudes in the  $r$ -band (or 17.51 in the  $i$ -band), then SDSS does not provide spectroscopic redshifts on the object. This condition limits the completeness of partner galaxies and, thus, the sample of host galaxies as well.

We want to now compute the upper bound on the redshift  $z_{upper}$  that results from the spectroscopic cutoff. To make this calculation, we place the faintest companion of the faintest host at the spectroscopic cutoff and compute the redshift this minimum condition would correspond to. The faintest companion of this faintest host is a free parameter and we, as researchers, must decide to determine what extent of completeness are we aiming for. To start, we saw that the absolute magnitude of a galaxy may be expressed in terms of this co-moving distance  $d$  and redshift  $z$  from Equation (2.13),

$$M = m - 5 \log \left( \frac{d_L}{10 \text{ pc}} \right) = m - 5 \log \left( \frac{1+z}{10 \text{ pc}} \times d \right), \quad (4.1)$$

where  $d_L (= (1+z)d)$  is the luminosity distance and  $m$  is the apparent magnitude (all magnitudes are measured in the  $i$ -band). We make a further substitution of  $d = cz/H_0$  and convert 10 pc to  $10^{-5}$  Mpc,

$$M = m - 5 \log \left( \frac{1+z}{10^{-5} \text{ Mpc}} \times \frac{cz}{H_0} \right), \quad (4.2)$$

$$\log \left( \frac{1+z}{10 \text{ pc}} \times \frac{cz}{H_0} \right) = \frac{m-M}{5} \quad (4.3)$$

$$z(1+z) = \frac{10^{-5} H_0}{c} 10^{m-M/5}. \quad (4.4)$$

The above formula is a quadratic relation that can be solved for the redshift  $z$  given an apparent  $m$  and absolute  $M$  magnitude value. We place our the faintest

companions of the faintest host at the spectroscopic cutoff of  $m_{sc} = 17.51$ . Suppose our faintest companions were 5% mass-of-host partners, then by the mass-to-light ratios developed in Equation (2.21), this 5% companion would corresponds the magnitude difference of,

$$\Delta M = -2.5 \log(\mu) = -2.5 \log(0.05) \approx 3.25 \quad (4.5)$$

Therefore, if the faintest 5% companion has an apparent magnitude of 17.51 then its associated host must have ( $m_H = 17.51 - 3.25 =$ ) 14.26 in apparent magnitude. If our sample of host varies between  $-23 \pm 0.5$ , then our faintest host is ( $M_H = -23 + 0.5 =$ )  $-22.5$ . From this information, we may determine the redshift of such a host to be,

$$z(1+z) = \frac{10^{-5} H_0}{c} 10^{m-M/5} \quad (4.6)$$

$$= \frac{10^{-5} H_0}{c} 10^{14.26 - (-22.5)/5} \quad (4.7)$$

$$\Rightarrow z(1+z) = 0.05071 \quad (4.8)$$

$$\Rightarrow z_{upper} = 0.048, \quad (4.9)$$

where the quadratic solution has provided two redshifts but the negative one is ignored because it has no physical value. We may also consider another cutoff for the 10% mass-of-host companions or  $\mu \geq 0.1$ :

$$z(1+z) = \frac{10^{-5} H_0}{c} 10^{15.01 - (-22.5)/5} = 0.07173 \quad (4.10)$$

$$\Rightarrow z_{upper} = 0.067. \quad (4.11)$$

### 4.2.3 Core Identity: Assigning Spectral Sub-Classifications

Spectroscopic information plays an important role not only in determining redshifts and distances, but it also took part in determining object classifications as non-AGNs and AGNs. We obtained the spectroscopic information from the `SpecObjA11` catalog, and capitalized on the availability of a wide range of Value-Added catalogs. Particularly, to identify core activity of galaxies, we used the *MPA-JHU* spectroscopic re-analysis catalog called `GalSpec`. The data were originally established and provide by the Max Planck Institute for Astrophysics and Johns Hopkins University, where the methods were developed and examined by the groups of Brinchmann et al. 2004, Kauffmann et al. 2003 and Tremonti et al. 2004.

Classifications in SDSS are stored under two parameters: (i) `class` and (ii) `subclass`. For this project, we require classification beyond the precision of `class = 'galaxy'`; that is, we need to consider the various subclassifications. Here are the six main sub-classifications given by SDSS:

1. **STARFORMING**: Galaxy has detectable emission lines that adhere to the following starforming criteria:

$$\log_{10} \left( \frac{[O \text{ III}]}{H\beta} \right) < 0.7 - 1.2 (\log_{10} ([N \text{ II}]/H\alpha) + 0.4). \quad (4.12)$$

2. **STARBURST**: If a galaxy has a positive **STARFORMING** match *and* an equivalent width of  $H\alpha$  greater than 50 Angstroms, then the object is recognized as a **STARBURST**.

3. **QSO**: Galaxy adheres to a pre-defined Quasar template.

4. **AGN**: Galaxy has detectable emission lines that adhere to the Seyfert and LINER criteria:

$$\log_{10} \left( \frac{[O \text{ III}]}{H\beta} \right) > 0.7 - 1.2 (\log_{10} ([N \text{ II}]/H\alpha) + 0.4). \quad (4.13)$$

5. **BROADLINE**: Any object with detected lines at the  $10\text{-}\sigma$  level with  $\sigma > 200$  km/s receives a **BROADLINE** classification.

6. **GALAXY**: General objects in the galaxy catalog that do not satisfy any of above conditions.

For this project, we particularly divided galaxy sub-classifications into two categories for simplicity:

$$C = \begin{cases} \mathbf{AGN} & \text{if subclass} = \{\mathbf{AGN}, \mathbf{AGN BROADLINE}\} \\ \mathbf{non-AGN} & \text{if subclass} = \{\mathbf{GALAXY}\} \end{cases}$$

We did not consider QSO objects in our study for AGNs. The majority of our identified active galaxies were Seyferts and LINERs based on the pre-defined emission criteria outlined above. The dominant morphology of Seyferts and LINERs are spiral galaxies. This is why we implemented a spiral confidence value of  $s > 0.6$ . This parameter was, to a degree, a free parameter that we could vary.

## *Summary of Chapter (4)*

- Chapter (2) and (3) focused a great deal on understanding the setup and goals of our model. In this chapter, we directly addressed the specifications of galaxy data and discussed specific numerical values used in the project;
- The data taken from SDSS needed to be calibrated and corrected for potential systematic errors. We identified three possibilities: (i) CMB rest-frame correction to the redshift, (ii)  $K$ -corrections to the redshift, and (iii) Extinction corrections to the magnitudes;
- We discussed the procedure taken to build a sample of host galaxies, which included localizing the absolute magnitude range, imposing a spectroscopic redshift limit to ensure completeness, and determining core identity from the `GalSpec` catalog;
- We are now ready to put the development from Chapters (2), (3), and (4) together to compute results.



# Chapter 5

## Results

Over the previous three chapters, we have set the foundation for the project. Chapter (2) involved defining our three-level model and the specific parameters used to control and calibrate the set-up. We delivered the idea that, to understand the spatial distribution of partners, we need to first build an ensemble of similarly configured host-partner systems constrained by the partners' mass ratios  $\mu$ . Chapter (3) involved defining the number density function  $n(r)$  and how we may go about computing this function in practice. In Chapter (4), we tackled the challenge of processing the raw data from SDSS to avoid potential systematic errors.

Now, we are ready to explore the results. This section is divided into two case studies that each explores different ensemble configurations:

### (#1) Gravitationally Non-Competitive (GNC) Case Study

- (a) **Minor Ensemble:** All companion galaxies in every host-partner system has a mass ratio of  $0.01 \leq \mu \leq 0.1$ .
- (b) **Intermediate Ensemble:** All companion galaxies in every host-partner system has a mass ratio of  $0.1 < \mu \leq 0.3$ .
- (c) **Comparable Ensemble:** All companion galaxies in every host-partner system has a mass ratio of  $0.3 < \mu \leq 0.6$ .

### (#2) Gravitationally Competitive (GC) Case Study

- (a) **Mixed Ensemble:** Unlike the GNC Case Study where we considered three different ensembles, in the GC Case Study, we consider only *one*

ensemble that is a mixture of different mass companions, referred to as the mixed ensemble.

- In the mixed ensemble, every host-partner system always has *one* massive perturbing partner with a mass ratio anywhere between  $1.0 \leq \mu \leq 3.0$  (thus, violating gravitational non-competitiveness condition).
- Along with this one massive partner, there exists a mixture of one or more lower-mass companions with a mass ratio anywhere between  $0.01 \leq \mu \leq 0.6$ .
- To understand where different mass companions are clustering around the host, we selectively filter different ranges of companion mass ratios, and individually model their number densities to understand *where* these particular mass companions are clustered.

The ultimate goal in each case study is to examine whether there are any:

1. Correlations between Companion Number Density and *Core Activity*?
2. Correlations between Companion Number Density and *Partner Mass Ratio*?
3. Correlations between Companion Number Density and *Gravitational Competitiveness Condition*?

## 5.1 Case Study (#1):

### *Gravitationally Non-Competitive (GNC) Environment*

This GNC Case Study explores the three individual ensembles depicted in Figures (5.1) to (5.3). It is important to note that all of these ensembles contain a localized range of partner mass ratios  $\mu$  (see above for definition). All partners have  $\mu \leq 0.6$  to ensure that the central host is the dominant source of the gravitational field in every host-partner system.

Even though there are three separate ensembles, there are two common trends associated with all of the number density curves in Figures (5.1) to (5.3). Starting from the edge of the counting volume at 3.0 Mpc to about 1.0 Mpc, AGN and non-AGN ensembles have similar number densities (ND) and are generally indistinguishable within the same range; this is seen in the near-zero value of the relative number density (RND). Within this interval, AGN and non-AGN hosts are seen to be placed in equally-dense environments of companions.

However, once we begin approaching the inner domain of about less than 0.5 Mpc, we begin to see a clear trend where the non-AGN ND continues increasing in a monotonic fashion to a maximum value in the last radial bin at  $[0.0, 0.3]$  Mpc, while the AGN ND is observed to reach a local maximum at a non-zero radius (*minor*:  $r_{max} \approx 0.4$  Mpc; *intermediate*:  $r_{max} \approx 0.4$  Mpc; *comparable*:  $r_{max} \approx 0.6$  Mpc) then progresses in a steady and declining fashion. The data seem to be indicating that the signal is strongly truncated within the inner 0.5 Mpc for the AGN curves in all three ensemble cases. The stronger non-AGN ND over the AGN ND within this inner 0.5 Mpc region results in the negative value of the RND, which indicates that AGN host are placed in an under-dense environment of companions within this inner domain of 0.5 Mpc. It may also be worth mentioning that not only is there a local maximum in the AGN ND that is not in the first or last bin, but there also exists two inflection points on both sides of the local maximum.

## Gravitationally Non-Competitive Environment: Minor Ensemble

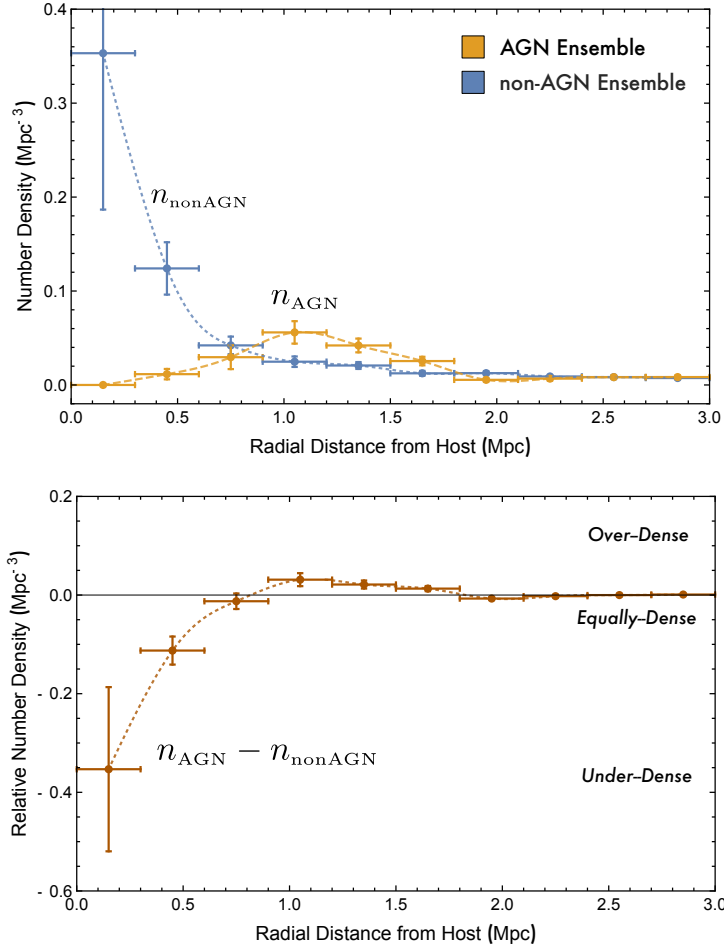
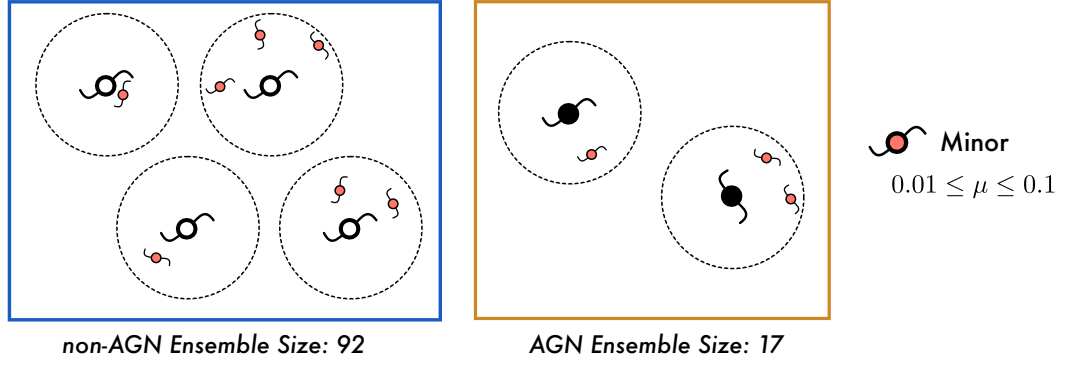


Figure 5.1: Number density and Relative Number Density for the non-AGN and AGN ensembles containing only companions with mass ratios  $0.01 \leq \mu \leq 0.1$ . All host were between  $0.010 \leq z \leq 0.048$ ; spiral galaxies ( $s > 0.6$ );  $M_{host} = -23 \pm 0.5$ . Companions were defined as neighbouring galaxies to the central host within a 3.0 Mpc volume. Data taken from SDSS DR 9.

## Gravitationally Non-Competitive Environment: Intermediate Ensemble

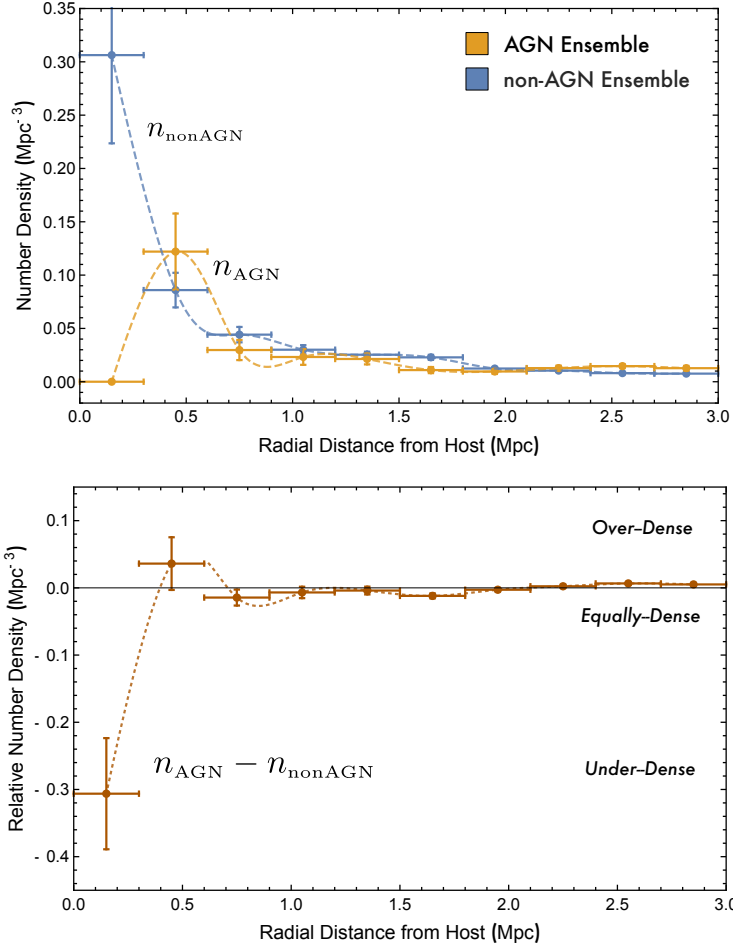
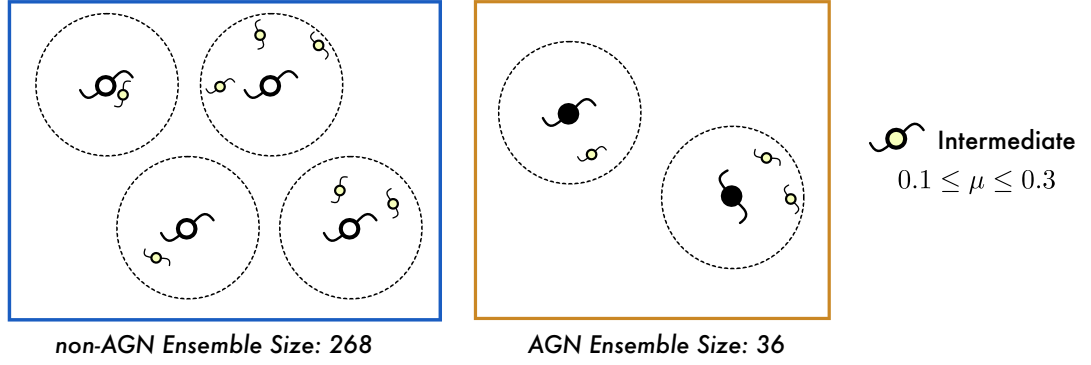


Figure 5.2: Number density and Relative Number Density for the non-AGN and AGN ensembles containing only companions with mass ratios  $0.1 \leq \mu \leq 0.3$ . All hosts were between  $0.010 \leq z \leq 0.067$ ; spiral galaxies ( $s > 0.6$ );  $M_{\text{host}} = -23 \pm 0.5$ . Companions were defined as neighbouring galaxies to the central host within a 3.0 Mpc volume. Data taken from SDSS DR 9.

## Gravitationally Non-Competitive Environment: Comparable Ensemble

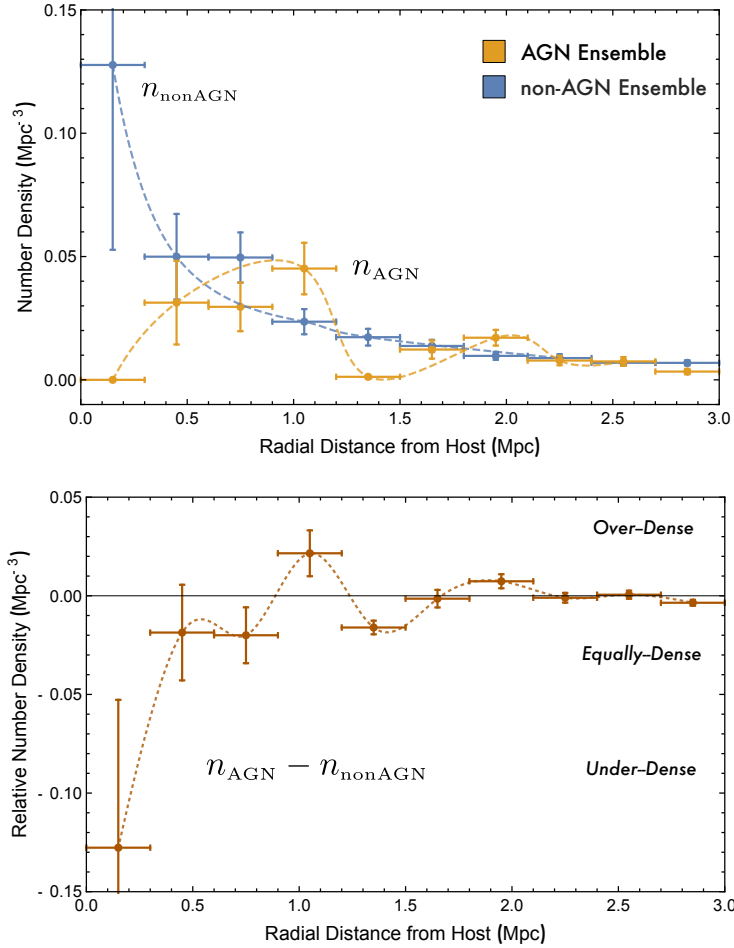
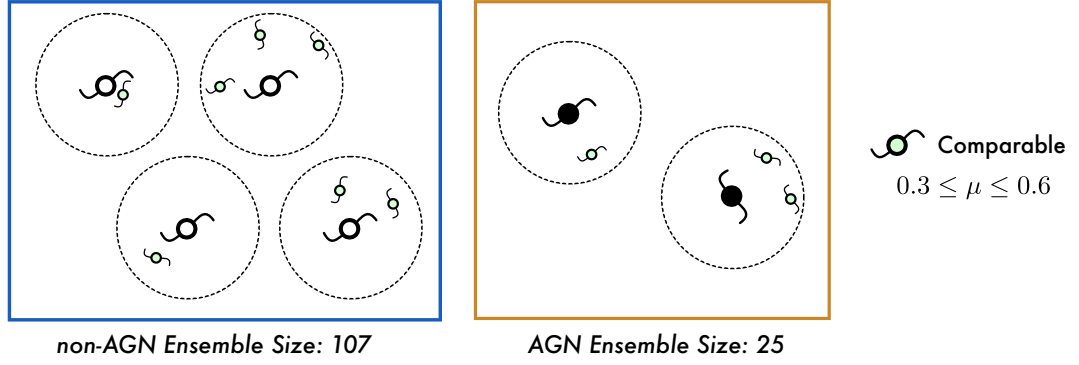


Figure 5.3: Number density and Relative Number Density for the non-AGN and AGN ensembles containing only companions with mass ratios  $0.3 \leq \mu \leq 0.6$ . All hosts were between  $0.010 \leq z \leq 0.067$ ; spiral galaxies ( $s > 0.6$ );  $M_{\text{host}} = -23 \pm 0.5$ . Companions were defined as neighbouring galaxies to the central host within a 3.0 Mpc volume. Data taken from SDSS DR 9.

We set out to investigate correlations between the spatial distribution and three parameters. This case study examines how core activity and partner mass ratios influence the spatial distribution of companions. Figures (5.1) to (5.3) clearly show that core activity and partner mass have significant influence on the companion NDs. AGNs are consistently placed in an under-dense environment of companions within 0.5 Mpc. The mass of a companion plays an important role in shifting the steepness of the curve for the non-AGN ND and, for the AGN ND, it plays a determining factor in the location of  $r_{max}$ .

We performed a quick calculation to determine the “missing” number of AGN companions relative to the non-AGN control within the first three radial bins (or about less than 1.0 Mpc). This would correspond to the following calculation,

$$N_{inner} = \int_{r=0}^{r=1} (n_{AGN} - n_{nonAGN}) dV \rightarrow \sum_{i=1}^3 (n_{AGN}^{(i)} - n_{nonAGN}^{(i)}) \cdot \Delta V_i, \quad (5.1)$$

where  $n^{(i)}$  is the number density within the  $i^{th}$  radial bin and  $\Delta V_i = \frac{4}{3}\pi(R_i^3 - R_{i-1}^3)$  represents the volume of the radial shell around the host. The results are summarized in Table (5.1). The negative sign in each case may be interpreted as the “missing”

<i>GNC Ensemble:</i>	$N_{inner}$
(1) <i>Minor</i> ( $0.01 \leq \mu \leq 0.1$ )	$-0.06 \pm 0.02$
(2) <i>Intermediate</i> ( $0.1 \leq \mu \leq 0.3$ )	$-0.011 \pm 0.005$
(3) <i>Comparable</i> ( $0.3 \leq \mu \leq 0.6$ )	$-0.04 \pm 0.01$

Table 5.1: Number of galaxies  $N_{inner}$  within the inner 0.5 Mpc AGN host galaxies relative to the non-AGN control sample. A negative value signifies an under-dense local environment around AGN host galaxies and a positive value signifies an over-density of companions.

number of AGN companions relative to the non-AGN control sample. Since there is a negative  $N_{inner}$  for each of the three GNC cases, this signifies an under-dense environment arising from a scarcity of AGN companions. In Table (5.1), the GNC environment with the minor ensemble contains the largest absence of companions within the inner domain of about 1.0 Mpc.

### 5.1.1 Examining the 95% Confidence Interval

In Figures (5.1) to (5.3), we plot the AGN number density (orange) and the non-AGN number density (blue) for a total of 10 radial bins that span the entire volume of radius 3.0 Mpc. In this subsection, we perform a statistical test aimed at comparing the AGN and non-AGN number density measurements in each radial bin and determining how statistically distinguished they are. We quantify this validity with the Confidence Value ( $C$ ) parameter, where  $0 \leq C \leq 1$ . In essence, two measurements are statistically distinguished, or highly confident with  $C \rightarrow 1$ , if the interval spanned by their error bars do not overlap in any significant manner.

To explain, for a single radial bin, there is a number density measurement  $n$  and its associated standard error bar  $\sigma$ , both for the AGN ensemble and non-AGN ensemble. If this is so, then the interval spanned by  $2\sigma$  around  $n$  (or  $n - 2\sigma$  to  $n + 2\sigma$ ) has a special statistical value – it represents an interval where we are 95% confident the “true” value of the measurement lies here. Now, if the non-AGN control measurement spans the 95% confidence interval of  $n_{nA} - 2\sigma_{nA}$  to  $n_{nA} + 2\sigma_{nA}$  for a particular radial bin, then the Confidence Value  $C$  determines to what extent the AGN measurement interval overlaps with this non-AGN control interval.

To quantify this description, we associate a Gaussian probability distribution with the AGN and non-AGN measurements and check for the AGN’s overlap in the control’s 95% confidence interval. Suppose we measure a number density of  $n$  with an error bar of  $\sigma$  for a particular radial bin, then we can represent the number density measurement as the following Gaussian probability distribution,

$$p(n') = \frac{1}{\sqrt{2\pi}\sigma} \exp\left(-\frac{(n' - n)^2}{2\sigma^2}\right). \quad (5.2)$$

To determine the Confidence Value  $C$ , we begin by measuring the overlap  $O$  of the AGN measurement distribution in the 95% confidence interval of the non-AGN measurement,

$$O = \frac{1}{\sqrt{2\pi}\sigma_A} \int_{n_{nA} - 2\sigma_{nA}}^{n_{nA} + 2\sigma_{nA}} \exp\left(-\frac{(n - n_A)^2}{2(\sigma_A)^2}\right) dn, \quad (5.3)$$

where  $n_{nA} \pm \sigma_{nA}$  is the non-AGN number density measurement and  $n_A \pm \sigma_A$  is the



AGN’s measurement. From this, we may define the confidence value  $C$  to be,

$$C = 1 - O. \tag{5.4}$$

It is important to note that  $C$  is for a specific radial bin. According to the above definition,  $C$  can be mathematically thought of as a measure of how much the AGN’s measurement *do not* overlap with the control’s 95% confidence interval.

We know that, after a typical radius of 1.0 Mpc, the AGN and non-AGN number density curves generally begin to merge. The interesting region is between 0.0 and 1.0 Mpc. Therefore, we only conduct the statistical test for the first 4 radial bins: (1) 0.0 to 0.3 Mpc; (2) 0.3 to 0.6 Mpc; (3) 0.6 to 0.9 Mpc; (4) 0.9 to 1.2 Mpc. The results are presented in the table below.

<i>Confidence Values C (%)</i>	0.0–0.3 Mpc	0.3–0.6 Mpc	0.6–0.9 Mpc	0.9–1.2 Mpc
Minor Ensemble	<b>99.9</b>	<b>99.9</b>	32.8	<b>95.4</b>
Intermediate Ensemble	<b>99.9</b>	56.8	50.2	42.6
Comparable Ensemble	<b>99.9</b>	17.3	48.8	<b>86.3</b>

Table 5.2: The confidence value represents how statistically distinguished the AGN and non-AGN number densities are in a particular radial bin. Mathematically, it may be thought of as a measure to determine how much the error bars of two measurements do not overlap. If there is high confidence between two measurements ( $C \rightarrow 1$ ), then this essentially means the interval spanned by their error bars do not overlap in any statistically significant manner.

From Table (5.2), we clearly observe that the inner most radial bin of 0.0–0.3 Mpc consistently has a high confident value of 99.9%. This implies that the AGN and non-AGN number densities are a distinguished and statistically valid measurement; that is, their error intervals do not overlap in any significant manner. Another interesting confidence measurement is the last radial bin (0.9–1.2 Mpc) in the minor and comparable ensemble. An examination of Figure (5.1) and Figure (5.3) reveal that, in this radial bin, the AGN number density reaches a maximum value before descending and, ultimately, merging with the background number density. The confidence value of 95.4% and 86.3% reveal that this maximum number density is a statistically distinguished feature in the AGN number density curve for the minor and comparable ensemble.

### 5.1.2 Fiber Collision in SDSS

An interesting observation in the GNC environment is the paucity of AGN companions in the inner volume compared to the non-AGN number density. In order to rule out any possible systematic effects that could lead to this observation, we had to rule out any technical issues that could play a role. We examined the possibility of SDSS fibre collisions. Because of the finite angular width of spectroscopic fibres, SDSS cannot study the spectroscopic information from two sources that are generally placed within 55 arcseconds of each other. Therefore, it is important to rule out fibre collisions as a possible explanation for the “missing” inner number density of companions.

A quick calculation reveals that this fibre collision angle of 55 arcseconds translates to the projected radius of 12 kpc for our closest redshift host galaxies at  $z = 0.010$  and 79 kpc for our farthest redshift at  $z = 0.067$ . With this said, our bin size is 300 kpc, which is much larger than the projected collision distance. If fibre collisions were a significant problem, then we would not get any measurement in the non-AGN number density within the inner radial bins as well – this is not the case. These observations suggest fibre collisions may not be a significant systematic issue.

### 5.1.3 Colour Distribution

The examination of galaxy colour in astrophysics often carries important information about star-formation history and galactic composition. Researchers have also observed that colour differences between matched samples of galaxies may possibly rise from interaction with neighbouring galaxies (Netzer, 2013; Sabater et al., 2013). Since the aim of our project is to examine how gravitational interactions influence companion clustering, in this sub-section, we compare the AGN and non-AGN companion colour distributions to examine for any potential difference between these matched sample of host galaxies.

When analyzing the number density function, we required a single data point (i.e. the average number density of companions) from a single bin. However, when discussing the colour distribution, we require a distribution of data points from a single bin. Therefore, this greatly restricts the size of our bins. We explore three different bin sizes: (i) 0.0 to 1.0 Mpc range, (ii) 1.0 to 2.0 Mpc range, and (iii) 2.0 to 3.0 Mpc range. In each range, we study three colour distributions of the companions around AGN and non-AGN hosts: (1)  $u - g$ , (2)  $g - r$ , and (3)  $r - i$ . In terms of the host galaxies used in the analysis, we took all the host galaxies from the GNC environment provided in the last section and examined their colours. There were a total of (Minor + Intermediate + Comparable = 92 + 268 + 107 =) 467 non-AGN hosts and a total of (17 + 36 + 25 =) 78 AGN hosts. Our results are illustrated in Figures (5.4) to (5.6).

<b>P-Values</b>	$u - g$	$g - r$	$r - i$
0.0 – 1.0 Mpc	0.295	0.397	0.667
1.0 – 2.0 Mpc	0.329	0.418	0.613
2.0 – 3.0 Mpc	0.352	0.397	0.666

Table 5.3: P-Values from the Kolmogorov-Smirnov Test with a 95% confidence level for the distribution depicted in Figures (5.4) to (5.6).

In the GNC environment, one of the key features observed in the number density of AGN companions was that it is differentiated from non-AGN number density within in the inner 0.5 Mpc region. The results from Figures (5.4) to (5.6) show that the AGN and non-AGN colour distribution of companion, however, do not appear to be differentiated in any statistically significant manner. In Table (5.1.3), we performed the Kolmogorov-Smirnov Test with a 95% confidence level and determined the  $p$ -values

for each of the nine total distributions depicted in Figures (5.4) to (5.6). The  $p$ -value is an important indicator we may use to decide if the null hypothesis is true or not. In our case, the null hypothesis is to determine whether the AGN and non-AGN colour distribution functions are different at a particular confidence level. The  $p$ -value ranges may be interpreted as,

→  $0.00 \leq p \leq 0.05$ : Significant result, i.e. The null hypothesis may be rejected and there is a significant statistical difference between the two distributions;

→  $0.05 < p \leq 0.15$ : Marginally significant result;

→  $0.15 < p \leq 1.00$ : No significant result, i.e. Null hypothesis is true.

With this information, none of the nine distributions shown in Figures (5.4) to (5.6) have  $p$ -values indicating a statistically significant result. The null hypothesis is true, i.e. AGN and non-AGN companions have similar colour distributions. The 0.0–1.0 Mpc range shows a somewhat significant variation in the  $u - g$  colour within the range of 1.5 to 2.5, but no other significant trend is observed.

Companion  
Colour  
Distribution for  
0.0 to 1.0 Mpc  
Range

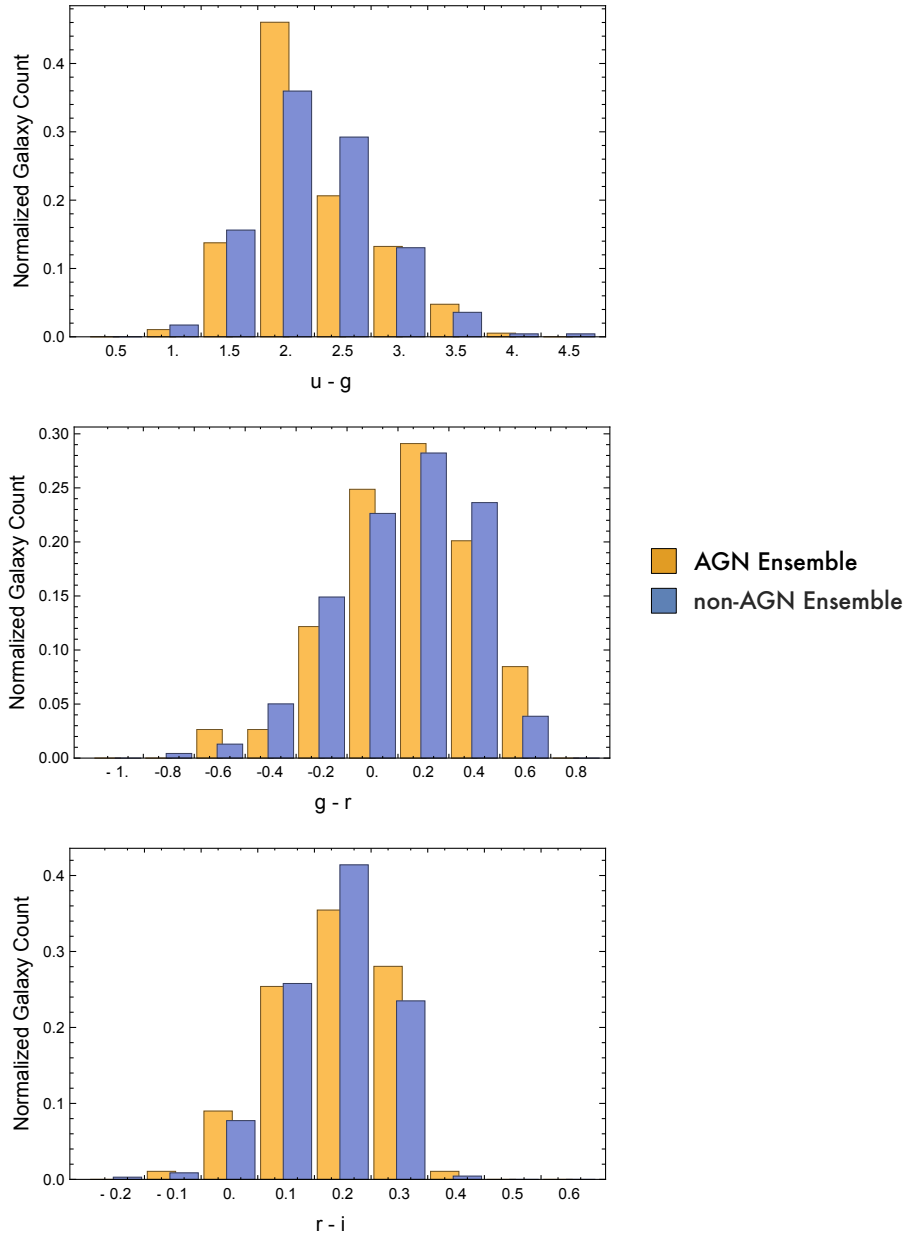


Figure 5.4: Three colour distributions ( $u-g$ ,  $g-r$ ,  $r-i$ ) for AGN and non-AGN companion galaxies within a 0.0 to 1.0 Mpc range around the central hosts. All host galaxies were taken from the GNC environment. There were a total of 78 AGN hosts and 467 non-AGN hosts.

Companion  
Colour  
Distribution for  
1.0 to 2.0 Mpc  
Range

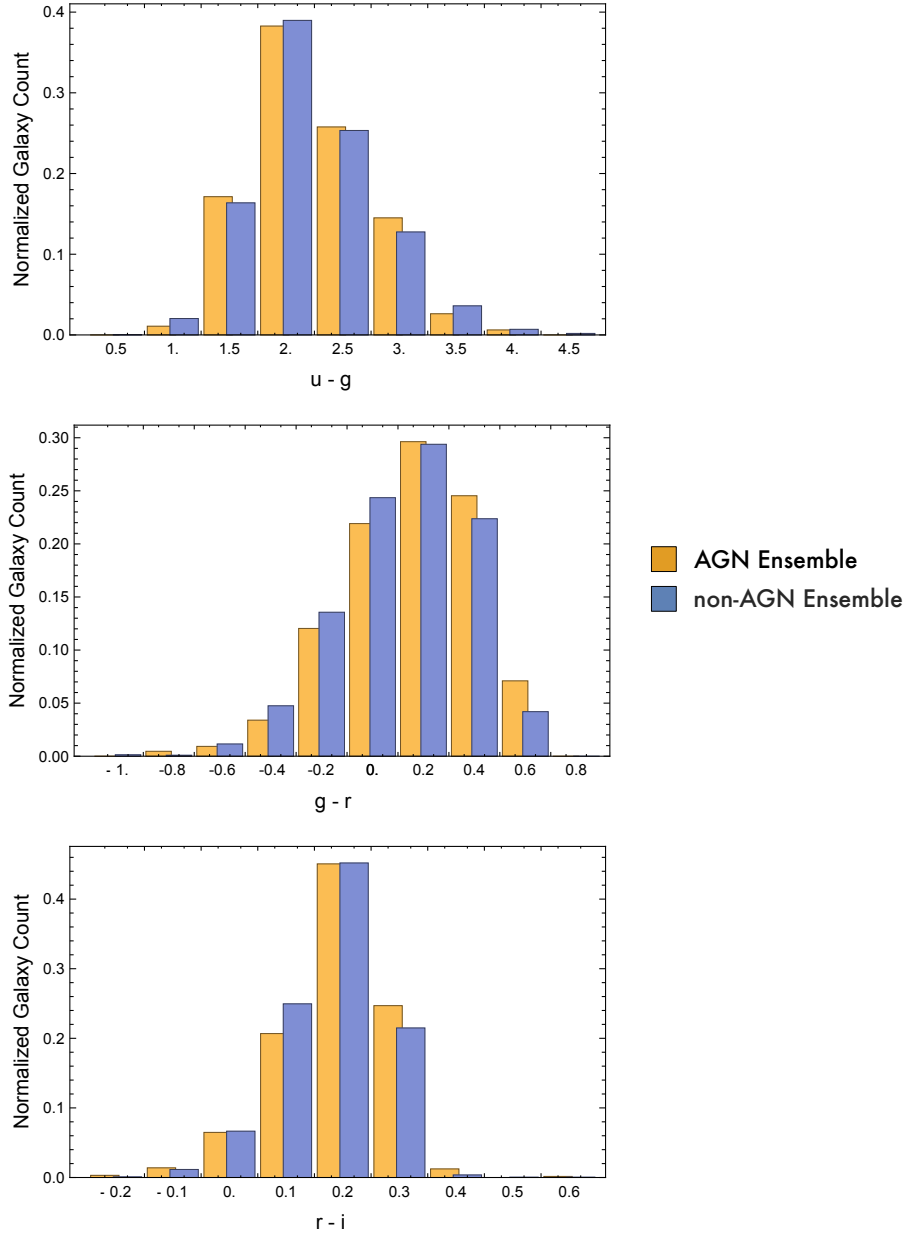


Figure 5.5: Three colour distributions ( $u-g$ ,  $g-r$ ,  $r-i$ ) for AGN and non-AGN companion galaxies within a 1.0 to 2.0 Mpc range around the central hosts. All host galaxies were taken from the GNC environment. There were a total of 78 AGN hosts and 467 non-AGN hosts.

Companion  
Colour  
Distribution for  
2.0 to 3.0 Mpc  
Range

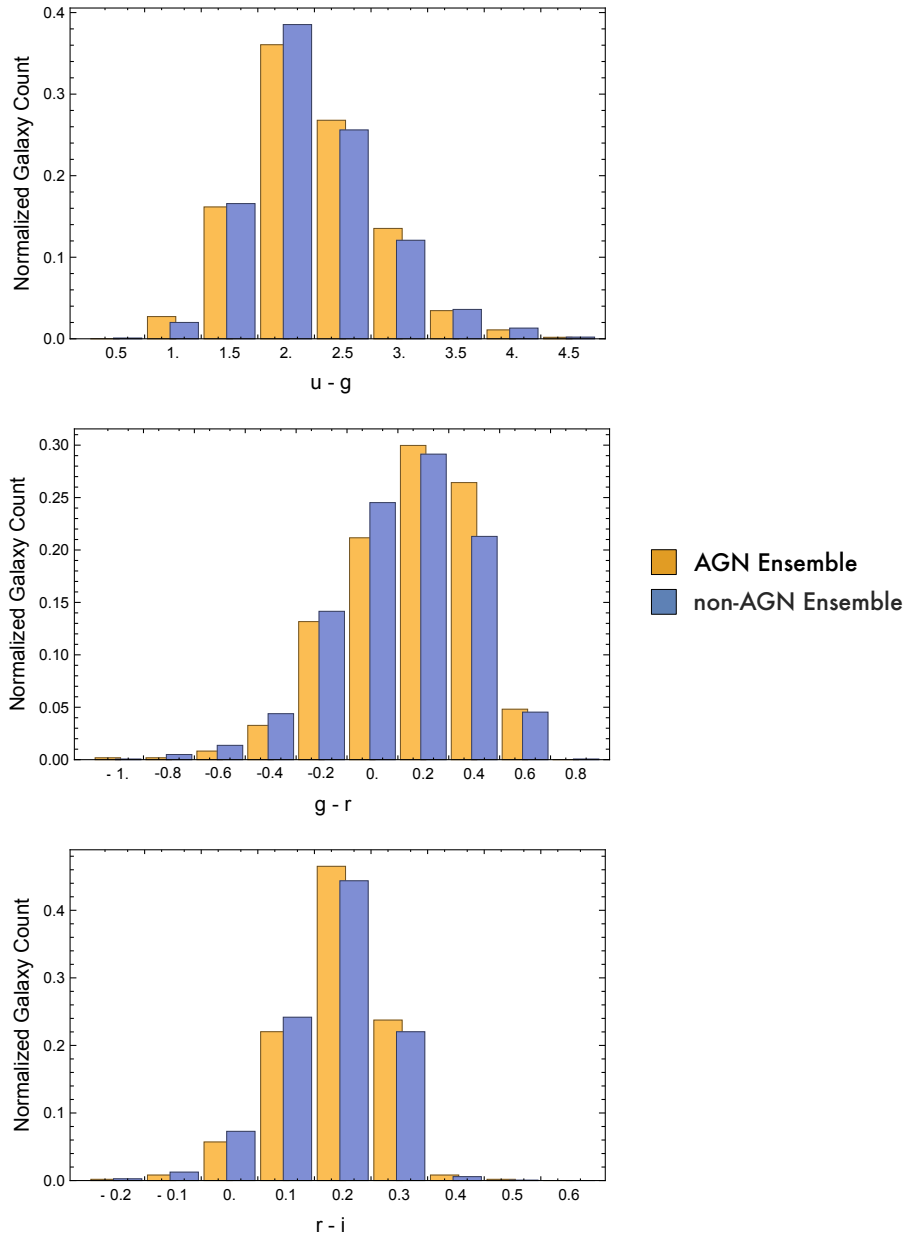


Figure 5.6: Three colour distributions ( $u-g$ ,  $g-r$ ,  $r-i$ ) for AGN and non-AGN companion galaxies within a 2.0 to 3.0 Mpc range around the central hosts. All host galaxies were taken from the GNC environment. There were a total of 78 AGN hosts and 467 non-AGN hosts.

## 5.2 Case Study (#2):

### *Gravitationally Competitive (GC) Environment*

Before we begin discussing the results of the GC case study, it is very important to understand the set-up of this case study because it is different from the GNC case. Unlike our GNC case study where we surveyed *three* separate ensembles and their NDs, for our GC case study, we surveyed only *one* ensemble, referred to as the mixed ensemble. Every host-partner system in the ensemble always has one massive perturbing companion ( $1.0 \leq \mu \leq 3.0$ ) and a mix of one or more lower-mass ( $0.01 \leq \mu \leq 0.60$ ) companions. Even though we have just one ensemble, Figures (5.7) to (5.10) produced four different plots because we selectively have filtered for different mass companions to examine how they specifically cluster around the central host. This mixed case study contains 30 AGN host-partner systems and 61 non-AGN host-partner systems.

Figure (5.7) is the ND function for *all mass-companions* contained in the counting volume. One of the most distinguishing features of Figure (5.7) is that AGN and non-AGN NDs are seen to strongly overlap; thus, producing a RND that is fluctuating near-zero in an equally-dense zone throughout the 3.0 Mpc domain, with one exception being the inner most radial bin of 0.0 to 0.3 Mpc where the uncertainty greatly grows. In this GC environment, we see for the first time the AGN and non-AGN NDs begin to resemble each other, as opposed to the GNC cases where the resemblance was only outside 1.0 Mpc.

Similar to the GNC Environment, we performed a quick calculation to determine the “missing” number of AGN companions relative to the non-AGN control within the first two radial bins (or about less than 0.5 Mpc). This would correspond to the following calculation,

$$N_{inner} = \int_{r=0}^{r=0.5} (n_{AGN} - n_{nonAGN}) dV \rightarrow \sum_{i=1}^2 (n_{AGN}^{(i)} - n_{nonAGN}^{(i)}) \cdot \Delta V_i, \quad (5.5)$$

where  $n^{(i)}$  is the number density within the  $i^{th}$  radial bin and  $\Delta V_i = \frac{4}{3}\pi(R_i^3 - R_{i-1}^3)$  represents the volume of the radial shell around the host. The results are summarized in the Table (5.4).



## Gravitationally Competitive Environment: Mixed Ensemble (Includes All Partners)

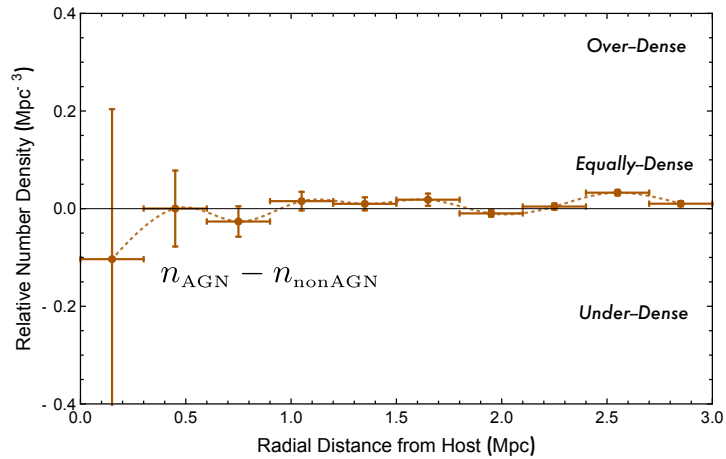
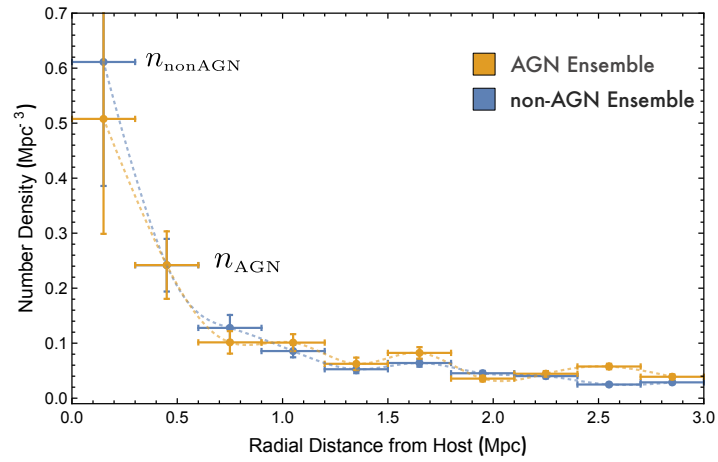
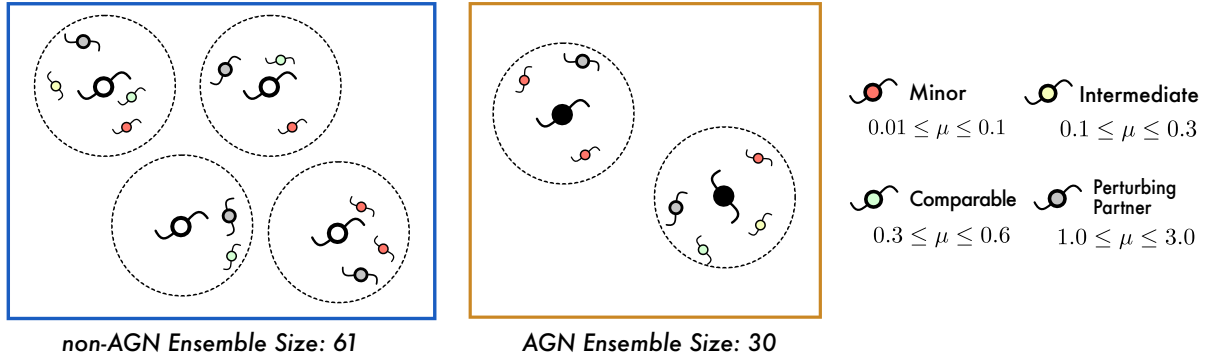


Figure 5.7: All non-AGN and AGN ensembles contain exactly one large perturbing companion with mass ratio  $1.0 \leq \mu \leq 3.0$  and any combination of lower-mass companions  $0.01 \leq \mu \leq 0.6$ . This plots includes all partners in the number density count. All host galaxies were between  $0.010 \leq z \leq 0.048$ ; spiral galaxies ( $s > 0.6$ );  $M_{host} = -23 \pm 0.5$ . Data taken from SDSS DR 9.

## Gravitationally Competitive Environment: Mixed Ensemble Selectively Filtered for Minors

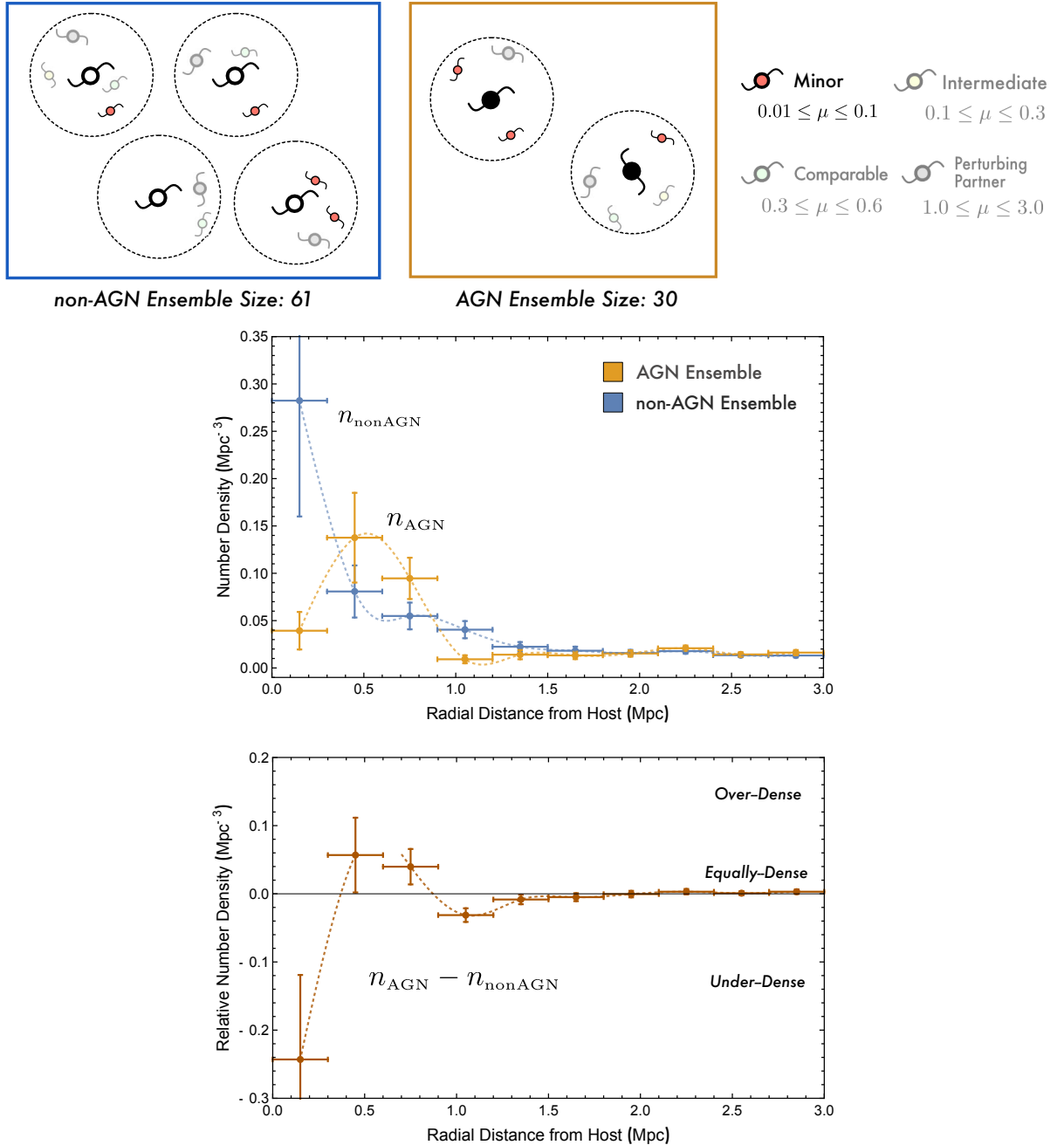


Figure 5.8: All non-AGN and AGN ensembles contain exactly one large perturbing companion with mass ratio  $1.0 \leq \mu \leq 3.0$  and any combination of lower-mass companions  $0.01 \leq \mu \leq 0.6$ . This plots selectively filters for minor companions in the number density count. All host galaxies were between  $0.010 \leq z \leq 0.048$ ; spiral galaxies ( $s > 0.6$ );  $M_{host} = -23 \pm 0.5$ . Data taken from SDSS DR 9.

## Gravitationally Competitive Environment: Mixed Ensemble Selectively Filtered for Intermediates

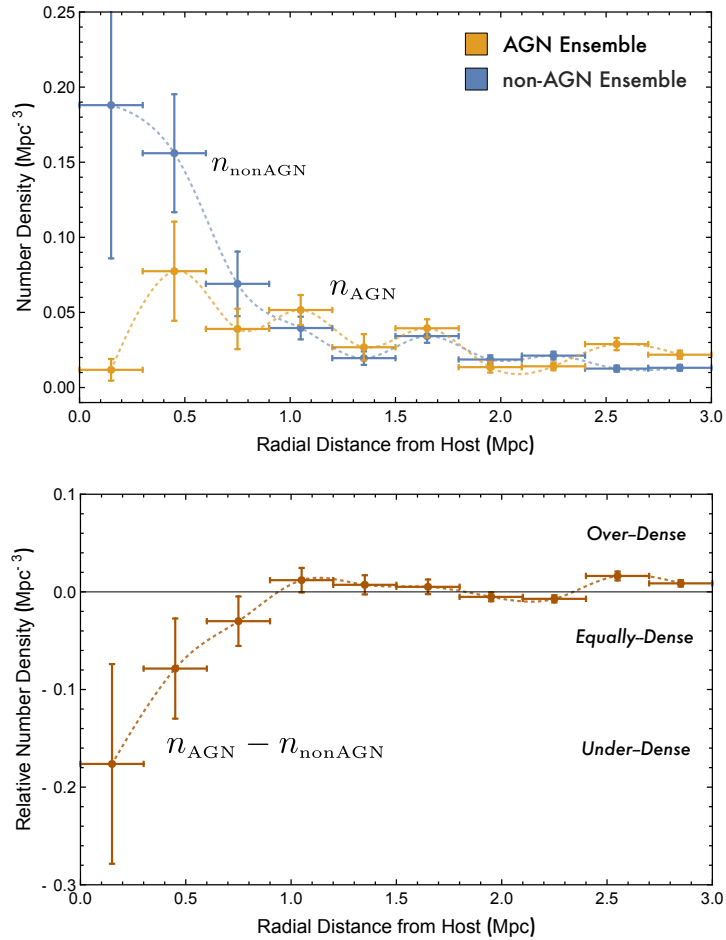
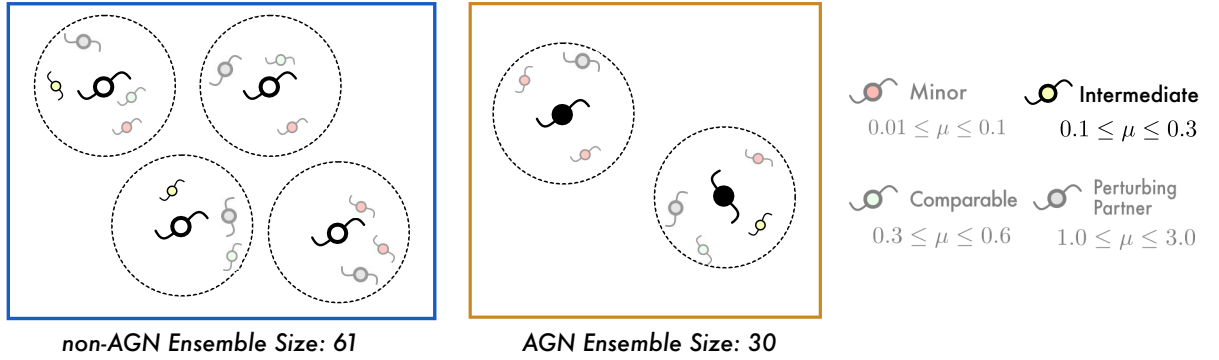


Figure 5.9: All non-AGN and AGN ensembles contain exactly one large perturbing companion with mass ratio  $1.0 \leq \mu \leq 3.0$  and any combination of lower-mass companions  $0.01 \leq \mu \leq 0.6$ . This plots selectively filters for intermediate companions in the number density count. All host galaxies were between  $0.010 \leq z \leq 0.048$ ; spiral galaxies ( $s > 0.6$ );  $M_{host} = -23 \pm 0.5$ . Data taken from SDSS DR 9.

## Gravitationally Competitive Environment: Mixed Ensemble Selectively Filtered for Comparables

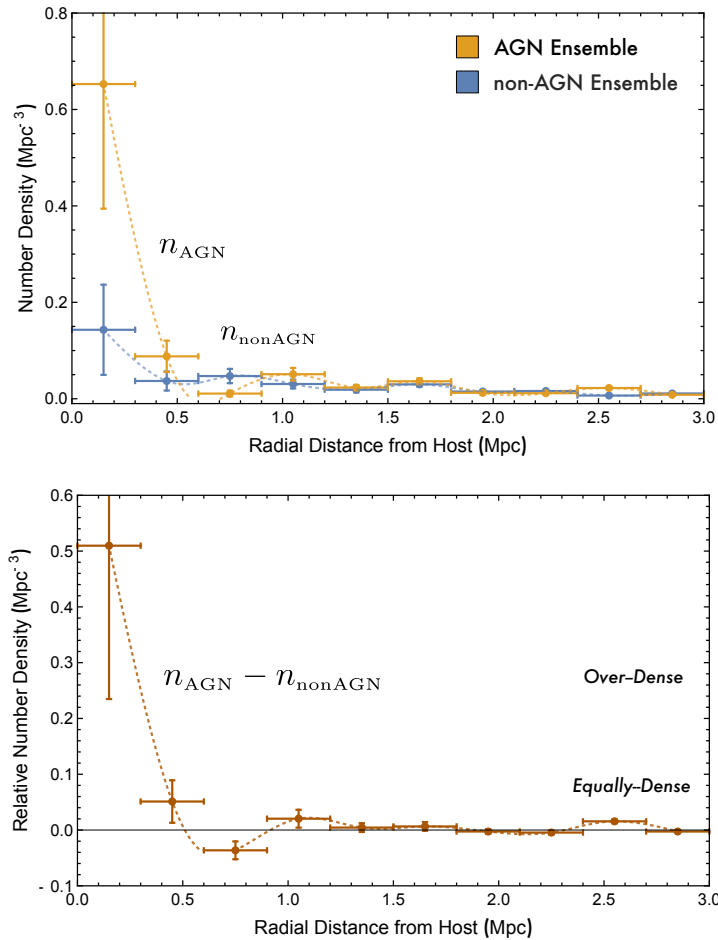
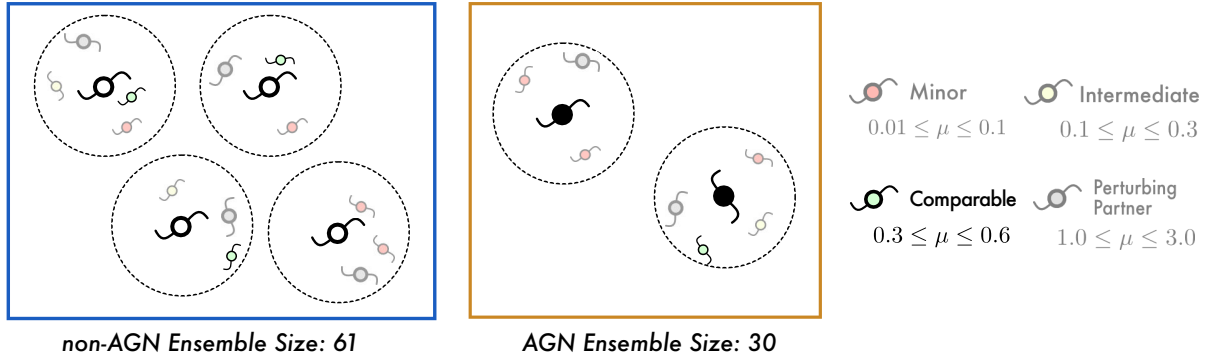


Figure 5.10: All non-AGN and AGN ensembles contain exactly one large perturbing companion with mass ratio  $1.0 \leq \mu \leq 3.0$  and any combination of lower-mass companions  $0.01 \leq \mu \leq 0.6$ . This plots selectively filters for comparable companions in the number density count. All host galaxies were between  $0.010 \leq z \leq 0.048$ ; spiral galaxies ( $s > 0.6$ );  $M_{host} = -23 \pm 0.5$ . Data taken from SDSS DR 9.

<i>GC Ensemble:</i>	$N_{inner}$
(1) <i>All Partners</i>	$-0.001 \pm 0.002$
(2) <i>Minor</i> ( $0.01 \leq \mu \leq 0.1$ )	$0.02 \pm 0.01$
(3) <i>Intermediate</i> ( $0.1 \leq \mu \leq 0.3$ )	$-0.030 \pm 0.007$
(4) <i>Comparable</i> ( $0.3 \leq \mu \leq 0.6$ )	$0.03 \pm 0.01$

Table 5.4: Number of galaxies  $N_{inner}$  within the inner 0.5 Mpc AGN host galaxies relative to the non-AGN control sample. A negative value signifies an under-dense local environment around AGN host galaxies and a positive value signifies an over-density of companions.

Now, in Figure (5.8), we take the same mixed ensemble and ask where are the minor companions ( $0.01 \leq \mu \leq 0.1$ ) particularly clustered around the host. Remember, the gravitational influence of the other companions, including the massive perturbing partner is still present, but just not incorporated in the counting of the number density. When we apply this selective filtering for minors in Figure (5.8), we begin to see a similar re-emergence of the trend seen in the GNC cases in the RND variation. The RND reveals a system where AGN host galaxies are placed in an under-dense inner domain of minors, while there is also a sudden surge in over-density of minors between 0.5 Mpc and 0.9 Mpc. Figure (5.9) for minor companions is similar again to the GNC case with the under-dense inner region.

Figure (5.10) is the most significant plot that breaks the so-far established norm. Up until now with the minor and intermediate companions, the RND has been consistently under-dense in the inner region. If this was always true, then the full ND seen in Figure (5.7) with all the partners would also have an inner under-density. However, it is the inclusion of the comparable companions seen in Figure (5.10) that causes over-dense deflection. This case is the only example of all the cases we have studied with an over-density in the inner domain of 0.5 Mpc.

### 5.2.1 Examining the 95% Confidence Interval

We perform the same Confidence Value ( $C$ ) calculations as outlined in Section 5.1.1. for the first 4 radial bins. The results are presented in the table below. One of the clear-cut differences seen in these confidence values compared to the GNC environment is that there are very few high confidence values. The presence of the massive perturber companion has significantly altered the statistics of the companion clustering. The last row on the comparable partner measurements is the only case where the confidence

values seems to be indicating a statistically distinguished result. The comparable partners were also the only case where the AGN number density was greater than the non-AGN number density in the inner radial shells, placing AGN host galaxies in an over-dense environment of companions.

<i>Confidence Values (C)</i>	0.0–0.3 Mpc	0.3–0.6 Mpc	0.6–0.9 Mpc	0.9–1.2 Mpc
All Partners	5.22	11.9	15.6	32.4
Minor Partners	46.7	52.4	70.2	<b>99.9</b>
Intermediate Partners	0.001	50.0	16.7	38.3
Comparable Partners	89.8	64.0	87.1	56.0

Table 5.5: The confidence value represents how statistically distinguished the AGN and non-AGN number densities are in a particular radial bin. Mathematically, it may be thought of as a measure to determine how much the error bars of two measurements do not overlap. If there is high confidence between two measurements ( $C \rightarrow 1$ ), then this essentially means the interval spanned by their error bars do not overlap in any statistically significant manner.

# Chapter 6

## Discussion

This project was ultimately motivated by the central question: *What pathway allows AGNs to efficiently supply their cores with gaseous fuel and engage in enhanced accretion onto the central supermassive black hole compared to non-AGNs? Where does this gas originate from?* Our approach to understanding this question involved asking: whether or not gravitational interactions with companion galaxies is the primary cause of core activity. By gravitational interaction, we refer to situations whereby a companion makes a direct contribution of gaseous fuel to the host's core (such as galactic collision or cannibalism) and/or the physical closeness of a partner induces gravitational disturbances in the host (such as galactic harassment or tidal stripping). Any of these scenarios may possibly stimulate gas inflow and lead to core activation.

While we recognize there are many details in the literature about the specific physical mechanics behind companion interactions, we are not necessarily concerned with the exact details. To understand how intensely companions are interacting with their host and what forms of gravitational interactions are being invoked, we were able to distill these two questions to: what is the spatial distribution of companion galaxies? By finding a collection of similarly configured host-partner systems (or equivalent ensemble), we were able to analyze the typical distribution of companions, quantified by the number density function  $n(r)$ .

We explored two different case studies that analyzed different ensemble possibilities: (i) a Gravitationally Non-Competitive Environment with three different ensembles; (ii) a Gravitationally Competitive Environment with one ensemble, referred to as the

mixed ensemble. In these different cases, we examined the correlation between the number density of companions and core activity/mass ratio of partners  $\mu$ .

An important gap in the literature is the lack of consistency among different environmental surveys about whether or not gravitational interaction with companions are linked to core activity and, if so, which particular form of interaction (i.e. collision, cannibalism, harassment, etc.) is primarily responsible for AGN activity. Our results aim at showing the importance of considering the relative number density, and how the condition of Gravitational Competitiveness can significantly alter the spatial distribution of companions around active host.

## 6.1 Observational Interpretation of the Results

### 6.1.1 Case Study (#1): Gravitationally Non-Competitive Environment

Figures (5.1) to (5.3) allow us to examine the correlation between the number density of companions and different parameters like core activity and mass ratio of partners. In this section, we discuss the possible physical interpretations between any observed correlations. The GNC environment results indicate that, when active galaxies occupy an isolated environment (within 3.0 Mpc), their inner domains (less than 0.5 Mpc) are consistently placed in an under-dense environment of companions. There are two significant parts to this statement that have important interpretations:

- (i) There is an *under-density* of companions within the *inner domain*;
- (ii) This inner under-density is *consistent* among all three companion mass ratios (minors, intermediates, comparables).

We now explore the possible interpretations behind these observations.

For the first observation, if the non-AGN number density represents the typical clustering of partners around a host such that gravitational interactions have not initiated core activity, then a deviation from this stable configuration may be possibly interpreted as a potential cause leading to core activity. Furthermore, deviations in the RND within the inner domain have particular significance because this is where



we would expect the strongest gravitational interactions to occur. In our case, an inner under-density may be possibly hinting at a history of past mergers, whereby a now-active host consumed its neighbours to acquire fuel. In other words, the absence of companions around AGN host, where one should expect to find companions as seen in the non-AGN cases, may be indicative of a past history of consumption. Another possibility is that active galaxies have engaged in some kind of physical mechanism whereby they have “pushed out” existing companions in the inner 0.5 Mpc out to 1.0 Mpc, explaining the local maximum number density near that range. However, based on the gravitational interaction schemes described in the introduction, it is not clear what kind of physical process would actually lead to this outward migration of companions. The effects of dynamical friction is like a “drag” force that decays orbits toward the system’s center-of-mass, as opposed to an outward movement.

The second observation is also significant. When we examined the GNC environment for three groups of mass-companions ranging from 1% to 60%, we observed an inner under-density in all three of these cases. This consistent behaviour across these three groups may be suggestive that active hosts have engaged in a wide range of gravitational interactions to merge with companions. There may possibly be multiple channels to initiate core activity. As discussed in the introduction, there were two main kinds of mergers: galactic collisions and galactic cannibalism. Galactic collisions can occur across all companion mass ratios, but it is interesting to note that galactic cannibalism, which is the orbital decay of smaller companions via dynamical friction, is typically seen when there is a stronger mass difference between the host and partner. With that said, the minor companions ( $0.01 \leq \mu \leq 0.1$ ) are also seen to have an inner under-density. AGNs may have engaged in multiple different merging mechanisms to possibly consume companions.

We can also draw inferences based on what we *do not* observe. Since the RND is not equally-dense or over-dense within the inner domain, this may imply that gravitational interactions associated with gravitational disturbances (such as galactic harassment and tidal stripping) may *not* play a significant role in the initiation of core activity in galaxies. Even though there is generally an equally-dense environment outside of 0.5 Mpc, the physical interactions associated with harassment and/or tidal stripping require a closeness within 0.5 Mpc. Therefore, the evidence seems to be suggesting that merging, as opposed inducing disturbances, is the primary gravitational interaction initiating core activity.

It is important to understand how different lines of reasoning may lead to different interpretations across the literature. For instance, Ellison et al. (2011) focus on finding merger candidates and examining the fraction of close range galaxy pairs that have AGNs. This work implies that the process of merging or, at least, the nearness of a comparable-sized candidate (in our study, this would be interpreted as galactic harassment) leads to core activity. However, it may not be clear whether the *act* of merging is initiating core activity, or the gravitational disturbances caused by the nearness of a comparable-sized companion, is the cause of core activity. Our study considers the *absence* of companions where one expects to find companions as also having important interpretational value.

### 6.1.2 Case Study (#2): Gravitationally Competitive Environment

With all of this said, how does the GC results add to the so-far developed narrative? In the GNC case study, we saw that, by finding host galaxies that are gravitationally dominant in a 3.0 Mpc volume, we were able to better define what it meant to be a *physical* host of an environment and how this influenced the number density of companions. We noticed that, in this kind of isolated environment, AGNs are consistently placed in an under-density within the 0.5 Mpc environment. However, as the GC results show, this behaviour is not always true.

In the GC case study, we include a single massive perturbing companion that significantly alters the gravitational field in the 3.0 Mpc volume and, thus, the central active/non-active host is not the only dominant source of gravity. There are two interesting observations in this case study:

- (i) By including all partners in the number density count, both non-AGN and AGN number densities look very similar and, thus, the RND fluctuates near zero or equally-dense;
- (ii) When we selectively examine how *specific* mass-companions cluster around the host, we suddenly notice a RND behaviour with similar trends as the GNC case study with one exception ( $0.3 \leq \mu \leq 0.6$ ), where there is a strong over-density in the inner domain.

The first observation has important implications. It shows that, when we allow for a mixture of different-mass partners in the counting volume, unlike the GNC case, it becomes difficult to distinguish the AGN and non-AGN number densities. This stresses the importance of the Gravitational Competitive constraint and it is important to consider this condition when studying active galaxies. In the second observation, when we selectively filter for different-mass partners studied in the GNC environment (satellites, minors, intermediates), we suddenly observe a change in the number density behaviour. We were able to differentiate number density curves when we begin to localize the partner mass.

### 6.1.3 Comparison to Ellison et al. (2011) Study

Ellison et al. and our study both explore the possibility of whether neighbouring galaxies play an important role in causing gas inflow toward the core and initiating/sustaining AGN activity. This surge of gas is what allows for enhanced accretion onto the central supermassive black hole. However, there is an undetermined component to this description. The question of whether of the inflowing gas originated from the galaxy’s own disk and/or was supplied by an external source, like the gaseous content of companions, is still an open question.

In the case of Ellison et al. (2011), they investigate the specific possibility of close range galaxy-galaxy interaction as a possible mechanism. That is, if a host galaxy has a nearby neighbouring galaxy that is close proximity to the host, then this places the host in an asymmetric gravitational potential, which may give rise to instabilities in *existing* gas of the host and ultimately cause a net inward migration of gas. Ellison et al. collect a sample of 11,060 galaxies from the Sloan Digital Sky Survey (SDSS) and examine the fraction of AGN occurring in these close-range galaxy pairs. Galaxies are paired if they are within a projected distance from each other of 80 kpc and  $\Delta V < 200 \text{ km s}^{-1}$ . Ellison et al. acknowledge SDSS fibre collisions may lead to a high incompleteness at separation angle less than 55 arcseconds. However, by using a methodology that involves adopting information from photometric catalogs to calculate separation angles and other available survey data, they were able to reduce the effects of this possible bias. They found a significant increase in the AGN fraction in close pairs with projected separation  $> 0.04 \text{ Mpc}$  by an average factor of 2.5 relative to the control sample, with an increase in the AGN fraction strongest in equal mass

galaxy pairs and weakest in unequal mass pairs. This supports the picture that the physical closeness of gravitational bodies, especially when unequal in mass, may be sufficient to cause the onset of gas inflow in the host and power AGN activity.

It is interesting to consider Ellison et al. (2011) study with respect to our research. A common ground is that we both explore the question of whether an external source is causing gas inflow to the core; however, Ellison et al. particularly look at the scenario of close-range galaxy pairs. The central investigative tool of our research, the number density function, maps out the spatial distribution. While Ellison et al. implement the specific constraint and only examine host galaxies with close-by neighbours, we do not implement such strict constraints. The number density functions allows us to measure the presence and, at the same time, the absence of the neighbours. That is, both of the paucity and the surplus of companions around active galaxies relative to the control have important interpretational value.

When we compare the results of the Ellison et al. to our study's outcomes, there is both a degree of consistency and indeterminacy among the results. For instance, in our Gravitationally Competitive environment in Figure (5.10), we see a similar result in line with the Ellison et al. conclusion, whereby there is an over-density of companions near active galaxies. This is suggestive that the physical nearness of companions may be a possible cause of AGN activity. However, there is also a degree of indeterminacy. One of the key ideas distinguishing our project is the notion of Gravitational Competitiveness. Ellison et al. do not place any major constraints more global environment ( $< 3$  Mpc) around the host. It is not clear if the examined galaxy pairs are in, by our definitions, a competitive and non-competitive environment and, therefore, we may not be able to make a fair comparison. As this work has demonstrated, this competitive environmental factor does seem to play an important role in the spatial distribution of neighbouring galaxies.

## 6.2 Theoretical Interpretation of the Results

Our ultimate goal in this project was to determine if the gravitational interaction with companion galaxies could be the primary *cause* of core activity. In the previous section, we examined the dependence of the number density of companions on variables like the host's core activity and mass ratio of partners. We observed that, in gravitationally

isolated environments (or GNC), active galaxies were consistently situated in an inner under-density for all partner mass-regimes. This scarcity of AGN companions may suggest that these galaxies became active via gravitational interaction, particularly mergers, with companion galaxies.

We now briefly explore the possibility of interpreting the number density of companions from a different perspective – a more theoretical viewpoint rooted in statistical physics/mechanics. Even though we recognize a full discussion and extension of these ideas are beyond the scope of this work, it is, nevertheless, worthwhile to mention and discuss the importance of these interpretations because they open up possibilities for future projects and have very interesting implications.

### 6.2.1 Importance of the GNC Case Study to Statistical Mechanics

Our motivation is simple: can we use statistical physics to relate the number density of companions  $n(r)$  to physical variables like energy, volume, and velocity? Can these theoretical relations be connected with our observational results seen in Figures (5.1) to (5.10)? The answer is yes. Our current observational models can indeed be connected to theoretical models by studying the statistical physics of self-gravitating collisionless systems. The idea is to represent galaxies as point-like particles in a “fluid” that move under the influence of a mean gravitational potential  $\phi$ , where we assume these particles do not undergo frequent collisions. With this said, it turns out that these criteria are satisfied by the GNC case study. The GNC results depicted in Figures (5.1) to (5.3) are a good approximation of a self-gravitating collisionless system, where galaxies are predominantly subjected to the gravitational potential  $\phi_H$  generated by the central host.

Even though a full discussion of these ideas may be outside the scope of this work, this section briefly explores a spherically symmetric collisionless model. We show that the non-AGN number density generally follows the behaviour predicted by an isotropic and isothermal model, but the AGN number density curve cannot be represented by an isothermal model. The local maximum consistently seen in the GNC case study in Figures (5.1) to (5.3) has significant implications regarding the kinematical configuration of the AGN companions. We want to show that they are

not in “thermal” equilibrium or, in other words, there exists a possible net flow of companions within the inner 0.5 Mpc around the AGN host that is not seen around the non-AGN host.

## 6.2.2 Spherically Symmetric + Isotropic Model

We follow the models and derivations developed by Longair (2008) and Binney & Tremaine (1987). These sources set out to provide a similar answer to the central goal of this thesis – can we understand the spatial density of galaxies in terms of statistical physics? They explore the possibility of modeling galaxies in a cluster environment as an ideal gas. At first glance, this may seem counter-intuitive, but the ideal-gas treatment becomes relevant when we consider more closely the similarities between the statistical physics of gas molecules and galaxies. If we assume the velocity distribution of galaxies in a cluster have reached some kind of stationary dynamical state and have well-defined distribution (like a Maxwell-Boltzmann distribution), then we can evaluate a mean kinetic energy for the galaxies, which may be interpreted as a kind of “temperature”. From this, we may define other quantities like pressure and proceed with a thermodynamic-like treatment of the galaxies. These kinds of statistical models have been used in the literature by different researcher such as King (1966), who generally predicted the spatial distribution of galaxies in cluster environments by modeling them as an isothermal gas sphere.

As for our project, we may follow a similar reasoning. Let’s assume we have a collisionless system of point-like particles (galaxies) subjected to the gravitational potential  $\phi_H$  of a central non-AGN/AGN host. Along with this, we begin with the simplest assumption that the system is isotropic, i.e. there is no preferred direction of motion or net flow in the movement of the companion galaxies. Within this model, we can now give meaning to the number density  $n(r)$ . Since we consider companion galaxies as particles in an ideal gas, we would expect galaxies to adhere to an equation of state,

$$P = \frac{\rho k_B T}{m} = nk_B T, \quad (6.1)$$

where  $k_B$  is the Boltzmann constant (for this point, we set  $k_B = 1$ ),  $P$  is pressure,  $T$  is temperature, and  $\rho$  is the mass density of this identical collection of particles each with an individual mass  $m$ . Borrowing another result from statistical mechanics, if

there is an equipartition of energy, we may relate the temperature to the degrees of motion (in this case, the three translational components) as,

$$\frac{3}{2}k_B T = \frac{1}{2}m\langle v^2 \rangle \Rightarrow T = \frac{m}{3k_B}\langle v^2 \rangle. \quad (6.2)$$

The companions are subjected to the gravitational potential of the central host:  $\phi_H = -GM_H/r$ , where  $G$  is the gravitational constant,  $M_H$  is the mass of the host, and  $r$  is the radius from the host. Now, if companions are like fluid particles with a pressure  $P$  and embedded in this gravitational potential, then the companions must be supported by a pressure gradient,

$$\frac{dP}{dr} = -\frac{d\phi_H}{dr}\rho = -\frac{GM_H}{r^2}\rho. \quad (6.3)$$

The mass density  $\rho$  is equal to the number density  $n(r)$  multiplied by the mass of an individual companion  $m$  (we assume all companions are of similar mass; this is why the GNC case's localized partner mass is particularly important). Along with the equation of state developed above and  $\rho = m \cdot n(r)$ , we may simplify the pressure gradient expression to

$$\frac{dP}{dr} = -\frac{GM_H}{r^2}\rho \Rightarrow \frac{d(nT)}{dr} = -\frac{GM_H}{r^2}(mn), \quad (6.4)$$

$$\Rightarrow \frac{d(n\langle v^2 \rangle)}{dr} = -\frac{3GM_H}{r^2}n. \quad (6.5)$$

Using this simple model, the developed differential equation describes the behaviour of the number density function  $n(r)$  as a function of other physical variables like mass of the central host  $M_H$ . We now explore possible solutions to this equation.

### 6.2.3 Spherically Symmetric + Isotropic + *Isothermal* Model

There are two unknowns in Equation (6.5): the number density  $n(r)$  and velocity component  $\langle v^2 \rangle$ . If we wanted to determine an analytical function for  $n(r)$ , we may assume  $\langle v^2 \rangle$  is some constant value and solve for  $n(r)$ . This assumption of a constant  $\langle v^2 \rangle$  may be regarded as an *isothermal* system, i.e. there is no “temperature” gradient or, equivalently, all radii have the same average kinetic energy. Now, we can to solve

the differential equation for  $n(r)$ ,

$$\frac{dn}{dr} = -\frac{3GM_H}{\langle v^2 \rangle r^2} n, \quad (6.6)$$

$$\Rightarrow \int \frac{dn}{n} = - \int \frac{3GM_H}{\langle v^2 \rangle r^2} dr, \quad (6.7)$$

$$\Rightarrow n(r) = n_0 \exp \left[ \frac{3GM_H}{\langle v^2 \rangle} \left( \frac{1}{r} - \frac{1}{r_0} \right) \right], \quad (6.8)$$

where  $n_0$  is representative of some background number density of companions near the edge of the counting volume at  $r_0 = 3.0$  Mpc.

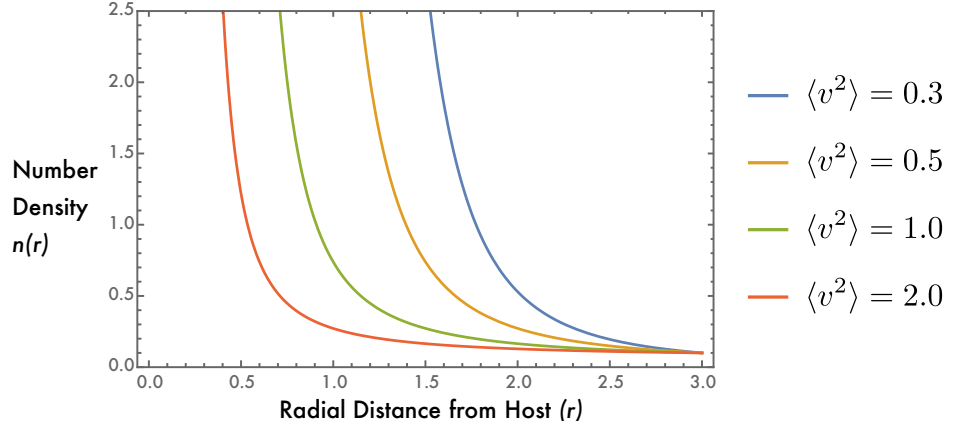


Figure 6.1: Sketches of the number density solution given in Equation (6.8) for the spherically symmetric, isotropic and isothermal model. We set  $G = M_H = 1$  and the initial condition to some background number density  $n_0 = 0.1$  at  $r_0 = 3$ . We know that  $T \propto \langle v^2 \rangle$  according to Equation (6.2); therefore, the four different  $\langle v^2 \rangle$  represent different isothermal curves. The monotonically decreasing nature of this solution is seen in the non-AGN number density curves in Figures (5.1) to (5.3).

Figure (6.1) provides quick sketches of Equation (6.8) for different values of  $\langle v^2 \rangle$ , given that  $G = M_H = 1$  and the initial condition is set to some background number density  $n_0 = 0.1$  at  $r_0 = 3$ . The solutions are seen to follow a monotonically decreasing nature. Even though we recognize a full curve fitting procedure is required to determine how good a fit the above curve is, this quick qualitative inspection has, nevertheless, shown that the non-AGN number density seen in the GNC case study seems to be reasonably represented by a spherically symmetric, isotropic and isothermal model.



## 6.2.4 Important Implications of AGN Number Density's Local Maximum

In the previous section, we attempted to model a spherically symmetric, isotropic and isothermal solution. We observed that this solution seemed to generally be a reasonable model for the non-AGN number density seen in the GNC case study. However, in this section, we want to demonstrate how the isothermal model *cannot* work at all for the AGN number density curve. Furthermore, we want to show that the local maximum seen in Figure (5.1) to (5.3) has significant physical implications on the kinematical configuration of the AGN companions.

By assuming isothermality, we begin by demonstrating a clear contradiction. Suppose  $\langle v^2 \rangle$  was independent of  $r$ , then we can pull it out of the derivative to get

$$\frac{d(n\langle v^2 \rangle)}{dr} = -\frac{3GM_H}{r^2}n \Rightarrow \frac{dn}{dr} = -\frac{3GM_H}{\langle v^2 \rangle r^2}n. \quad (6.9)$$

Now, we use an observation from the data. Figures (5.1) to (5.3) clearly show the AGN number density to generally increase from the 0.0 Mpc to about 1.0 Mpc, reach a local maximum and then generally decrease toward 3.0 Mpc. This means that the derivative of the number density is  $dn/dr' \geq 0$  for the interval between the origin and the local maximum. Mathematically, this means

$$\frac{dn}{dr'} \geq 0 \Rightarrow -\frac{3GM_H}{\langle v^2 \rangle (r')^2} \geq 0, \quad (6.10)$$

$$\Rightarrow \frac{3GM_H}{\langle v^2 \rangle (r')^2} \stackrel{?}{\leq} 0. \quad (6.11)$$

However, this cannot be true. None of the variables seen on the left-side of Equation (6.11) can be negative or zero. This simple consideration shows that isothermality cannot work for the AGN number density.

The simplest correction would be to assume  $\langle v^2 \rangle$  was dependent on the radius  $r$ . If we were to consider  $\langle v^2 \rangle$  as a function of  $r$  and apply the local maximum constraint,

we would get,

$$\frac{d(n\langle v^2 \rangle)}{dr} = \langle v^2 \rangle \frac{dn}{dr} + n \frac{d\langle v^2 \rangle}{dr} = -\frac{3GM_H}{r^2}, \quad (6.12)$$

$$\text{If } \frac{dn}{dr} = 0 \text{ at local max. } \Rightarrow n_{max} \frac{d\langle v^2 \rangle}{dr} = -\frac{3GM_H}{(r_{max})^2}, \quad (6.13)$$

$$\Rightarrow \frac{d\langle v^2 \rangle}{dr} < 0 \text{ (at local max.)} \quad (6.14)$$

This is a very interesting result. It implies that the region where the AGN number density and non-AGN number density begin to deviate (i.e. near the AGN’s local maximum) represents a fundamental change in the kinematical configuration of the companions. In other words, the AGN number density is not isothermal and the system is not in “thermal” equilibrium. There is a net flow within the inner region of 0.5 Mpc. This theoretical implication adds more strength to the idea that AGN host galaxies have consumed companions acquiring fuel because AGN companions may kinematically be in a preferred infall state.

The statistical mechanics of self-gravitating collisionless systems has given us a means to interpret the number density  $n(r)$  that was observationally determined. If we have a host’s gravitational potential  $\phi_H$  and a statistical arrangement of collisionless galaxies, then we can expect a regular distribution of these companions to cluster around the host. However, this number density of companions is dependent on the velocity distribution of the galaxies. We saw that the monotonically decreasing non-AGN number density in the GNC case study was indicative of a generally uniform average companion velocity of  $\langle v^2 \rangle$  across 3.0 Mpc. However, the violation of monotonicity seen in the AGN number density (i.e. the local maximum) is a clear sign that the kinematical nature of the companions has to be different. These AGN companions cannot be in thermal equilibrium and there seems to be a net flow within the inner radial domain of 0.5 Mpc.

As a future project, it would further be interesting to investigate *which* component of the companion’s velocity is changing. We started with an isotropic model where all velocity components were equal  $\langle v_r^2 \rangle = \langle v_\theta^2 \rangle = \langle v_\phi^2 \rangle$ . However, Binney and Tremaine (2008) explore the possibility of *anisotropic* flow, where only  $\langle v_\theta^2 \rangle = \langle v_\phi^2 \rangle = \text{constant}$

and  $\langle v_r^2 \rangle$  is dependent on  $r$ , or

$$\frac{d}{dr} (n \langle v_r^2 \rangle) + \frac{2n}{r} (\langle v_r^2 \rangle - \langle v_\theta^2 \rangle) = -\frac{d\phi}{dr} n. \quad (6.15)$$

Notice, anisotropy introduces the extra term,  $\frac{2n}{r} (\langle v_r^2 \rangle - \langle v_\theta^2 \rangle)$ , which otherwise would be zero if the velocity component were equal and reduce to Equation (6.9). A full investigation of these possibilities are beyond the scope of this thesis, but are nevertheless intriguing to consider.

## 6.3 Assumptions and Limitations of the Model and Methods

### 6.3.1 Redshift Range and Relation to Cosmic Timescale

One important constraint affecting our dataset was that all galaxies used in the sample were between the redshift range of  $0.010 \leq z \leq 0.064$ . Redshift is not only a measure of distance, but it is indicative of cosmic time as well. Using the cosmology relation given by Ryden (2011),

$$t_{\text{past}} = H_0^{-1} \left( 1 - \frac{1}{1+z} \right), \quad (6.16)$$

where  $H_0$  is the Hubble constant, the redshift range given above corresponds to 150 million to 890 million years into the past. To put this time in more perspective, it takes approximately 220 million years for the Sun to make one complete orbit around the Milky Way. Therefore, this time range may be equivalently stated as 0.68 to 4.04 Milky Way years.

In cosmology, the study of key epochs plays an important role in understanding galaxy formation and the growth of supermassive black holes (SMBH), which power AGNs. Our spatial distributions depicted in the results are based on galactic evolution and SMBH sizes within recent cosmological timescales. It would be interesting to examine how these spatial distributions would change according to different cosmic epochs. For us, we are significantly limited the SDSS data. It is not that higher redshift objects are not be measured by SDSS beyond  $z > 0.067$ , but, to make accurate distance estimates, we need spectroscopic information and, therefore, the spectroscopic cutoff prevents us from examining fainter objects.

### 6.3.2 Selection Bias to AGN Type

Due to the selection process outlined by the value-added catalog, the AGNs used in our project were predominantly Seyferts and LINERs. These active galaxies are on the scale of AGNs with weaker core activity. It is not clear if more energetic AGNs such as quasars and radio galaxies would be placed in the same environment as these galaxies. One would expect that these more powerful AGNs to have adopted a much more larger in-take of gaseous fuel and may have possibly consumed more companions and/or larger ones.

# Chapter 7

## Conclusion

We set out to investigate whether gravitational interaction with companion galaxies was the primary cause leading to core activity. By gravitational interaction, we refer to situations whereby a companion makes a direct contribution of gaseous fuel to the host's core (such as galactic collision or cannibalism) and/or the physical closeness of a partner induces gravitational disturbances in the host (such as galactic harassment or tidal stripping).

Our approach to investigating this problem was to conduct a 3.0 Mpc environmental survey around a matched sample of active and non-active host galaxies, and to examine how the number density of companions radially varied within this volume. If active galaxies have been engaging in gravitational interaction with their neighbour galaxies, then we would expect some kind of difference in the spatial arrangement of companions around these host, which could potentially be observable in the number density function. Our model also adopted an important constraint known as Gravitational Competitiveness. This condition particularly investigated how a host's gravitational dominance in its environment influenced the spatial distribution of companions.

Here is a summary of our main results, their implications, and possible future works:

1. When active galaxies are placed in an isolated environment (i.e. Gravitationally Non-Competitive (GNC) within 3.0 Mpc), their inner domains within about 0.5 Mpc seem to consistently be placed in an under-dense environment of companions (minors, intermediates, & comparables) relative to their non-active counterparts.

- In this GNC environment, the number density of companions follow consistent trends. The non-AGN number density is seen to be a monotonically decreasing curve starting from a maximum value in the inner-most radius and decaying to some background density at 3.0 Mpc. The AGN number density is similar to the non-AGN number density outside about 1.0 Mpc, but there is an important change that occurs within the inner domain – the AGN curve reaches a local maximum and then decays to a near-zero value.
  - This absence of AGN companions where one should expect to find companions (according the standard set by the non-AGN control) may possibly be indicative of a history of mergers and consumptions of neighbour galaxies to power these now-active host.
  - We may also model the GNC case study from the perspective of a self-gravitating collisionless system. In this light, the local maximum seen in AGN number density may have important interpretational value as a change in the kinematical configuration of the companions. That is, AGN companions may not be in equilibrium and there may be a preferred net flow of companions. This implication further supports the idea that AGNs have consumed neighbour galaxies.
2. In the Gravitationally Competitive (GC) environment, we allowed for one massive perturbing partner to be present in the counting volume and one-or-more lower-mass companions. The presence of this massive companion had noticeable impacts on the spatial distribution of the lower-mass partners.
- The results from the GC study show how the presence of a massive partner can significantly alter the spatial distribution of companions. When attempting to consider all partners in the count for the number density, the AGN and non-AGN number density curves started to become indistinguishable.
  - It was only when we selectively analyzed specific partner masses that the number densities became distinguishable. This shows that different mass-companions cluster in different arrangements around hosts.

3. Overall, the results of this study support the idea that, in gravitationally isolated environments, active galaxies are placed in different environments than their non-active counterparts, which may be directly suggestive of a history of mergers and consumptions. These findings support the idea that gravitational interactions with neighbour galaxies may lead to core activation.
4. In terms of future work, there are many different directions we can take to further test and refine the hypotheses. Here are a few examples:
  - For simplicity, we explored two relatively straightforward ensemble setups: the GNC environment and GC environment with a single massive perturber. It would be interesting to explore different ensemble configurations with more competitive environments. Perhaps, it may be worthwhile to look into how two or more AGNs in a close range environment influence the clustering of companions around them;
  - As mentioned in the discussion section, based on the selection process implemented, our active galaxies were mainly Seyferts and LINERs. It would be interesting to examine how neighbouring galaxies cluster around other types of active galaxies, like radio galaxies and Quasars. Since these active galaxies are often more energetic, they require more fuel to power their AGN engines. It would be interesting to investigate how this increased fuel demand to power the supermassive black hole would change the number density of companions within the inner volume around these host galaxies;
  - SDSS posed limitations on our surveying depth and our dataset. Future works with other telescopes with more richer spectroscopic data may allow for a deeper redshift range. Since the redshift is also related to cosmological time, it would be interesting to explore how the number density function of AGN companions changes over different cosmic timescales.

# Bibliography

- [1] Besla, G., Kallivayalil, N., Hernquist, L., Marel, R. P., Cox, T. J., & Keres, D. (2010). Simulations Of The Magellanic Stream In A First Infall Scenario. *The Astrophysical Journal*, 721(2). doi:10.1088/2041-8205/721/2/197
- [2] Binney, J., & Tremaine, S. (2008). *Galactic Dynamics*. Princeton: Princeton University Press.
- [3] Blanton M. R., Eisenstein D., Hogg D. W., Schlegel D. J. & Brinkmann J. (2005). Relationship between Environment and the Broadband Optical Properties of Galaxies in the Sloan Digital Sky Survey. *The Astrophysical Journal*, 629, 143157.
- [4] Cisternas, M., Sheth, K., Salvato, M., Knapen, J. H., Civano, F., & Santini, P. (2015). The Role Of Bars In Agn Fueling In Disk Galaxies Over The Last Seven Billion Years. *The Astrophysical Journal*, 802(2), 137. doi:10.1088/0004-637x/802/2/137
- [5] Conidis, G. J., (2013). Analogues of the Local Sheet. *Master of Science Thesis in Physics and Astronomy*. York University, Toronto Canada.
- [6] Combes, F., Baker, A. J., Schinnerer, E., Garca-Burillo, S., Hunt, L. K., Boone, F., A. Eckart, R. Neri & Tacconi, L. J. (2009). Molecular gas in NUclei of GALaxies (NUGA). *Astronomy & Astrophysics*, 503(1), 73-86. doi:10.1051/0004-6361/200912181



- [7] Ellison, S. L., Patton, D. R., Mendel, J. T., & Scudder, J. M. (2011). Galaxy Pairs in the Sloan Digital Sky Survey - IV. Interactions Trigger Active Galactic Nuclei. *Monthly Notices of the Royal Astronomical Society*, 418(3), 2043-2053. doi:10.1111/j.1365-2966.2011.19624.x
- [8] Fabian, A. (2012). Observational Evidence of Active Galactic Nuclei Feedback. *Annual Review of Astronomy and Astrophysics*, 50(1), 455-489. doi:10.1146/annurev-astro-081811-125521
- [9] Khabiboulline, E. T., Steinhardt, C. L., Silverman, J. D., Ellison, S. L., Mendel, J. T., & Patton, D. R. (2014). Changing Ionization Conditions In Sdss Galaxies With Active Galactic Nuclei As A Function Of Environment From Pairs To Clusters. *The Astrophysical Journal*, 795(1), 62. doi:10.1088/0004-637x/795/1/62
- [10] Haan, S., Schinnerer, E., Emsellem, E., Garca-Burillo, S., Combes, F., Mundell, C. G., & Rix, H. (2009). Dynamical Evolution Of Agn Host Galaxies Gas In/out-Flow Rates In Seven Nuga Galaxies. *The Astrophysical Journal*, 692(2), 1623-1661. doi:10.1088/0004-637x/692/2/1623.
- [11] Hashimoto, Y., Funato, Y., & Makino, J. (2003). To Circularize or Not To Circularize? – Orbital Evolution of Satellite Galaxies. *The Astrophysical Journal*, 582(1), 196-201. doi:10.1086/344260
- [12] Lynden-Bell, D. (1969). Galactic Nuclei as Collapsed Old Quasars. *Nature*, 223(5207), 690-694. doi:10.1038/223690a0
- [13] Mo, H., Bosch, F. V., & White, S. (2010). *Galaxy Formation and Evolution*. Cambridge: Cambridge University Press.
- [14] McCall M. L. (2004). On Determining Extinction from Reddening. *The Astrophysical Journal*, 128, 21442169.

- [15] Netzer, H. (2013). *The Physics And Evolution Of Active Galactic Nuclei*. Cambridge: Cambridge University Press.
- [16] Netzer, H. (2015). Revisiting the Unified Model of Active Galactic Nuclei. *Annual Review of Astronomy and Astrophysics*, 53(1), 365-408. doi:10.1146/annurev-astro-082214-122302
- [17] Ogiya, G., & Burkert, A. (2016). Dynamical friction and scratches of orbiting satellite galaxies on host systems. *Monthly Notices of the Royal Astronomical Society*, 457(2), 2164-2172. doi:10.1093/mnras/stw091
- [18] Osterbrock, D. E., & Ferland, G. J. (2006). *Astrophysics of Gaseous Nebulae and Active Galactic Nuclei*. Sausalito: University Science Books.
- [19] Putman, M. E., Staveley-Smith, L., Freeman, K. C., Gibson, B. K., & Barnes, D. G. (2003). The Magellanic Stream, High-Velocity Clouds, and the Sculptor Group. *The Astrophysical Journal*, 586(1), 170-194. doi:10.1086/344477
- [20] Richstone, D., E. A. Ajhar, R. Bender, G. Bower, A. Dressler, S. M. Faber, A. V. Filippenko, K. Gebhardt, R. Green, L. C. Ho, J. Kormendy, T. R. Lauer, J. Magorrian & S. Tremaine (1998). Supermassive black holes and the evolution of galaxies. *Nature Review*, 395(6701), A14-A19
- [21] Sabater, J., Best, P. N., & Argudo-Fernandez, M. (2013). Effect of the interactions and environment on nuclear activity. *Monthly Notices of the Royal Astronomical Society*, 430(1), 638-651. doi:10.1093/mnras/sts675
- [22] Satyapal, S., Ellison, S. L., Mcalpine, W., Hickox, R. C., Patton, D. R., & Mendel, J. T. (2014). Galaxy pairs in the Sloan Digital Sky Survey IX. Merger-induced AGN activity as traced by the Wide-field Infrared Survey Explorer. *Monthly Notices of the Royal Astronomical Society*, 441(2), 1297-1304. doi:10.1093/mnras/stu650

- [23] Schlegel D. J., Finkbeiner D. P. & Davis M. (1998). Maps of Dust Infrared Emission for Use in Estimation of Reddening and Cosmic Microwave Background Radiation Foregrounds. *The Astrophysical Journal*, 500, 525.
- [24] Seth, A., Ageros, M., Lee, D., & BasuZych, A. (2008). The Coincidence of Nuclear Star Clusters and Active Galactic Nuclei. *The Astrophysical Journal*, 678(1), 116-130. doi:10.1086/528955
- [25] Tanaka, I., Yagi, M., & Taniguchi, Y. (2017). Morphological evidence for a past minor merger in the Seyfert galaxy NGC 1068. *Publications of the Astronomical Society of Japan*, 69(6). doi:10.1093/pasj/psx100
- [26] Tully, R. B., Shaya, E. J., Karachentsev, I. D., Courtois, H. M., Kocevski, D. D., Rizzi, L., & Peel, A. (2008). Erratum: “Our Peculiar Motion Away from the Local Void” (*ApJ*, 676, 184 [2008]). *The Astrophysical Journal*, 686(2), 1523-1523. doi:10.1086/591904
- [27] Vaduvescu O., McCall M. L., Richer M. G. & Fingerhut R. L. (2005). Infrared Properties of Star-forming Dwarf Galaxies. I. Dwarf Irregular Galaxies in the Local Volume. *The Astrophysical Journal*, 130, 15931626.